An Investigation of Inorganic Compound Scattering.

A Dissertation Presented for the

Doctor of Philosophy

Degree

The University of Tennessee, Knoxville

Karl Jay Bernstein

May 2015

DEDICATION

This dissertation is dedicated to improvement the human life, even if in the minutest of ways.

ACKNOWLEDGEMENTS

I have many people to acknowledge in the process of my work. First and foremost I must give praise my family. There are many, many of you; each and every one of you has given me your support in my life and I simply cannot express my gratefulness enough for that. A special heartfelt thanks goes to Angela Belic, for her loving dedication, both in life and in the reduction of errors in this document! Thank you Angela!

In my graduate studies I'd like to first express my appreciation to my group mates: Nasrin Misraleh-Kohan Vighter Iberi, DJ Simmons, Hobbie Turley, Xin Gu, and Sarah Griffin for their help and support over the years. We've all learned so very much from each other over these years!

I must also express my gratitude to Prof Robert Harrison and his research group: Deborah Penchoff, Scott Thornton, Nick Vence, Jacob Fosso-Tande, Tara Michaels-Clark, and Bryan Sundahl, as well as to Prof George Schweitzer and members of his group: John Auxier, Britney Miner, Kaitlyn Roussert, and Melissa Lassig for your lengthy chats and advice!

An enormous thank you goes out to Prof David Jenkins and group members for their patience and guidance. To each of you: Chi-Linh Do-Thanh, Heather Bass, Alan Cramer, Chris Murdock, Brianna Hughes, Preeti Chandachud and Scott McCullough. I know an analytical chemist idea of clean is far different from that of a synthetic chemist!

I'd like to recognize my graduate committee: Prof Michael Sepaniak, Prof David Jenkins, Prof Sheng Dai, Prof Ramki Kalyanaraman for your academic guidance and support.

Finally, I'd like to express my appreciation the University of Tennessee Department of Chemistry and Dr. Jon Camden for their financial support through these last several years.

ABSTRACT

Raman and its associated forms of spectroscopy are powerful tools that have been under-utilized. Presented within are three studies of inorganic compounds performed with some form of Raman spectroscopy: normal Raman, hyper-Raman (HR), surface-enhanced Raman spectroscopy (SERS), surface-enhanced hyper-Raman spectroscopy (SEHRS), or resonance Raman spectroscopy (RR).

The first study involves the investigation of phosphine binding with silver metal. Phosphines find wide use in synthetic circles yet have had little study into their method of binding, unlike similar compounds comprised of sulfur. In order to understand the binding of phosphines, several tertiary phosphines, secondary phosphines and secondary phosphine oxides are examined with SERS. SERS is a surface technique, providing a probe into the surface interaction of the phosphines and silver. By analyzing the results of SERS experiments and using the process of elimination, the secrets of phosphine binding begins to unravel.

The second study involves the use of Raman spectroscopy, along with several other chemistry techniques to characterize a new uranium complex. This particular uranium complex is of interest due to applications to uranium capture and uranium sensing; however, this work did not progress to these points. Detailed in the study are the various facets concerning the complex, using many techniques for characterization.

The third study centers around the investigation of uranium compounds with HR, RR and SEHRS. There are no published works on this subject to the author's knowledge. Non-linear spectroscopies such as HR offer the benefit of accessing modes forbidden to one-photon spectroscopies, such as traditional linear spectroscopies like Raman and IR. This can lead to new possibilities for identification and sensing not previously accessible.

TABLE OF CONTENTS

LIST OF FIGURES

INTRODUCTION

Statement of Purpose

Raman spectroscopy as a field has blossomed with the advent of inexpensive, monochromatic laser sources. Much as infrared spectroscopy has been a long used process to probe chemical systems; now too Raman can be used. While for many, the first experience with spectrophotometry occurs in an organic chemistry class, these spectroscopies are equally valuable for work with inorganic species. Vibrational spectroscopies provide information on functionalization, bond characteristics and more.

The work presented in this document draws heavily on various forms of Raman spectroscopy to investigate a number of inorganic compounds. There are a multitude of advantages to these forms of spectroscopy that have aided in the understanding of phosphine binding to silver, the exploration of a new uranium complex, and exploring new avenues of spectroscopic characterization. In this first chapter, background material is given for a number of techniques used in the included studies.

Literature Background

Raman Spectroscopy

The Raman phenomenon was first described by C.V. Raman and his student K.S. Krishna in 1928.[1] The new scattering process, the fundamental process at heart of Raman Spectroscopy, was named after it's discoverer and earned Raman a Nobel in 1930 demonstrating the impact of this discovery on science. Unlike the previously discovered Rayleigh scattering, Raman scattering is the inelastic scattering of light. The difference of energy can be a reduction or gain

in net energy yielding Stokes and anti-Stokes scattering respectively.[2] This difference in energy coincides with the loss or gain of energy from vibrational states of the interacting medium as illustrated with a Jablonski diagram in Figure 0.1.

Raman spectroscopy is usually performed using light in the visible region of the electromagnetic spectrum. However, fluorescence often occurs in this range and generally overpowers Raman scattering in intensity. To alleviate issues arising from fluorescence, experimenters often move further into the red where there is insufficient energy for the process. In general, Raman scattering is a very weak process; for instance, a typical absorption experiment will absorb 90 percent of the incident light over a 1 cm path length, but only one in 10^{10} incident photons will undergo Raman scattering.[2] This fundamental limitation is a challenge when using Raman spectroscopy. The classical depiction of Raman scattering is that a polarization is induced in a molecule by an oscillating electric field of incoming light. The induced dipole then radiates scattered light, without (Rayleigh) or with (Raman) exchanging energy with vibrations in the medium (e.g. molecule). The magnitude of the induced polarization, P, scales with the polarizability, α, and the incident electric field E:

$$P = \alpha E$$

Given this equation, the only methods to increase the magnitude of Raman scattering is to change the polarizability (e.g. your sample) or to raise the intensity of the electric field (e.g. light source).

Hyper-Raman Spectroscopy (HR)

Hyper-Raman scattering is the two photo form of Raman scattering, requiring that two

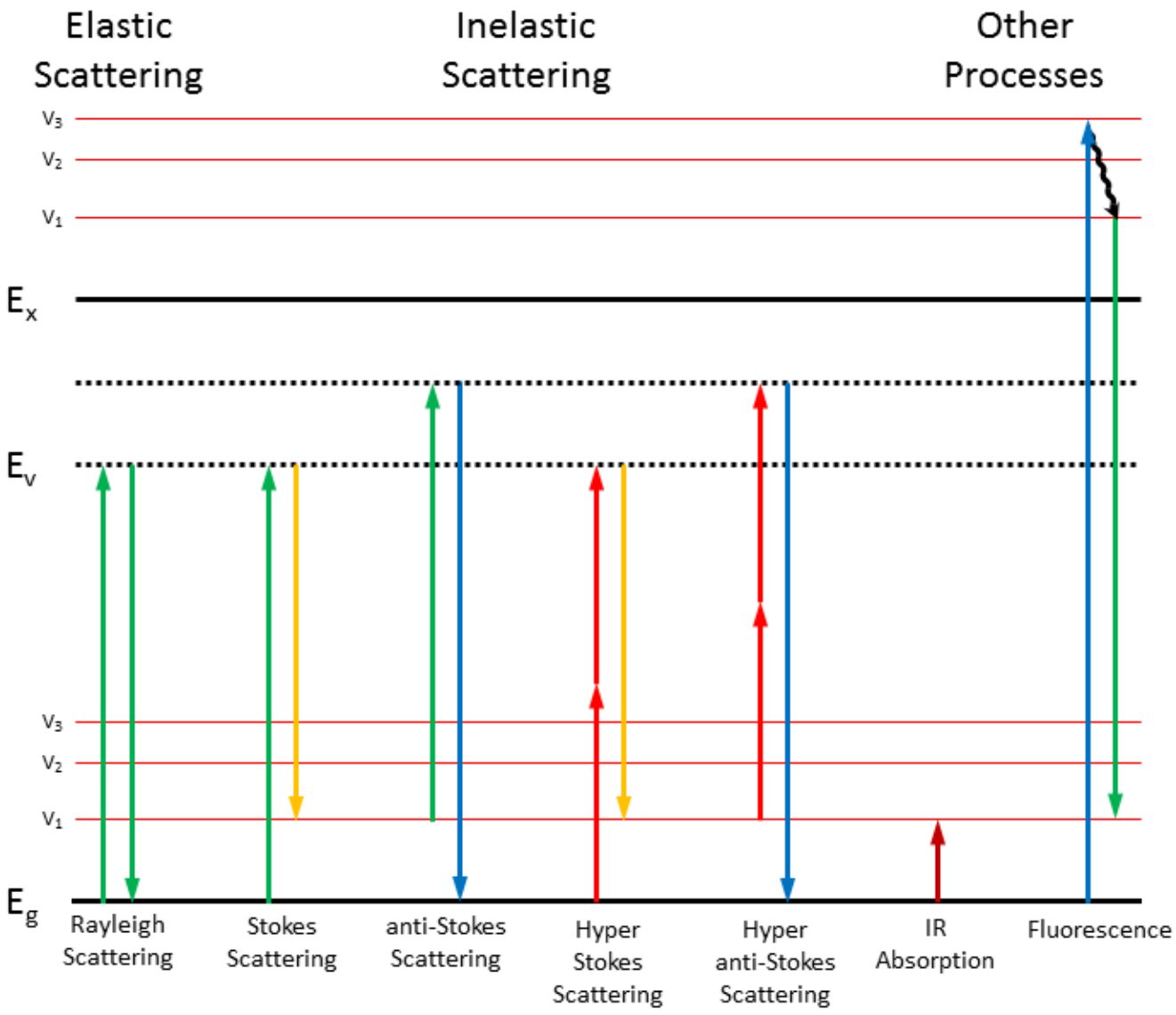

Figure 0.1. Jablonski diagram of Rayleigh, Raman, Hyper-Raman, IR (absorption), and Fluorescence.

photons scatter at the same time. The process was first documented in 1965 by Terhune, Maker, and Savage.[3] While intensities, selection rules, and depolarization ratios for ordinary Raman are represented by the linear terms in the expansion of the dipole moment of a molecule, the description for hyper-Raman is represented mathematically by the first set of nonlinear terms in the equation:

$$P = \alpha E + \frac{1}{2}\beta E^2 + \cdots$$

The magnitude of P scales with α and E for normal Raman and is added to the second polarizability, the hyperpolarizability, represented by half β and the electric field, E, squared. The Raman activity of the analyte is determined by the polarizability and the Hyper-Raman activity is determined by the hyperpolarizability. Two researchers, Long and Stanton, explored hyperpolarizability in 1970 and found the polarizability to generally be six orders of magnitude, greater than the hyperpolarizability.[4] A benefit of hyper-Raman is differing selection rules from either IR or Raman, meaning that inactive vibrational modes in IR and Raman may be observed in hyper-Raman.

Surface-Enhanced Raman Spectroscopy (SERS)

Raman scattering is a weak process that can lack sensitivity needed for many experiments. However, the physics behind Raman can dictate that the process be used for a specific experiment. Assuming that the sample (and α) cannot be changed, E must be increased in order to get a stronger signal for more sensitivity; yet high electric fields result in photo bleaching and sample degradation. The answer to these challenges is often surface-enhanced Raman spectroscopy.

First observed and documented by Fleischmann, Hendra and McQuillan in 1974[5] and later in 1977, described simultaneously by two groups.[6,7] SERS is a method which utilizes incredibly intense, localized electric fields while avoiding destroying the sample. While there is still some debate concerning the exact mechanism of SERS, it is generally agreed that there is an electromagnetic enhancement aspect. The electromagnetic enhancement is derived from the excitation of localized surface plasmon resonance (LSPR), which is essentially an "electron wave" (Figure 0.2) that oscillates in resonance with incident electromagnetic fields.[8] As the name indicates, LSPRs are highly localized, creating an enhancement generally no more than two to ten nanometers from the surface they originated from. Therefore, in order to utilize SERS, the analyte must be on or very near the surface of the enhancing substrate. While there are substantial experimental constraints to SERS, an average enhancement of seven to eight orders of magnitude is routinely achieved and enhancements of eleven orders of magnitude have been reported.[9-11] The enormous boost in intensity allows the experimenter to use much lower powers, for less time, and still receive more signal than they would get with higher power and longer experiments. SERS also provides the benefit of quenching competing fluorescence which can be of great benefit to experimenters.

Plasmonic Surfaces

SERS requires plasmonic surfaces to support LSPRs and provide an enhancement; Figure 0.3 provides illustrations of two types of substrates. Fleischmann et al. initial work used a silver electrochemically etched electrode.[5] The electrode was cycled numerous times which led to the surface becoming roughened or microscopically textured. This was important as it was the coarseness of the surface that permitted the formation of LSPRs and SERS enhancement. While

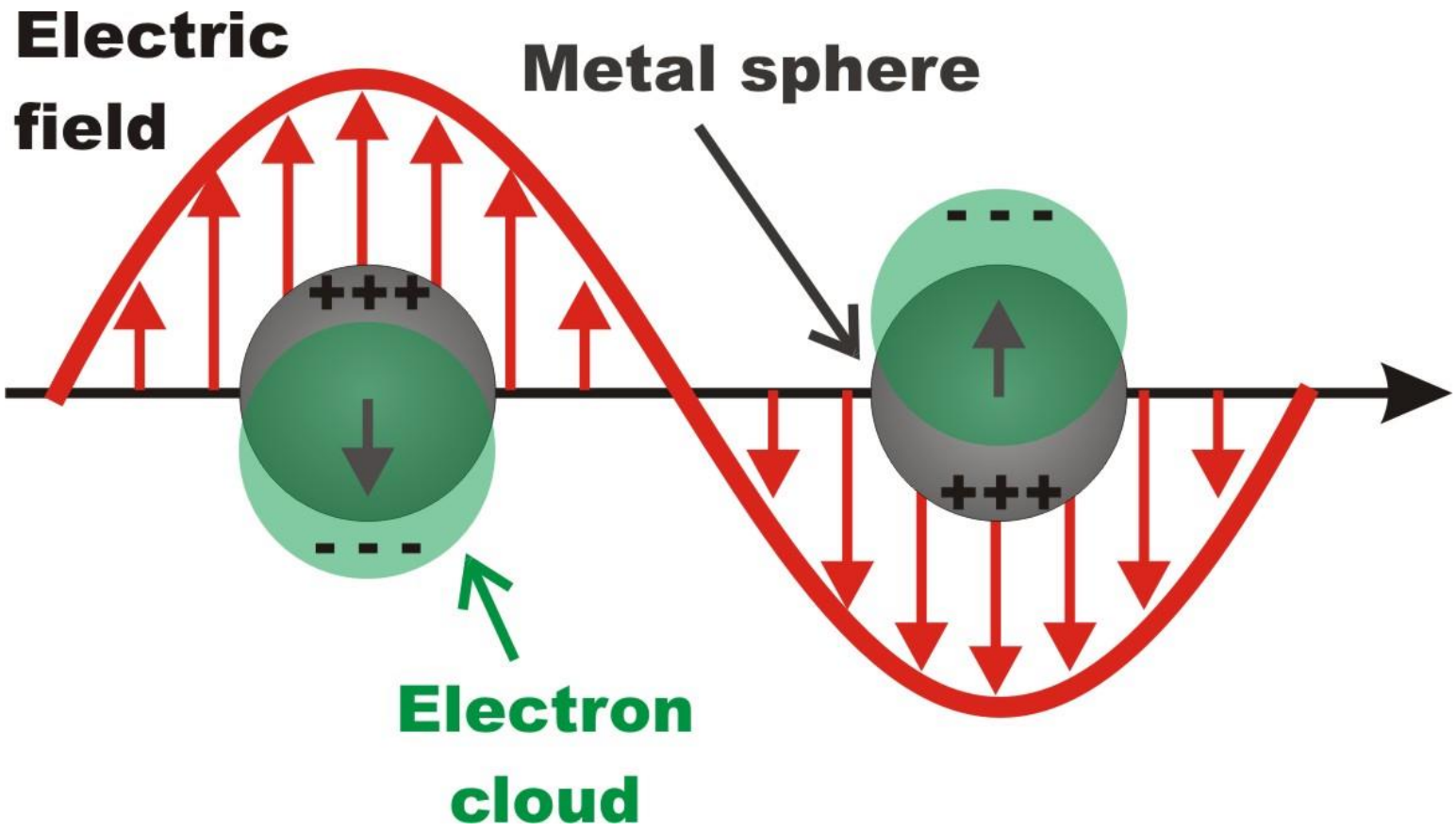

Figure 0.2. When nanoparticles are excited by electromagnetic radiation, their electrons oscillate. These oscillations are knows as localized surface plasmon resonance (LSPR).

electrochemically roughened electrodes are rarely used today in SERS work, the prerequisite of a microscopically textured surface is still key to the substrates used in all SERS work.[8] The fact that the electrode was silver is also important as the LSPRs of silver and gold typically resonate within the visible spectrum of light. Most SERS active substrates consist of either gold or silver.

Popular SERS substrates are colloidal aggregates. Typically, colloids are chemically synthesized from silver or gold as a colloidal suspension, made up of small spherical particles.[12,13] A sample is introduced to the suspension where it must then migrate to the surface of the colloids. Initially, very little if any enhancement of the colloidal-sample complex suspension is observed. However, after a sufficient amount of time, the complex generally self-aggregates. If not, a salt is added to force aggregation. Aggregation causes the complex to crash out of solution, collecting at the bottom of the container. When the complex collects in an aggregate, the spheroid particles end up touching, or nearly touching, and it is at these junctions between particles that hotspots are excited and provide enormous SERS enhancement.[11] Another popular substrate is thin island films.[14] Named for the thin amount of material present in island like patches, these films are often made using physical vapor deposition. This process vaporizes small amounts of gold or silver metal and deposits them onto a substrate such as glass. Only a very thin layer, around ten nanometers, is typically used. The process creates a rough surface of island-like collections of the metal that provide the texture necessary for LSPR formation and SERS enhancement.

Aryl Phosphines

The binding of thiols and aryl thiols is a well understood process; when binding with metals, it has been well established that thiols lose a proton to form strong covalent bonds to metals.[15] This method of binding has been used extensively in modifying the surface of

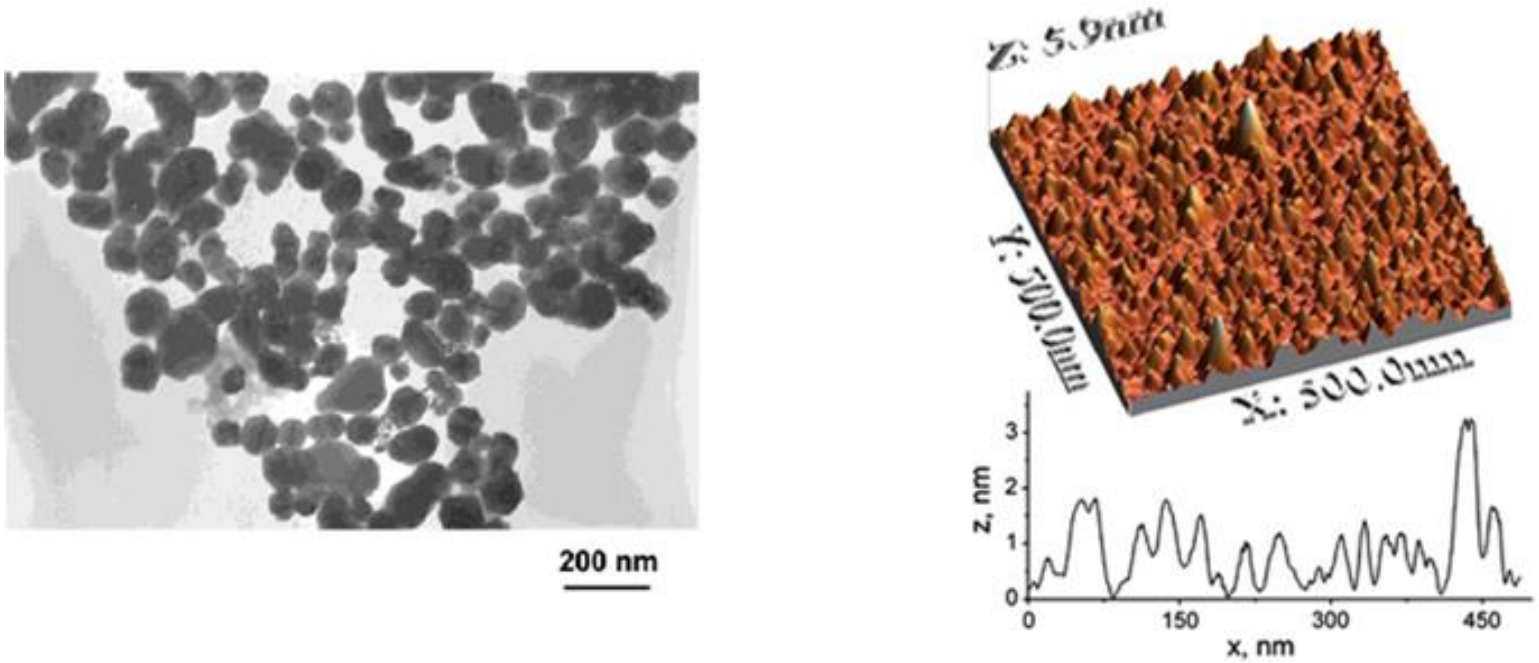

Figure 0.3. Examples of a colloidal aggregate (left) and a section of topology from a silver island film (right).

nanoparticles.[16] However, the binding of phosphines, with their central phosphorus atoms a direct neighbor to sulfur on the periodic table, have yet to have their binding explored.

Phosphines have a variety of uses throughout academia, industry and the medical field. Frequently found in synthetic methods for the hydroformylation of olefins[17] and a number of hydrogenation schemes[18], phosphine compounds offer a method to tune activity, selectivity (including exceptionally high enantioselectivity) and recoverability of catalytic intermediates used in reactions. Of particular use is the ability to perform highly selective dehydrogenation, which is utilized in pharmacology for the production of the highly chiral compounds necessary for medicinal use. For example, the latter method has been utilized in the production of 3,4-dihydroxyphenylalanine ((S)-DOPA) to treat Parkinson's disease and also in production of (S)-cyclopentaneglutarate as an intermediate in the synthesis of Pfizer's Candoxatril, used in the treatment of chronic heart failure.[19] Phosphine compounds can also be used as stabilizers for copper[20], gold and palladium nanoparticles[21].

Uranium Complexation

Recent interest in amidoxime functional groups has been largely driven by uranium seawater extraction efforts.[22,23] Initial media used for the extract of uranium lacked the necessary durability and selectivity that was desired.[24,25] Following a functionalization screening study, it was found that amidoximes were highly selective to uranium and when combined with a polymer backbone were far superior at enduring the harsh conditions present in seawater.[24,25]

Work by Vukovic et al.[26] performed a theoretical investigation into the binding of amidoximes to the uranyl cation and suggested that η^2 binding was the method of binding most likely to occur contrary to previous suggestions in the literature.[27-29] This was confirmed in single X-ray crystal structures obtained of uranyl complexed with acetamidoxime and

benzamidoxime[26] and further supported in work by another group, Barber et al.[30] The research started by Vukovic et al. was continued by the same group in a publication by Kang et al. investigating the formation and stability of cyclic imide dixomes, a variant that occurs during functionalization of poly(acrylonitriles) to poly(acrylamidoximes).[31] It was found that heating an analogue of poly(acrylamidoximes), bisamidoxime, at 130 °C for 3 hours resulted in quantitative yields of the analogous cyclic imide dioxime, glutarimidedioxime. Also examined was the stability of the compounds in acidic conditions as previous reports had noticed diminishing efficacy after acid processing to remove the bound uranium.[25] Investigated were the simple acetamidoxime, bisamidoxime and glutarimidedioxime in 1 M DCl; acetamidoxime was found to be stable for several months, bisamidoxime for a couple of weeks and glutarimidedioxime for less than 20 hours in the acidic solution.

It was believed that the cyclic imide dioxime variants played an important role in uranium uptake[25], thus the loss of functionality of the cyclic imide dioximes would ultimately reduce efficacy of any sorbent based on poly(acrlamidoximes). Kang et al. reported that acid degradation of the cyclic forms was due to nucleophilic attack of water on the imino carbon and demonstrated that by lowering the charge on the carbon with an aromatic ring would slow the deterioration of the functionality.[31]

Work by Tian et al. demonstrated that the cyclic imide dioxime analog, glutarimideioxime, formed a very strong tridentate complex with UO_2^{2+}.[32] More importantly, that glutarimidedioxime could effectively compete with carbonate for complexing UO_2^{2+} at seawater pH. Tian's work also demonstrated 1:2 uranium-ligand binding motif in which the imide group on the ligand was deprotonated and the oxime groups experienced a hydride shift. These changes result in a large conjugated ligand system that coordinates UO_2^{2+} via the equatorial plane in a

tridentate mode. It was noted that improved electron density on the imide nitrogen should result in better uranium binding. Further work by Tian demonstrated the poly(acrylamidoxime) variant, represented by glutardiamidoxime, was unable to compete with carbonate to complex UO_2^{2+} at seawater pH.[33]

A combined study of phthalimidedioxime, the compound used by Kang[31] previously, demonstrated that the aromatic backbone reduces the strength of the uranium-ligand binding.[34] However, it was able to compete with carbonate for uranium and was far superior to glutarimidedioxime at withstanding the acid baths used to remove the bound uranium. Highlighted was the possibility of tuning the electronic properties of the ligands to enhance uranium binding; an important finding given recent advances in alternative methods for removal of sorbed uranium.[35]

Uranium Spectroscopy

A recent joint working group of the American Physical Society and the American Association for the Advancement of Science publication has recommended that "[a] program should be undertaken to develop and manufacture advanced, automated, field deployable equipment that would allow the necessary measurements to be made rapidly" and that "[s]uch field equipment is not now readily available."[36] This suggestion likely reflects the current state of the art instruments for tasks such as uranium isotopic discrimination; bulky, immensely expensive lab based mass spectrometers that require extensive sample preparation before samples can be analyzed.

When a border agent intercepts questionable material, it is at best "cumbersome" to have to remove a sample of the material and then ship it to a lab; where additional chemical digestions and extensive sample preparation is performed prior to analysis and eventual dissemination of

pertinent information. An ideal situation, when dealing with interdicted material, would entail the ability to rapidly (within an hour) identify material and characterize isotopic makeup.

Vibrational spectroscopy, such as Raman spectroscopy, is a nondestructive technique that provides rapid information about functionalization, bonds and isotopic makeup that unambiguously fingerprints samples. Furthermore, Raman spectroscopy requires little if any preparatory work up before analysis, often allowing for non-invasive sampling. Instrumentation can be constructed such that no moving parts are required, allowing for rugged, reliable instrumentation. Other vibrational techniques such as infrared spectroscopy (IR) typically require that samples be prepared into pellets or encased in between salt plates. Moreover, the excitation is often absorbed by optically transparent materials; notably, water, thus making noninvasive sampling impossible. Given the harmless nature of Raman spectroscopy, its compatibility with samples and lack of required sample prep, it can be performed in advance of or in tandem with other, destructive techniques to provide additional characterization.

Raman spectroscopy is particularly suited for unambiguous uranium identification due to the clarity of uranyl containing spectra in contrast to the IR spectra of the same compounds.[37] While IR spectra contain numerous modes in the cluttered finger print region, the uranyl mode in Raman is clear and unmistakable. Thus with Raman spectroscopy, the identification of the uranyl stretch in a compound borders on trivial - an ideal situation for rapid, field based identification and characterization.

In the case of uranyl containing compounds, the uranium containing stretch that is allowed in Raman via selection rules is the totally symmetric uranyl stretch. This stretch involves both oxygen atoms bound to the uranium atom stretching away from and then compressing into the central uranium atom in synchrony. The uranium atom experiences no movement in this

situation. For hyper-Raman and IR, the anti-symmetric uranyl stretch is the allowed mode. In this stretch one oxygen atom stretches away from the uranium atom while the other compresses in closer, both moving at the same rate before reaching the extent of their motion and the process reverses. An important difference between these two stretches is that a change in the central atoms mass will change the frequency of the anti-symmetric stretch and not the totally symmetric. Thus normal Raman spectra will show no difference between isotopes of uranium. However, IR and HR spectra will have a variation in the frequency of the uranyl stretch between uranium isotopes. The broader line width of IR and experimental difficulties associated with the technique would make it cumbersome, presenting HR as an ideal method to spectroscopically observe isotopic differences of uranium compounds.

Introduction References

[1] Raman, C. V.; Krishnan, K. S. *Nature* **1928**, *121*, 501.

[2] McCreery, R. L. *Raman Spectroscopy for Chemical Analysis*; John Wiley & Sons, 2005.

[3] Terhune, R. W.; Maker, P. D.; Savage, C. M. *Physical Review Letters* **1965**, *14*, 681.

[4] Long, D. A.; Stanton, L. *Proceedings of the Royal Society of London Series a-Mathematical and Physical Sciences* **1970**, *318*, 441.

[5] Fleischm.M; Hendra, P. J.; McQuilla, A. J. *Chemical Physics Letters* **1974**, *26*, 163.

[6] Jeanmaire, D. L.; Vanduyne, R. P. *Journal of Electroanalytical Chemistry* **1977**, *84*, 1.

[7] Albrecht, M. G.; Creighton, J. A. *Journal of the American Chemical Society* **1977**, *99*, 5215.

[8] Moskovits, M. *Journal of Chemical Physics* **1978**, *69*, 4159.

[9] Kneipp, K.; Wang, Y.; Kneipp, H.; Perelman, L. T.; Itzkan, I.; Dasari, R.; Feld, M. S. *Physical Review Letters* **1997**, *78*, 1667.

[10] McFarland, A. D.; Young, M. A.; Dieringer, J. A.; Van Duyne, R. P. *Journal of Physical Chemistry B* **2005**, *109*, 11279.

[11] Nie, S. M.; Emery, S. R. *Science* **1997**, *275*, 1102.

[12] Lee, P. C.; Meisel, D. *J. Phys. Chem.* **1982**, *86*, 3391.

[13] Leopold, N.; Lendl, B. *Journal of Physical Chemistry B* **2003**, *107*, 5723.

[14] Schlegel, V. L.; Cotton, T. M. *Analytical Chemistry* **1991**, *63*, 241.

[15] Daniel, M. C.; Astruc, D. *Chemical Reviews* **2004**, *104*, 293.

[16] Stewart, A.; Zheng, S.; McCourt, M. R.; Bell, S. E. J. *Acs Nano* **2012**, *6*, 3718.

[17] Zhu, H. J.; Ding, Y. J.; Yan, L.; Xiong, J. M.; Lu, Y.; Lin, L. W. *Catalysis Today* **2004**, *93-5*, 389.

[18] Blaser, H. U.; Malan, C.; Pugin, B.; Spindler, F.; Steiner, H.; Studer, M. *Advanced Synthesis & Catalysis* **2003**, *345*, 103.

[19] Crepy, K. V. L.; Imamoto, T. *Advanced Synthesis & Catalysis* **2003**, *345*, 79.

[20] Decaro, D.; Wally, H.; Amiens, C.; Chaudret, B. *Journal of the Chemical Society-Chemical Communications* **1994**, 1891.

[21] Tamura, M.; Fujihara, H. *Journal of the American Chemical Society* **2003**, *125*, 15742.

[22] Kim, J.; Tsouris, C.; Mayes, R. T.; Oyola, Y.; Saito, T.; Janke, C. J.; Dai, S.; Schneider, E.; Sachde, D. *Separation Science and Technology* **2013**, *48*, 367.

[23] Sodaye, H.; Nisan, S.; Poletiko, C.; Prabhakar, S.; Tewari, P. K. *Desalination* **2009**, *235*, 9.

[24] Schenk, H. J.; Astheimer, L.; Witte, E. G.; Schwochau, K. *Separation Science and Technology* **1982**, *17*, 1293.

[25] Astheimer, L.; Schenk, H. J.; Witte, E. G.; Schwochau, K. *Separation Science and Technology* **1983**, *18*, 307.

[26] Vukovic, S.; Watson, L. A.; Kang, S. O.; Custelcean, R.; Hay, B. P. *Inorganic chemistry* **2012**, *51*, 3855.

[27] Zhang, A.; Asakura, T.; Uchiyama, G. *React. Funct. Polym.* **2003**, *57*, 67.

[28] Choi, S.-H.; Nho, Y. C. *Radiation Physics and Chemistry* **2000**, *57*, 187.

[29] Katragadda, S.; Gesser, H. D.; Chow, A. *Talanta* **1997**, *45*, 257.

[30] Barber, P. S.; Kelley, S. P.; Rogers, R. D. *Rsc Advances* **2012**, *2*, 8526.

[31] Kang, S. O.; Vukovic, S.; Custelcean, R.; Hay, B. P. *Industrial & Engineering Chemistry Research* **2012**, *51*, 6619.

[32] Tian, G. X.; Teat, S. J.; Zhang, Z. Y.; Rao, L. F. *Dalton Trans.* **2012**, *41*, 11579.

[33] Tian, G. X.; Teat, S. J.; Rao, L. F. *Dalton Trans.* **2013**, *42*, 5690.

[34] Sun, X.; Tian, G.; Xu, C.; Rao, L.; Vukovic, S.; Kang, S. O.; Hay, B. P. *Dalton Trans.* **2014**, *43*, 551.

[35] Pan, H.-B.; Liao, W.; Wai, C. M.; Oyola, Y.; Janke, C. J.; Tian, G.; Rao, L. *Dalton Transactions* **2014**, *43*, 10713.

[36] Science, J. W. G. o. t. A. P. S. a. t. A. A. f. t. A. o. *Nuclear Forensics: Role, State of the Art, and Program Needs*, 2008.

[37] Bernstein, K. J.; Do-Thanh, C.-L.; Penchoff, D. A.; Alan Cramer, S.; Murdock, C. R.; Lu, Z.; Harrison, R. J.; Camden, J. P.; Jenkins, D. M. *Inorganica Chimica Acta* **2014**, *421*, 374.

CHAPTER 1.

SERS STUDY OF PHOSPHINES AND PHOSPHINE OXIDES ON SILVER

Abstract

An investigation of phosphorus binding to silver in aryl phosphines has been carried out with Raman and surface-enhanced Raman spectroscopy (SERS). The phosphines studied include tertiary aryl phosphines and secondary aryl phosphine oxides. The resistance to oxidation of both the tertiary phosphines and secondary phosphine oxides allowed for their examination using solution based colloidal substrates. Secondary phosphines are readily oxidized and SERS can be highly sensitive to impurities. Thus, solution free, silver island films (SIFs) were used for the second portion of experimentation. The results of the work demonstrate phosphorus bonding to silver metal via Lewis acid/base adducts or L-type bonds. An examination of secondary aryl phosphines was attempted to complete this series of experiments; however experimental limitations prevented the completion of sequence.

Rational For Phosphine Surface Experiment

Organic group (R-groups) binding to metals typically occur in either a Lewis acid/base type adduct or in a covalent manner, known respectively as an L-type or X-type bond as proposed by Green et al.[1] Aryl thiols have been used widely to create monolayers on metal surfaces and are known to bind by the loss of a proton to create robust covalent bonds with the metal surface.[2] Phosphorus directly neighbors sulfur on the periodic table and would be expected to have similar chemistry. Yet the bonding motif of aryl phosphines has yet to be explored. Phosphines are widely used in synthetic and catalytic processes which are used extensively in industrial applications.[3,4] Phosphines also find specialized use as highly chiral selective reagents for pharmaceuticals.[5] A better understanding of how phosphines bind to metals would increase the fundamental understanding of phosphine chemistry. An investigation of phosphorus-metal

bonds was started by examining the binding of a select group of tertiary phosphines, secondary aryl phosphines and secondary aryl phosphine oxides, illustrated in Figure 1.1-2, with SERS.

These specific phosphines were chosen for the select ways in which they can bind. Tertiary phosphines are covalent-bond saturated and may only bind via an L-type bond using lone pairs. The secondary phosphines may bind with either lone pairs for an L-type bond or by losing the proton for an X-type bond. The secondary phosphine oxide may bind via an L-type bond only using one of the oxygen's lone pair or by again losing a proton and forming an X-type bond. By investigating the selected phosphines with a surface specific technique such as SERS and utilizing the process of elimination, the binding modes of the phosphines should be easily determined.

Experimental Limitations

Initial experiments were performed with normal Raman and spectra were recorded from crystalline material without issue. The tertiary phosphines used were triphenylphosphine (tpp), triphenylphosphine d-15 (tppd15), tris(4-methylphenyl)-phosphine (t4mpp), and tris(4-fluorophenyl)-phosphine (t4fpp). In order to record SERS spectra the silver colloidal solution method was chosen. To begin with Lee and Meisel's method was used to fabricate the silver colloids; this colloidal synthesis, as most are, was performed in aqueous solution.[6] Phosphines will generally be insoluble in water due to their low affinity for water. To combat this issue the colloids were resuspended in ethanol by centrifuging the aqueous suspension, decanting the aqueous supernatant and resolvating in alcohol. Within a few hours of incubation with the phosphines, the colloidal solution began to clear and no SERS activity was observed. A different colloid synthesis by Leopold and Lendl was also resuspended in alcohol, which crashed out with

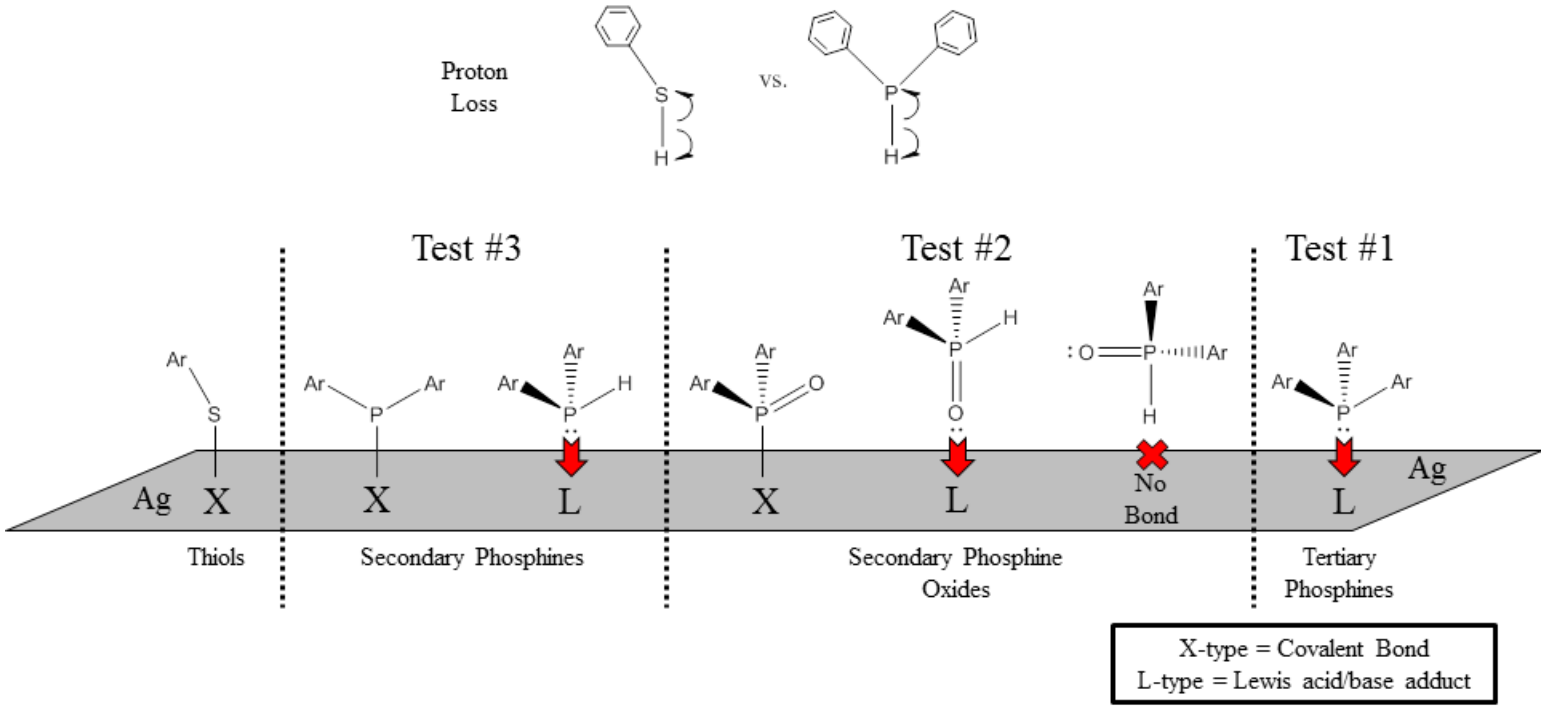

Figure 1.1. A schematic representation of the bonding mode of aryl thiols on a silver surface vs. the potential bonding modes of secondary phosphines, secondary phosphine oxides, and tertiary phosphines.

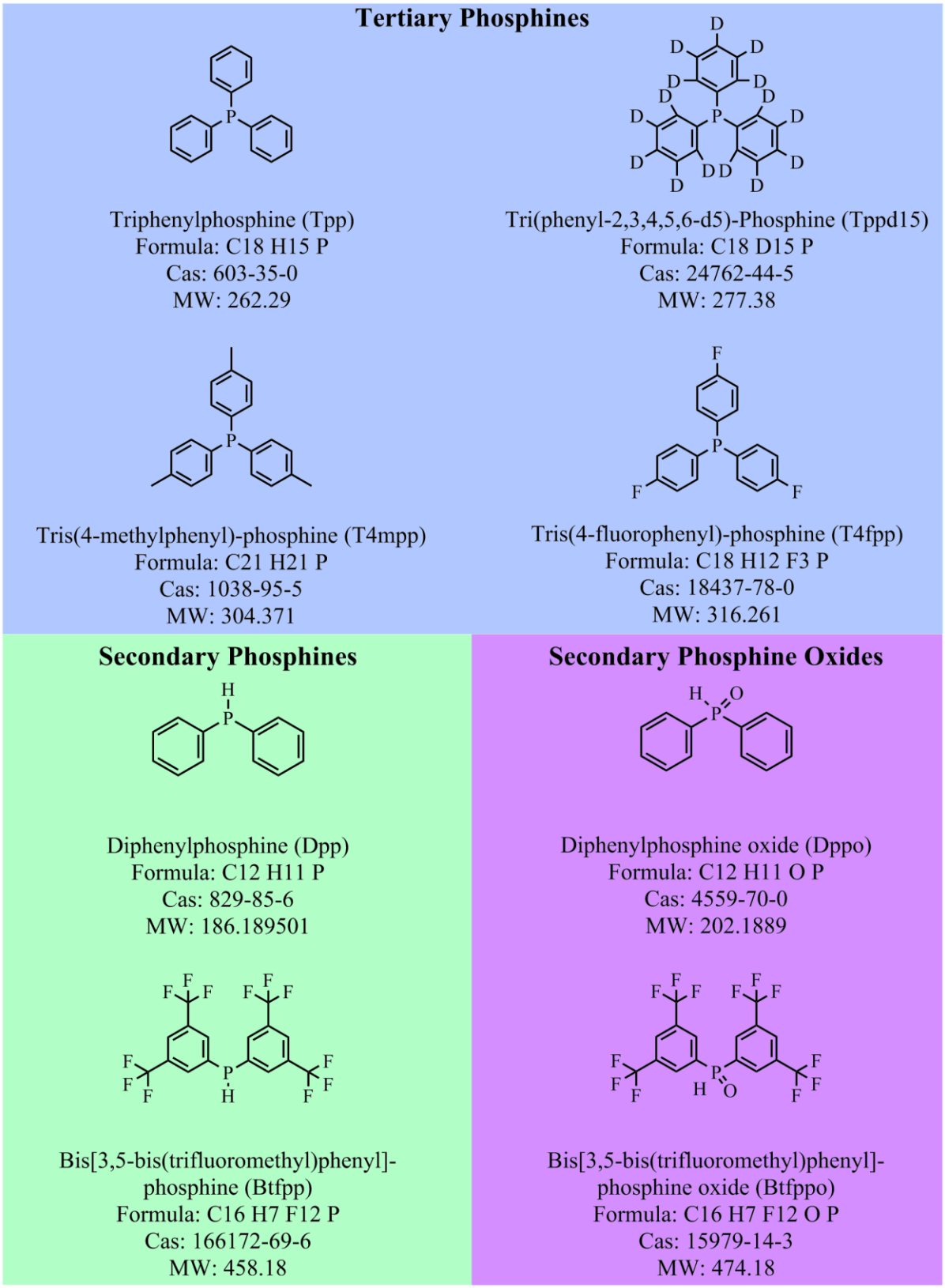

Figure 1.2. Selection of Phosphines for studies.

phosphine concentrations in the millimolar range or less after 12 hours of incubation.[7] Colloid solutions with less than micromolar concentrations of phosphines failed to crash out. This second colloidal fabrication technique yielded particles with a greater size distribution than the synthesis of Lee et al. and it is believed that this greater distribution of sizes is what led to the colloids working.

Results and Discussion

Tertiary Phosphines

The Raman spectrums of tpp, tppd15, t4mpp and t4fpp share several spectral features, displayed in Figure 1.3 with a few differences. The incredibly intense benzene breathing mode is a dominant feature in all four spectra, for tpp this mode is located at 1000 relative cm^{-1}, for tppd15 at 960 rel cm^{-1}, for t4mpp and t4fpp at 1100 rel cm^{-1}. Another very characteristic peak for all the compounds were the C-H stretches from the benzene rings at 3050, 2290, 3050, 3050 rel cm-1 for the four respective compounds. The replacement of hydrogen with deuterium gives Tppd15 C-D stretches in the 2300 rel cm^{-1} range. The unique para groups on T4mpp and T4fpp give rise to additional strong peaks at 800 and 1600 rel cm^{-1}. Of special note on t4mpp, with the methyl groups off the para position of the aromatic rings shows a “trident” like set of peaks at 2870, 2920, 2980 rel cm^{-1} with the central peak being the most intense. Note, the dip at roughly 1970 rel cm^{-1} is an artifact from the experimental procedure and not an aspect of the spectrum.

When comparing the normal Raman spectrum to the SERS spectrum of tpp in Figure 1.4, it must first be noted that the presence of solvent contributions to the SERS spectrum which are denoted with a star or asterisk (*). Other than these additions the two spectra correspond quite closely. The benzene breathing modes, C-H stretches, and several of the other rather intense

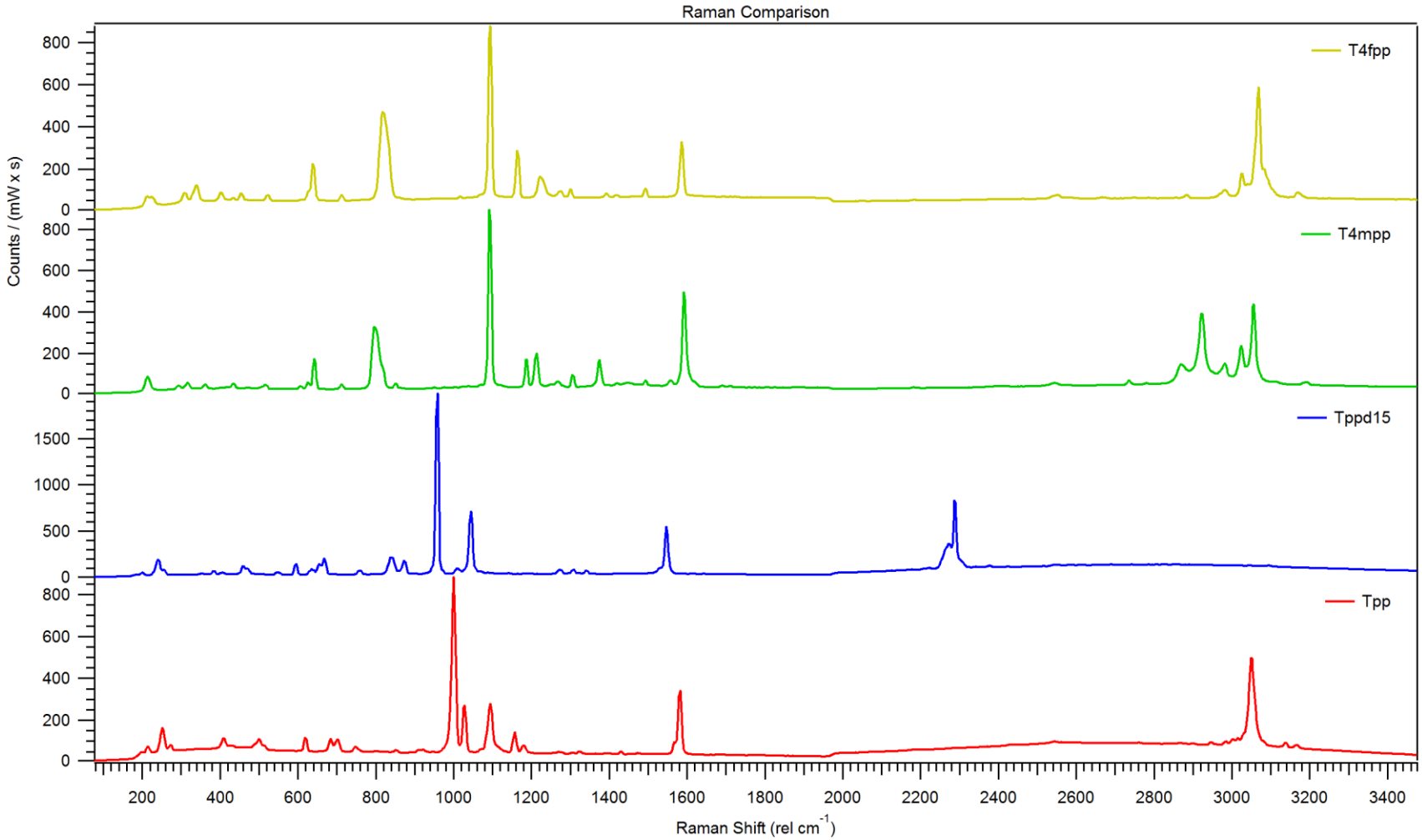

Figure 1.3. The normal Raman spectrums of tpp, tppd15, t4mpp, and t4fpp.

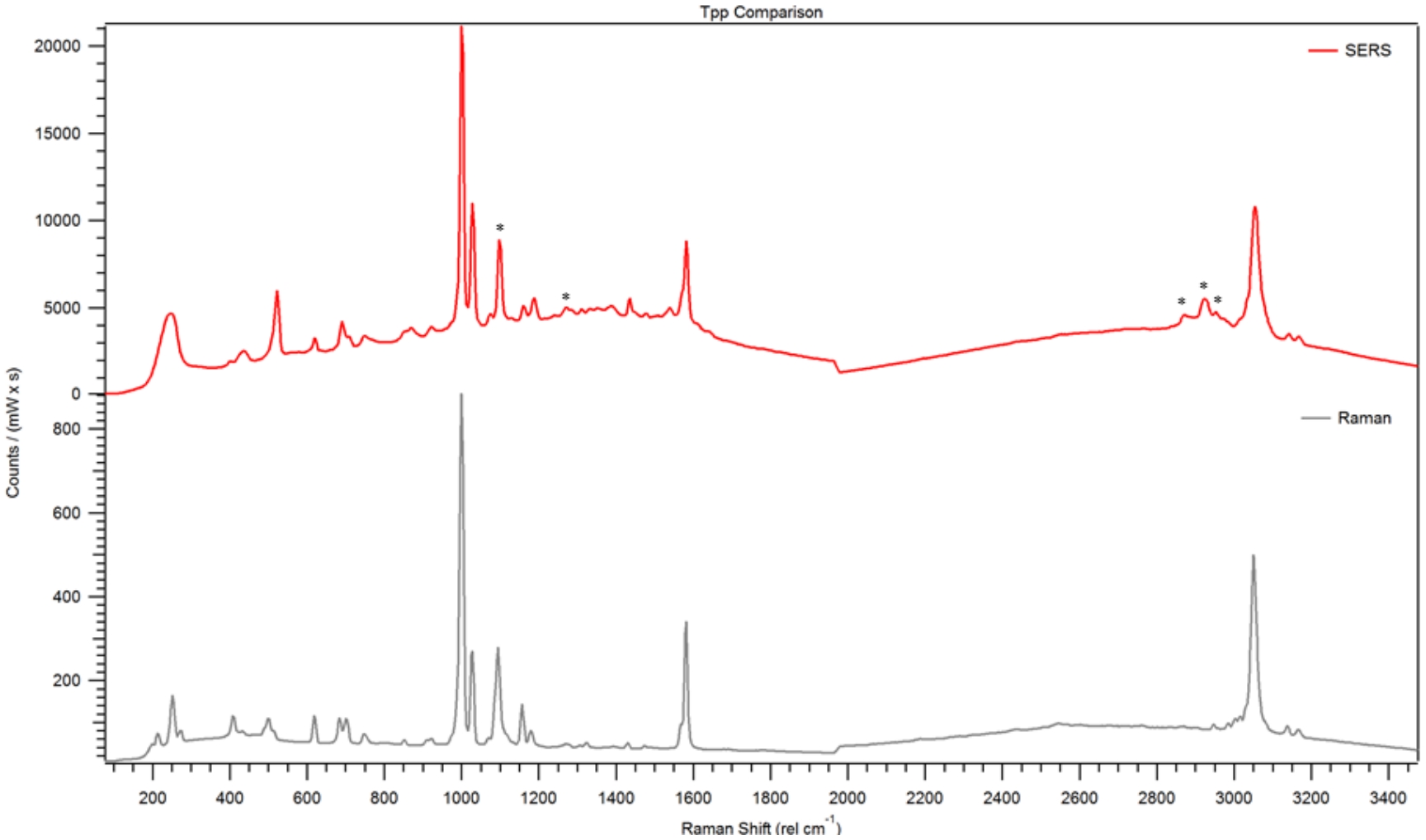

Figure 1.4. SERS spectrum of Tpp (top) and normal Raman spectrum (bottom). Contributions from solvent marked with an asterisk (*).

peaks match up closely confirming that tpp was observed in the SERS spectrum. Furthermore, the normal Raman spectrum was recorded from a crystal over twenty five seconds with 6.45 mW of laser power while the SERS spectrum was taken of a milimolar concentration tpp solution over twenty five seconds at 588 uW of laser power. An order of magnitude less laser power and several orders of magnitude lower concentration while getting more than an order of magnitude more signal demonstrates that an enhancement is occurring and that this is indeed a SERS spectrum.

Examining the comparison plots for tppd15, t4mpp and t4fpp in Figures 1.5-7 the same trends repeat, the benzene breathing modes, C-H stretches and several of the other intense peaks match up nearly exactly. Of special note in t4mpp is the incredibly intense "trident" like set of peaks. This is due to the methyl group on the para position of the benzene rings and the ethanol solvent overlapping, making these peaks much more intense than they otherwise would be.

This phase of experimenting verified that SERS spectra of the four tertiary phosphines had been obtained. Given that SERS spectra have been confirmed for all four tertiary phosphines as shown again in Figure 1.8 and there is not a proton present to be lost, L-type bonding must be the method of binding. This is the first of three test in the series of experiments to be performed with the phosphines.

Secondary Phosphine Oxide

Tests were then run with the secondary phosphine oxide, Bis[3,5-bis(trifluoromethyl)phenyl]-phosphine oxide (Btfppo), in colloids. Unlike the triphenylphosphines, the colloids when incubated with btfppo failed to crash out at the same concentrations and when salts were added to force the crash out no activity from btfppo was

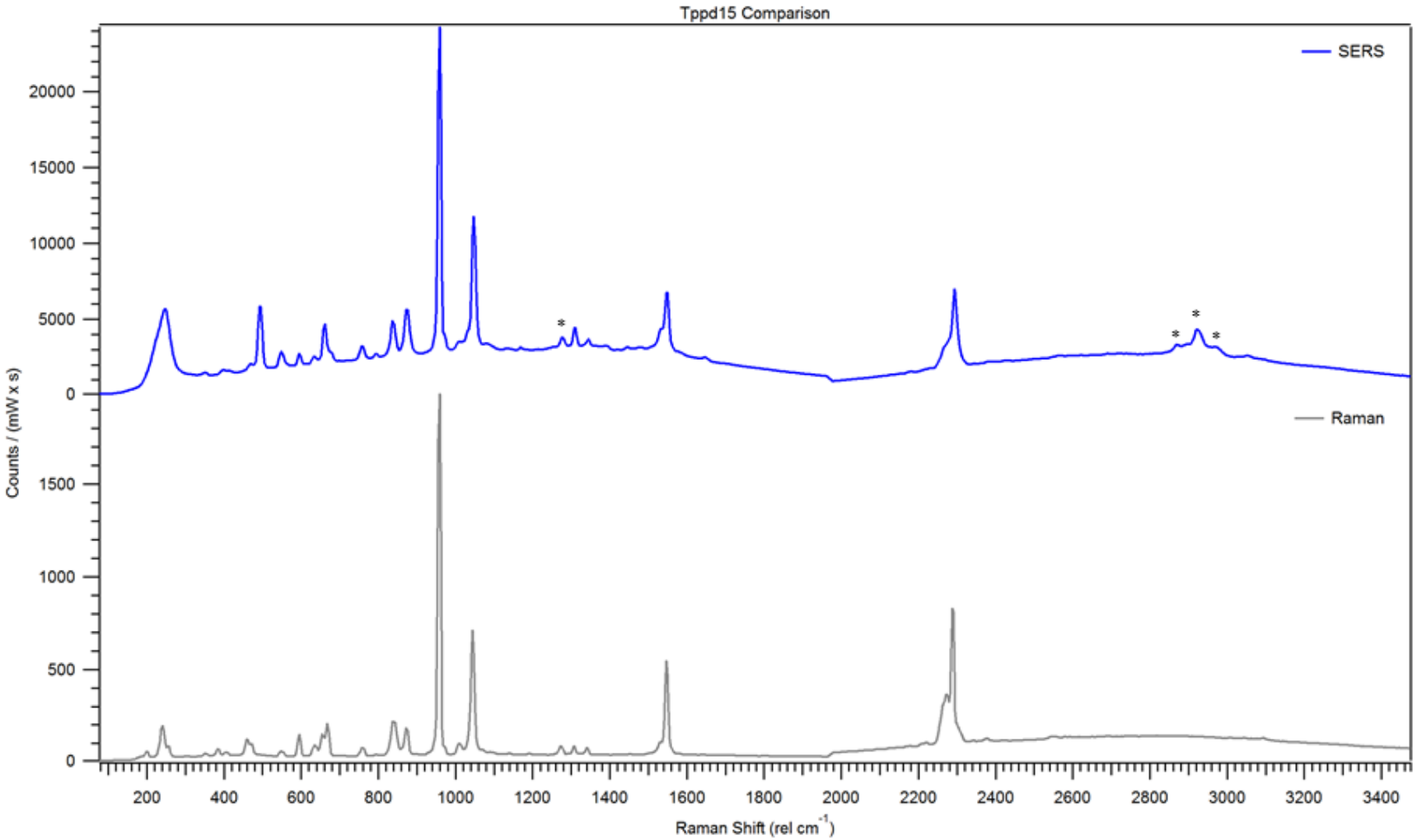

Figure 1.5. SERS spectrum of Tppd15 (top) and normal Raman spectrum (bottom).

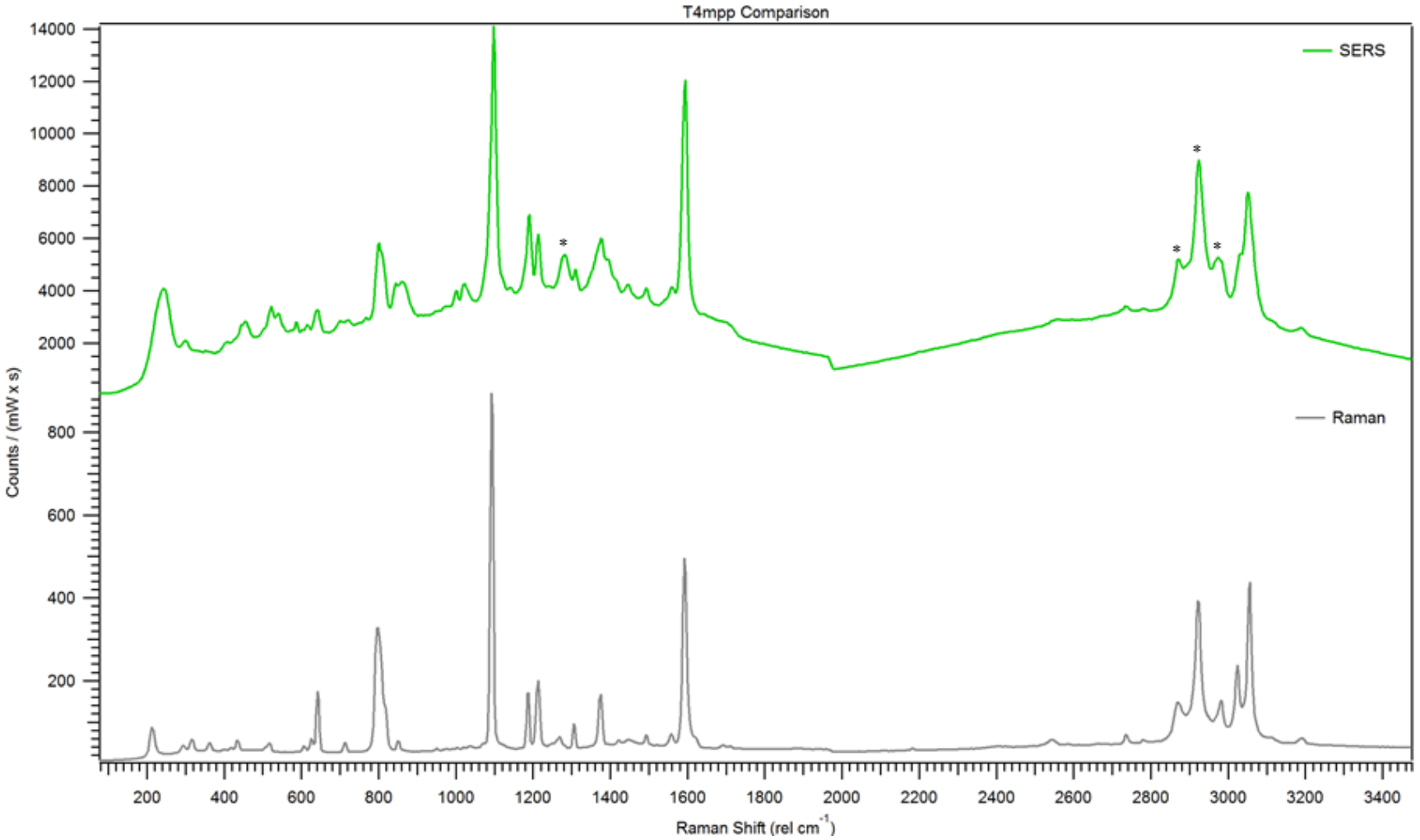

Figure 1.6. SERS spectrum of T4mpp (top) and normal Raman spectrum (bottom).

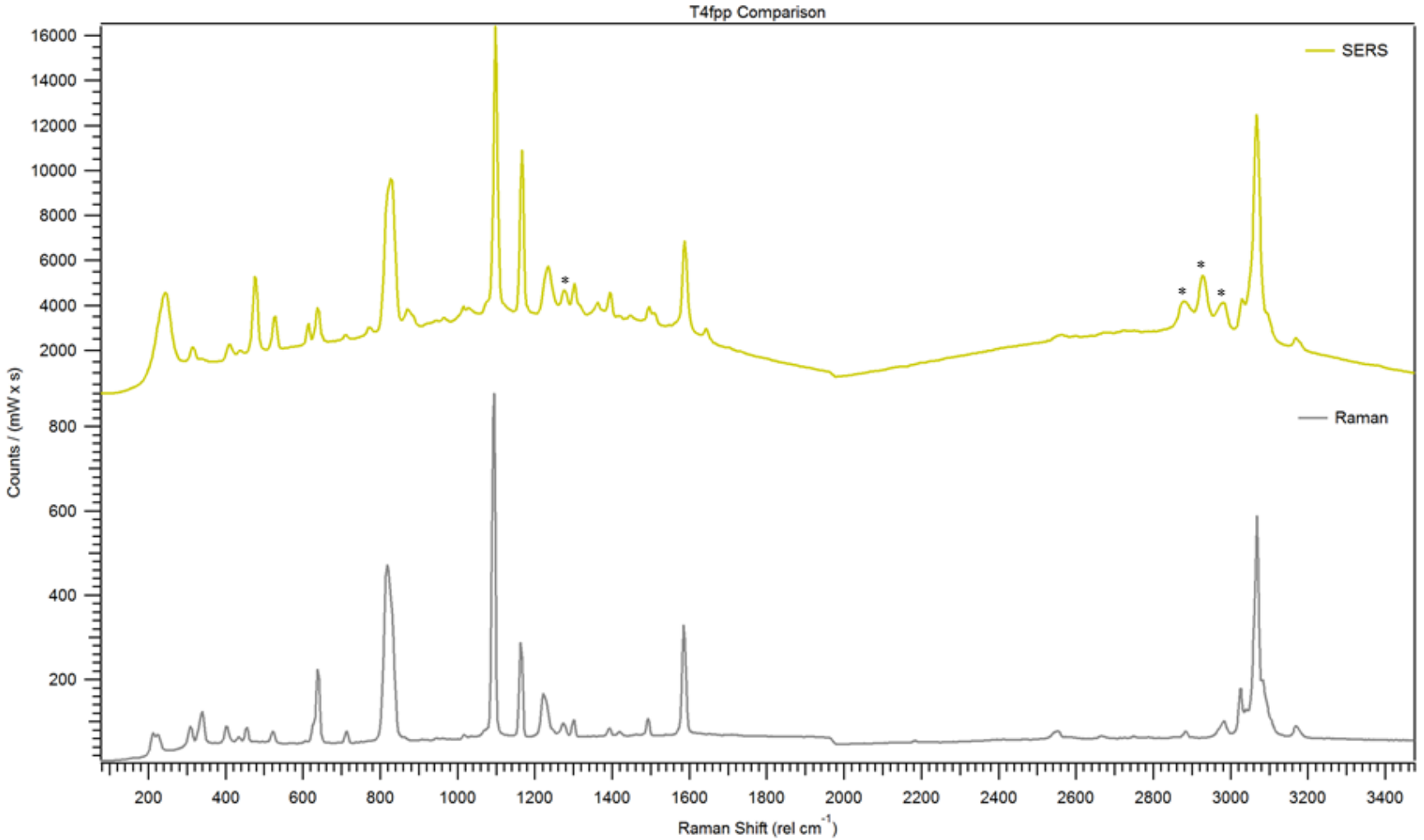

Figure 1.7. SERS spectrum of T4fpp (top) and normal Raman spectrum (bottom).

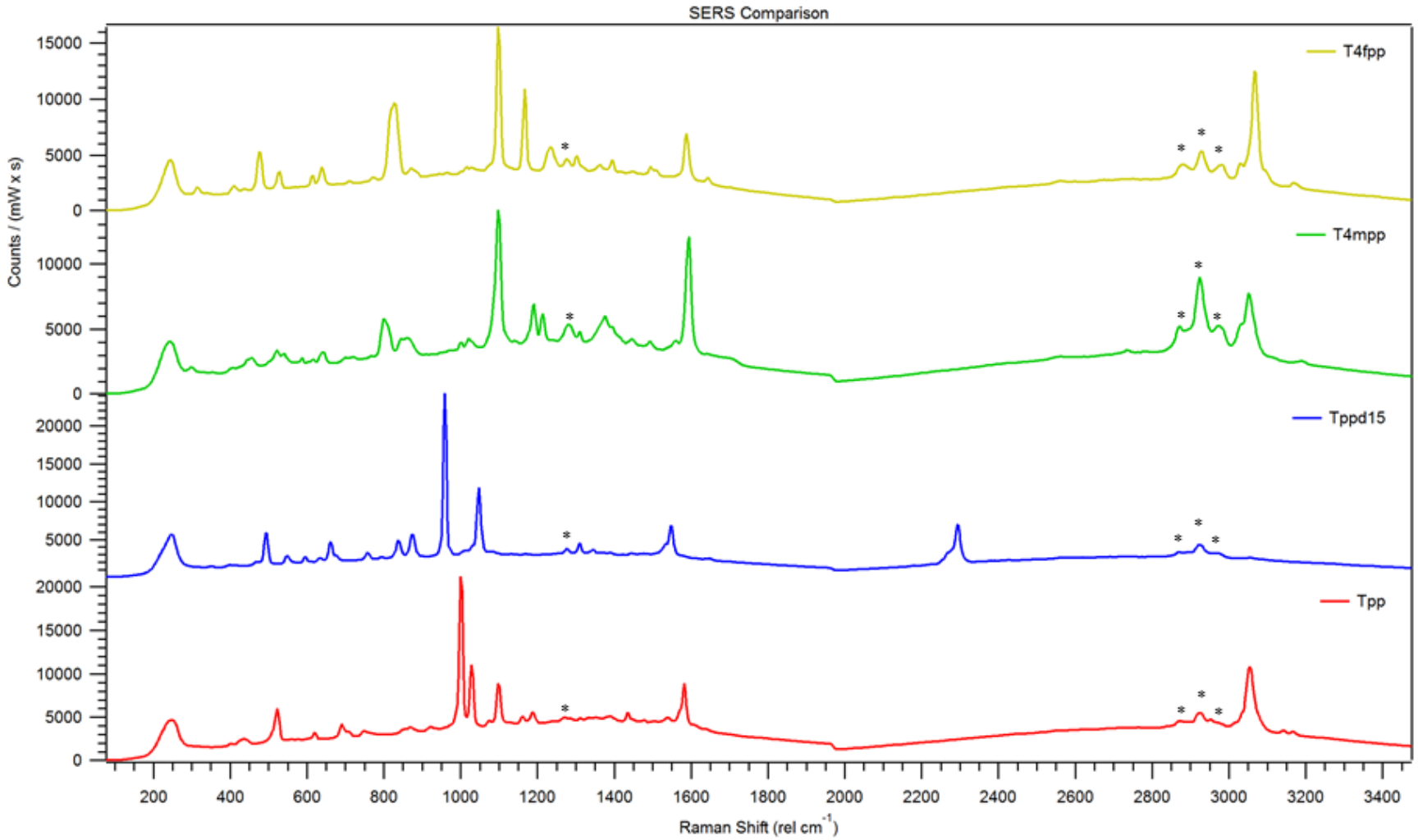

Figure 1.8. SERS spectra of all four tertiary phosphines, Tpp on the bottom and going up, Tppd15, T4mpp and T4fpp at the top. Contributions from solvent marked with an asterisk (*).

observed as shown in Figure 1.9. While several modes are clearly visible in the plot labeled SERS, this is not SERS from the analyte, but from the capping agent and other compounds from the colloids. This is further confirmed by comparing the Raman and SERS spectrum of btfppo to the analogous spectra of the tertiary phosphines in Figures 1.10 and 1.11. The benzene breathing mode is not present, the C-H stretch is at the wrong frequency, and the modes at 700, 1600, and 2400 rel cm^{-1} are completely absent. In addition, the peaks in the 800-1400 rel cm^{-1} range do not match up. Thus there does not appear to be SERS activity from the analyte. The absence of bound btfppo, a secondary phosphine oxide, indicates that an X-type covalent binding method with the loss of a proton is not possible nor is the L-type binding through the attached oxygen. The only option left is an L-type bond through the absent phosphine lone pair; thus binding does not occur, giving a conclusion to the second of three tests in the series.

Films For Oxygen Free Environment

Secondary Phosphines

The secondary phosphines, diphenylphosphine (dpp) and Bis[3,5-bis(trifluoromethyl)phenyl]-phosphine (Btfpp), can be oxidized by atmospheric oxygen, thus all initial Raman measurements were made in sealed containers under inert atmosphere. In order to prevent selective enhancement from causing even the smallest amount of oxygen impurity to show up as an overwhelming majority, an alternative substrate to colloidal suspensions were required. A suitable alternative of silver island films (SIFs) were chosen.[8] Unlike aqueous solution suspended colloids, the thin films were a solid metal substrate that could be pumped under a vacuum or put under inert atmosphere without harm. The films were first tested with the

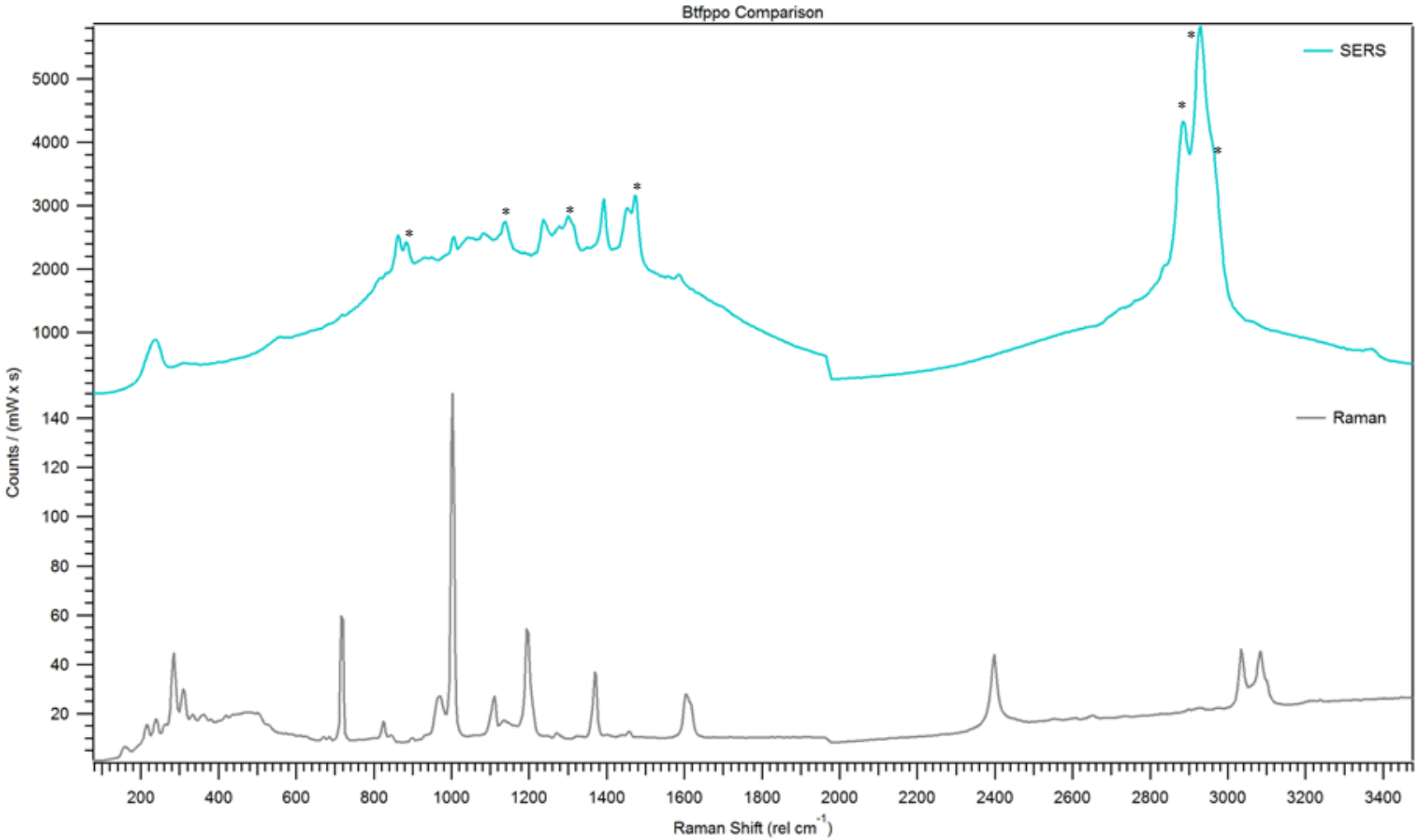

Figure 1.9. The attempted SERS spectrum of Btfppo (top) and normal Raman spectrum (bottom).

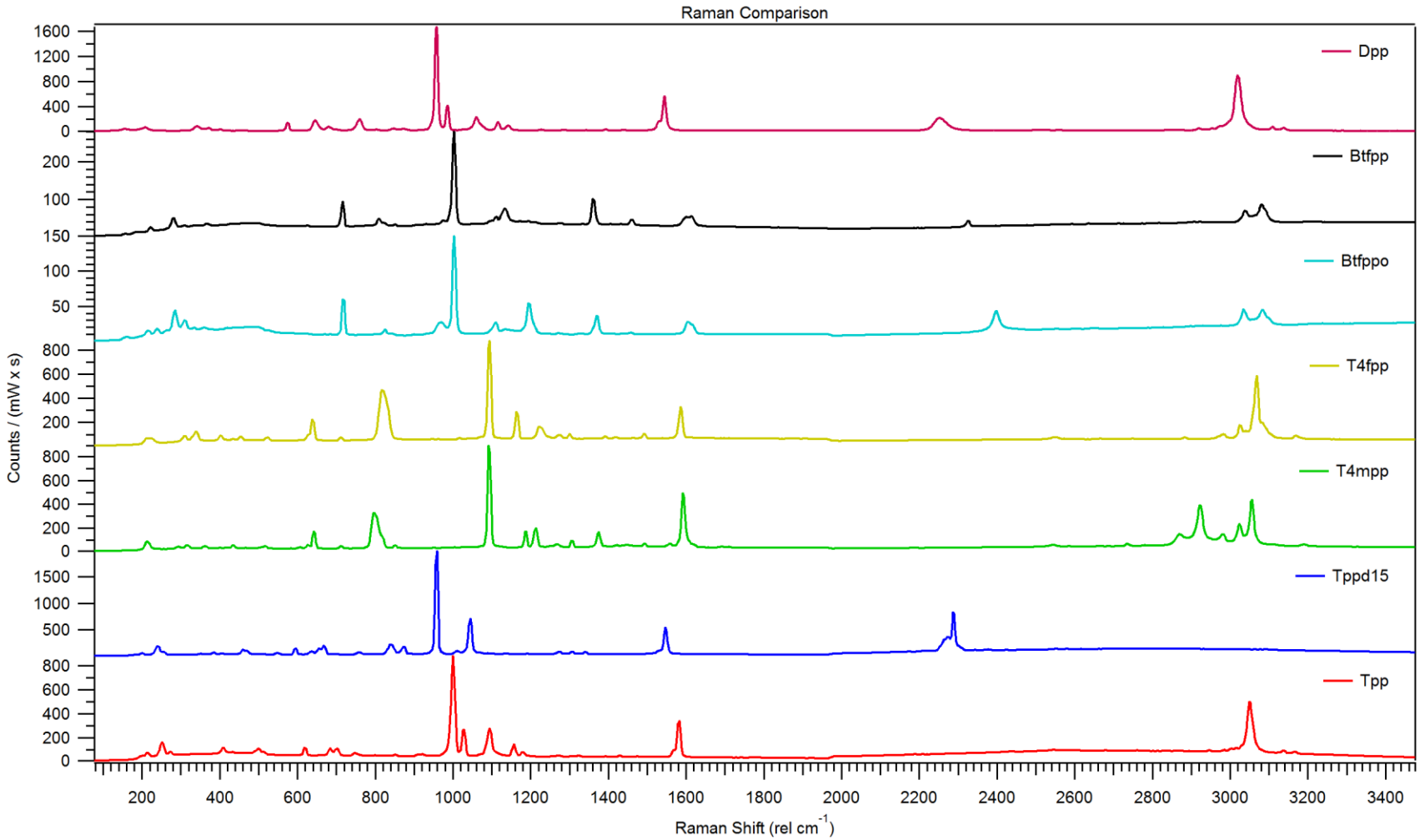

Figure 1.10. The normal Raman spectrums of Dpp, Btfpp, and Btfppo compared with the four tertiary phosphines: (from top to bottom) T4fpp, T4mpp, Tppd15 and Tpp.

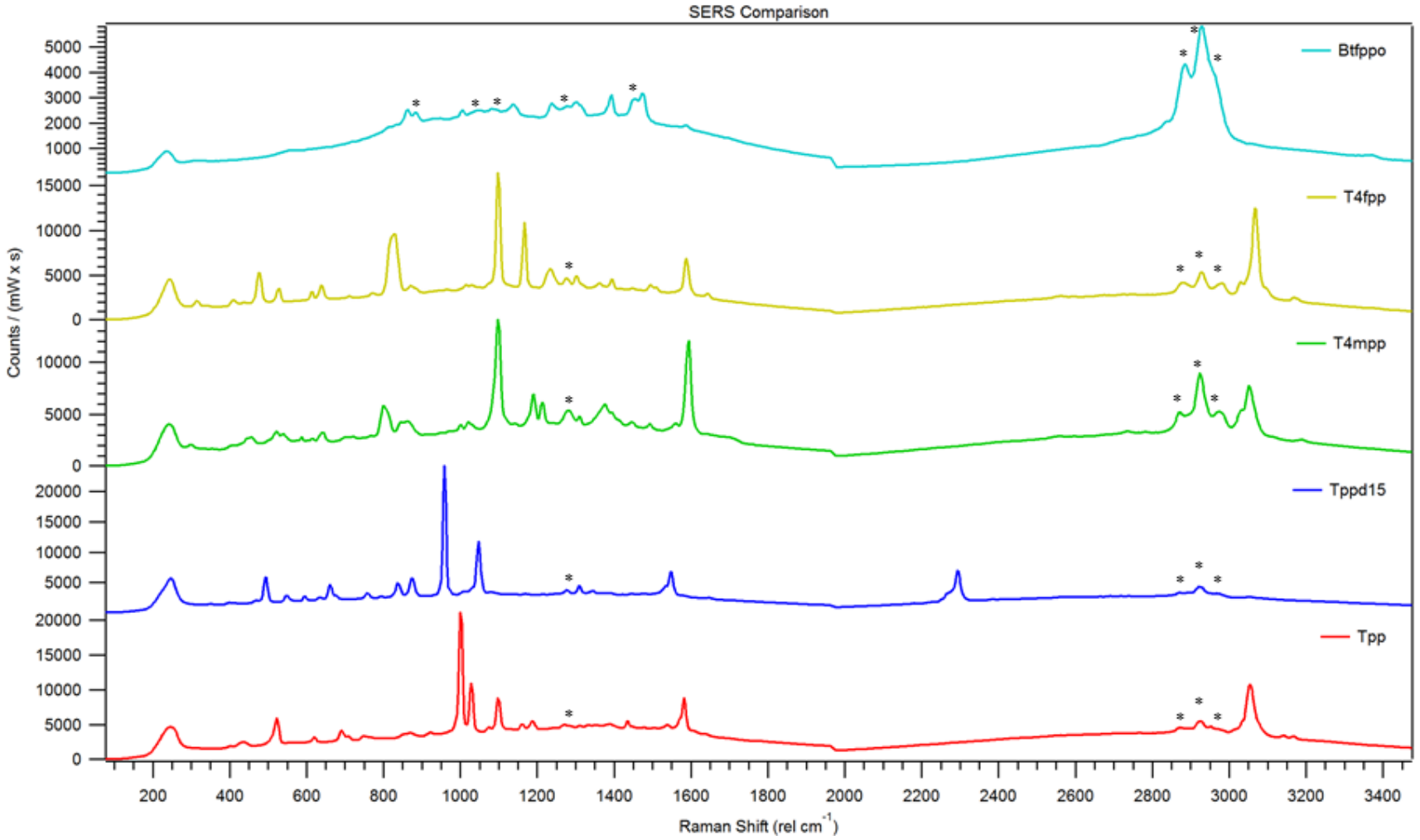

Figure 1.11. The SERS acquisition of Btfppo compared to the SERS spectra of (top to bottom) T4fpp, T4mpp, Tppd15, and Tpp.

tertiary phosphines to establish experimental parameters. It was found that the phosphines completely strip the silver from the glass substrate even at very low concentrations. Several different exposures were tested but all resulted in the stripping of the film. Thus the SIFs would not work and the final experiment in the series of three could not be completed.

Until a method to test the secondary phosphines in an oxygen free atmosphere can be utilized, this series of experiments will ultimately be inconclusive. The experiments that were completed indicate that phosphines bind in an L-type method exclusively (see Figure 1.12). This was the type of binding that was observed with the tertiary phosphines and the method unavailable to the secondary phosphine oxide.

Further Work

Just as the challenges with the initial work on silver colloids fabricated with the synthetic method of Lee et al. were overcome using an alternate synthetic route by Lepoldt et al. so too the issues associated with SIFs might be overcome using a differing method of analysis. Another form of film called film over nanosphere or FONs is likely to overcome the difficulties associated with phosphine stripping of the silver. FONs typically have a much thicker layer of the critical metal, with typical layers of 200 nm as opposed to the 6-8 nm layer in SIFs, deposited over a monolayer of beads. This much thicker layer of metal is far less likely to be completely stripped by the phosphine, increasing the likelihood of successful phosphine deposition on the critical plasmonic metal surface. This change would remove the obstacle to experimentation that halted the current work and likely allow for the completion of the study.

Conclusion

An investigation into the binding mode of aryl phosphines has been conducted utilizing tertiary phosphines and secondary phosphine oxides. The tertiary phosphines were found to bind readily in an L-type binding motif. The secondary phosphine oxide was found to not bind, demonstrating that the phosphine would not lose a proton analogous to thiols; demonstrating that without a lone pair of electrons on the phosphorus for L-type binding, no bond would occur. Ultimately, this work is incomplete until secondary phosphines can be studied to confirm L-type binding and the presence of the proton retained on the phosphorous atom.

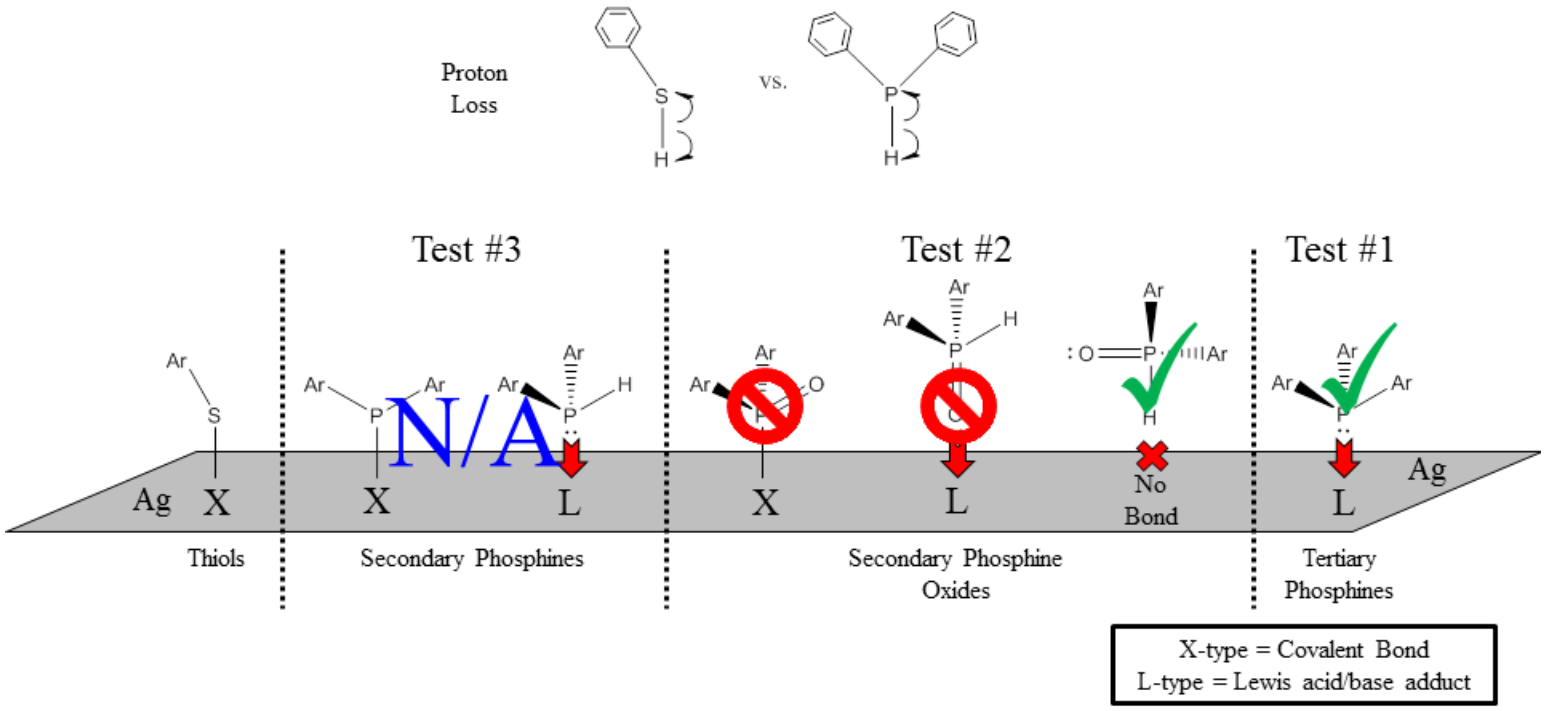

Figure 1.12. A schematic representation of the outcome of bonding mode of aryl thiols on a silver surface vs. the potential bonding modes of secondary phosphines, secondary phosphine oxides, and tertiary phosphines. Test #1 demonstrated an L-type binding motif while Test #2 proved the phosphine would not bind in an X-type motif losing a proton or an L-type motif through the oxygen present. Test #3 could not be performed due to experimental difficulties.

Experimental

Instrumentation

Excitation was provided by a frequency doubled ND:YAG laser (Princeston Instruments) with a laser line of 532 nm and a power of 0.5 mW at the objective. An inverted microscope (Ti-U, Nikon Eclipse) with a 10x, 0.30 NA dry objective (Nikon) in the 180° configuration was used in conjunction with Rayleigh filter and dichroic (Semrock) to collect the Raman scattering. Spectra were recorded with a 300 cm focal length spectrometer (Acton, Princeton Instruments) containing a 1200 groove mm^{-1} holographic grating, and a 10 μm slit with an attached liquid-nitrogen-cooled deep-depletion charge-coupled device (CCD, Spec10, Princeton Instruments). Spectra were calibrated with cyclohexane.

Materials

Tertiary phosphines and Diphenylphosphine were purchased from Sigma-Aldrich and purified via sublimation to extremely high purity and confirmed by NMR and MS analysis. Solvents were obtained at the highest level of purity possible.

Synthesis of bis[3,5-bis(trifluoromethyl)phenyl]phosphine oxide

Under a N2 atmosphere, a solution of diethylphosphite (0.65 g, 4.7 mmol) in THF (10 mL) was added dropwise to (3,5-bis(trifluoromethyl)phenyl)magnesium bromide (0.5 M solution, 34 mL, 1.7 mmol) in 20 mL of THF. The mixture was heated to 50 °C and stirred for 1 hr. After the hour elapsed, the mixture was cooled to room temperature and hydrolyzed with a saturated ammonium chloride solution (20 mL). The aqueous layer was separated and the product was extracted from the aqueous layer with methylene chloride (3 X 20 mL), which was

subsequently dried with magnesium sulfate. The resulting methylene chloride portion was run over a silica plug then was dried under reduced pressure leaving a light brown solid. To get rid of further impurities, the product was washed with petroleum ether (4 X 4 mL) and dried under reduced pressure leaving the pure, light brown product (0.34 g, 15.5%). 1H NMR (CDCl3, 300.1 MHz): δ8.31 (d, *JPH* = 504 Hz, 1H), 8.20 (d, *JPH* = 13.5 Hz, 4H), 8.16 (s, 2H). 19F NMR (CDCl3, 282.3MHz): δ -63.0. DART/MS (*m*/*z*): [M+H]+ 475.1.

References for Chapter 1

[1] Green, M. L. H. *Journal of Organometallic Chemistry* **1995**, *500*, 127.

[2] Daniel, M. C.; Astruc, D. *Chemical Reviews* **2004**, *104*, 293.

[3] Zhu, H. J.; Ding, Y. J.; Yan, L.; Xiong, J. M.; Lu, Y.; Lin, L. W. *Catalysis Today* **2004**, *93-5*, 389.

[4] Blaser, H. U.; Malan, C.; Pugin, B.; Spindler, F.; Steiner, H.; Studer, M. *Advanced Synthesis & Catalysis* **2003**, *345*, 103.

[5] Crepy, K. V. L.; Imamoto, T. *Advanced Synthesis & Catalysis* **2003**, *345*, 79.

[6] Lee, P. C.; Meisel, D. *J. Phys. Chem.* **1982**, *86*, 3391.

[7] Leopold, N.; Lendl, B. *Journal of Physical Chemistry B* **2003**, *107*, 5723.

[8] Schlegel, V. L.; Cotton, T. M. *Analytical Chemistry* **1991**, *63*, 241.

CHAPTER 2.

THE SYNTHESIS AND SPECTROSCOPIC CHARACTERIZATION OF AN AROMATIC URANIUM AMIDOXIME COMPLEX

A version of this chapter was originally published by Karl J Bernstein, Chi-Linh Do-Thanh, Deborah A. Penchoff, S. Alan Cramer, Christopher R. Murdock, Zheng Lu, Robert J. Harrison, Jon P. Camden and David M. Jenkins:

Bernstein, K. J., Do-Thanh, C., Penchoff, D. A., Cramer, S. A., Murdock, C. R., Lu, Z., Harrison, R. J., Camden, J. P., and Jenkins, D. M. **THE SYNTHESIS AND SPECTROSCOPIC CHARACTERIZATION OF AN AROMATIC URANIUM AMIDOXIME COMPLEX.** *Inorganica Chimica Acta* (2014), 421, 374-379.

The article is represented in the published form, with the exception that the following Inorganica Chimica Acta sections have been removed: Article history, Keywords, acknowledgements. The Supporting Information section of the manuscript has been added as an appendix. The dissertation author was primarily responsible for the complexation, vibrational spectroscopy, and shared responsibility for the DFT calculations with D. A. Penchoff. The 1,8-naphthalimide dioxime, **3**, (Np-CAO-H3) molecule was synthesized by C. Do-Thanh, Mass spectroscopy and 2D NMR were led by S. A. Cramer, solid state NMR were led by C. R. Murdock, single crystal X-ray analysis and structure deconvolution was performed by Z. Lu, these four individuals were under the guidance of D. M. Jenkins. DFT calculations and analysis were performed by D. A. Penchoff under the guidance of R. J. Harrison. All authors participated in the discussion of results and approved the final manuscript.

Abstract

A tridentate aromatic amidoxime ligand and its corresponding uranyl complex have been synthesized. The complex was rigorously characterized with single-crystal X-ray diffraction, solid-state NMR, infrared absorption, and Raman spectroscopy. Unlike previous amidoxime complexes, the crystal structure confirms the complexation of only a single tridentate amidoxime

ligand to the uranium, and solid state NMR confirms uranyl binding in the bulk sample. The Raman spectrum of the complex is dominated by the strong U═O vibration which exhibits a significant shift from the U═O vibration in unbound uranyl. Density functional theory (DFT) aided in calculations of vibrational modes as well as providing insight into the electronic structure of this uranyl complex.

Published Work

Introduction

Aqueous uranyl chemistry is experiencing a renaissance due to two distinct, but related, applications: extraction of uranium from seawater and nuclear forensics.[1-4] Due to the very low concentration of uranium for each application, sorption methods are considered the only viable option as a result of financial and environmental considerations.[5,6] The oceans contain the uranyl ion at an uniform concentration of 3.3 ppb (ppb);[7,8] this ubiquity of uranium in nature and its destructive potential as a weapon underpin the necessity of nuclear forensics. This field is concerned with who has harnessed uranium's deadly capabilities and it has typically relied heavily on lab-based mass spectrometry for analysis.[2,9] Uranyl extraction from seawater and spectroscopic detection for nuclear forensics could benefit from the development of highly selective uranyl binding ligands. Several complexing agents for sorptive methods of uranyl extraction have been investigated, and evaluated based on selectivity, robustness, loading capacity, and rate of uptake.[5,10–13] After extensive methodology evaluation, amidoxime functionalized polymers were selected as optimal.[5] Further investigation of the uranyl complexing polymers revealed the presence of cyclic, polydentate amidoximes alongside the normal amidoximes.[10] Recent advances in understanding the binding of polydentate amidoximes

to uranyl by Hay[14] and Rao[15–17] provided insight into the structural motifs that are possible when employing these ambidentate ligands. While simple amidoximes have been well characterized by a variety of spectroscopic techniques, their cyclic counterparts have received far less attention.[18] To our knowledge, detailed spectroscopic measurements, such as NMR, IR, and Raman, have not been collected on any of the cyclic amidoxime uranyl complexes. Vibrational spectroscopy is of particular interest since these initial measurements would be necessary to determine if these systems could be viable in the field of nuclear forensics. In this manuscript, we describe the synthesis of a tridentate amidoxime ligand that complexes with uranyl in a 1:1 fashion. The uranyl complex was structurally characterized by single crystal X-ray diffraction. In addition to the structural characterization, additional solid state spectroscopic methods such as NMR, IR, and Raman were employed. The Raman spectroscopy suggests that conjugated ligands like this one could lead to novel detection methods for actinides.

Experimental

Materials

The compound acenaphtho[1,2-c][1,2,5]thiadiazole 8,8-dioxide (1) was prepared via a modification of the published procedure of Qian [19]. Compound **1** was also prepared by Wright.[20] 1,8-dicyanonaphthalene (**2**) was synthesized in a manner similar to Ege's pyrolysis approach (Ege provided no characterization of the product except melting point).[21] 1,8-naphthalimide dioxime (**3**) was prepared via adaptation of the published procedures of Forrester.[22] Our detailed synthetic procedures and analytical data are described below. All other reagents were purchased from commercial vendors and used without further purifications.

Methods and instrumentation

^{1}H and $^{13}C\{^{1}H\}$ solution spectra were recorded at ambient temperature on a Varian VNMRS 500 MHz narrow-bore system. ^{1}H, $^{13}C\{^{1}H\}$, HSQC, and HMBC NMR chemical shifts were referenced to the residual solvent. Solid ^{13}C CP MAS NMR samples were recorded on a Varian Inova 400 MHz spectrometer and referenced to an external adamantane sample. ^{13}C CP MAS with interrupted decoupling (to suppress protonated carbons) was applied using a spin rate of 6 kHz with the dipolar dephasing turned on for 100 μs. All mass spectrometry analyses were conducted at the Mass Spectrometry Center located in the Department of Chemistry at the University of Tennessee. The DART analyses were performed using a JEOL AccuTOF-D time-of flight (TOF) mass spectrometer with a DART (direct analysis in real time) ionization source from JEOL USA, Inc. (Peabody, MA). The ESI/MS analyses were performed using a QSTAR Elite quadrupole time-of-flight (QTOF) mass spectrometer with an electrospray ionization source from AB Sciex (Concord, Ontario, Canada). Sample solutions of complexes for mass spectrometry were prepared in acetonitrile, tetrahydrofuran, or DMSO (for uranium complex, **4**, only). Carbon, hydrogen, and nitrogen analyses were obtained from Atlantic Microlab, Norcross, GA.

X-ray structure determination

Data was collected on a Bruker SMART APEX II three circle diffractometer equipped with a CCD area detector and operated at 1800W power (45 kV, 40 mA) to generate Mo Kα radiation (λ = 0.71073 Å). The incident X-ray beam was focused and monochromated using Bruker Excalibur focusing optics. Single crystals were mounted on nylon CryoLoops (Hampton Research) with Paratone-N (Hampton Research) and frozen at -173 °C. Initial scans of each

specimen were taken to obtain preliminary unit cell parameters and to assess the mosaicity (i.e. breadth of spots between frames) of the crystal to select the required frame width for data collection. For all cases frame widths of 0.5° were judged to be appropriate and full hemispheres of data were collected using the BRUKER APEX2 software suite to carry out overlapping φ and ω scans at detector setting of $2\theta = 28°$. Following data collection, reflections were sampled from all regions of the Ewald sphere to re-determine unit cell parameters for data integration. Following exhaustive review of collected frames the resolution of the dataset was judged, and, if necessary, regions of the frames where no coherent scattering was observed were removed from consideration for data integration using the BRUKER SAINTPLUS program.[23] Data was integrated using a narrow frame algorithm and was subsequently corrected for absorption. Absorption corrections were performed for both samples using the SADABS program.[23] Space group determination and tests for merohedral twinning were carried out using XPREP.[23] In all cases, the highest possible space group was chosen. Final models were refined anisotropically (with the exception of H atoms). The *Addsym* subroutine of PLATON[24] was utilized to assure that no additional symmetry could be applied to the models.

Vibrational spectroscopy

Excitation was provided by a HeNe laser (HNL100L, Thorlabs) with a laser line of 632.8 nm and a power of 0.6 mW at the objective. An inverted microscope (Ti-U, Nikon Eclipse) with a 10x, 0.30 NA dry objective (Nikon) in the 180° configuration was used in conjunction with Rayleigh filter and dichroic (Semrock) to collect the Raman scattering. Spectra were recorded with a 300 cm focal length spectrometer (Acton, Princeton Instruments) containing a 1200 groove mm^{-1} holographic grating, and a 10 μm slit with an attached liquid-nitrogen-cooled deep-depletion charge-coupled device (CCD, Spec10, Princeton Instruments). Spectra were calibrated

with cyclohexane. Infrared spectra were collected on a Thermo Scientific Nicolet iS10 with a Smart iTR accessory for attenuated total reflectance. Raman and IR spectra were both obtained from the crystalline solid.

Computational methodology

Geometry optimizations and vibrational frequencies were obtained with the NWCHEM[25] package using density functional theory (DFT), and the B3LYP functional.[26–28] The Stuttgart RSC 1997 effective core potential and its corresponding basis set was used for uranium[29] (with the most diffuse S, P, D, and F functions removed, i.e., those with exponent 0.005, since they pertain only to the neutral metal atom and cause numerical problems in molecules), and the 6-311++g** basis set was used for oxygen, nitrogen, carbon, and hydrogen atoms.[30] The ECP accounts for relativistic effects and replaces 60 electrons of uranium with a pseudopotential. Basis sets were obtained from the EMSL database.[31,32] This computational protocol has been established as producing reliable geometries and energetics for uranyl complexes.[33] Geometry optimizations were performed with tight convergence settings. Frequency calculations were performed to obtain thermochemical corrections, and to verify that the structures reflect local minima. Volumetric data was generated with NWCHEM, modeled with Visual Molecular Dynamics (VMD)[34] and plotted with Persistence of Vision Raytracer (Pov-Ray).[35]

Synthesis of acenaphtho[1,2-c][1,2,5]thiadiazole 8,8-dioxide, 1

Sulfamide (15.8 g, 161 mmol) and *p*-toluenesulfonic acid monohydrate (1.36 g, 7.14 mmol) were added to acenaphthenequinone (10.0 g, 53.8 mmol) in absolute ethanol (400 mL), and the mixture was heated at 80 °C for 3 days. After cooling to room temperature, the solvent was removed by rotary evaporation. The residue was then extracted with methylene chloride (2 x

350 mL) from water (350 mL), and a light brown precipitate formed above the organic layer. The precipitate was collected, and the combined organic layers were dried with magnesium sulfate, filtered, and concentrated. The concentrate was combined with the precipitate and recrystallized from boiling pyridine (200 mL) to give the product as a light brown powder (7.35 g, 56.4% yield).

^{1}H NMR (DMSO-d_6, 499.74 MHz): δ 8.49 (d, J = 7.8 Hz, 2H), 8.45 (d, J = 7.8 Hz, 2H), 8.01 (t, J = 7.7 Hz, 2H). ^{13}C NMR (DMSO-d_6, 125.67 MHz): δ 166.24, 148.57, 133.26, 130.77, 129.71, 126.80, 123.13. IR (neat): 1630, 1581, 1485, 1415, 1355, 1170, 1091, 1070, 1038, 986, 942, 920, 831, 776, 738, 694, 663 cm^{-1}. HRDART/ MS (*m/z*): $[M+H]^+$ 243.0219 (found); $C_{12}H_7N_2O_2S$ 243.0228 (calcd).

Synthesis of 1,8-dicyanonaphthalene, 2

Acenaphtho[1,2-c][1,2,5]thiadiazole 8,8-dioxide (1) (2.04 g, 8.41 mmol) was pyrolyzed under vacuum (150 mTorr) at 180 °C in a water-cooled sublimation apparatus overnight. The resulting solids were collected and resublimed under vacuum (150 mTorr) at 180 °C overnight to give the product as a pure yellow solid (1.36 g, 90.6% yield).

^{1}H NMR ($CDCl_3$, 499.74 MHz): δ 8.18 (d, J = 8.4 Hz, 2H), 8.13 (d, J = 8.4 Hz, 2H), 7.68 (t, J = 7.6 Hz, 2H). ^{13}C NMR ($CDCl_3$, 125.67 MHz): δ 138.00, 134.68, 133.55, 128.99, 126.84, 116.81, 109.05. IR (neat): 3061, 2227, 2215, 1586, 1571, 1512, 1372, 1360, 1230, 1218, 1174, 1111, 1092, 990, 970, 943, 828, 779, 761, 694, 666 cm^{-1}. HR-DART/MS (m/z): $[M+H]^+$ 179.0605 (found); $C_{12}H_7N_2$ 179.0609 (calcd).

Synthesis of 1,8-naphthalimide dioxime, 3, (Np-CAO-H3)

Hydroxylamine hydrochloride (0.982 g, 14.1 mmol) and potassium hydroxide (0.793 g, 14.1 mmol) were added to 1,8-dicyanonaphthalene (0.504 g, 2.83 mmol) in water (18 mL) and ethanol (6 mL). The reaction mixture was stirred at 80 °C overnight and then cooled to room temperature, filtered, and washed with cold ethanol. The solid residue was recrystallized from boiling absolute ethanol (50 mL) and dried under vacuum for 1 h to give the product as yellow needles (0.351 g, 54.6% yield). The product was stored under nitrogen to prevent oxidation that occurs over a 4 d period to form the dark red-brown 1,8-naphthalimide.

^{1}H NMR (DMSO-d_6, 499.74 MHz): δ 11.05 (s, 2H), 8.96 (s, 1H), 8.14 (d, J = 7.0 Hz, 2H), 8.06 (d, J = 7.9 Hz, 2H), 7.63 (t, J = 7.6 Hz, 2H). ^{13}C NMR (DMSO-d_6, 125.67 MHz): δ 141.02, 132.40, 129.42, 126.40, 125.66, 121.90, 120.59. ^{13}C SSNMR (Adamantane standard, 100.53 MHz): δ 144.65, 130.84, 127.05, 125.19, 120.97. ^{13}C SSNMR (interrupted decoupling, Adamantane standard, 100.53 MHz): δ 144.82, 131.16, 125.33, 120.95. IR (neat): 3407, 3384, 3058, 2813, 1642, 1606, 1469, 1433, 1387, 1332, 1217, 1165, 1085, 1003, 957, 898, 872, 827, 794, 764, 719, 685, 667, 641, 610 cm^{-1}. HR-DART/ MS (m/z): $[M+H]^+$ 228.0773 (found); $C_{12}H_{10}N_3O_2$ 228.0773 (calcd).

Synthesis of (Np-CAO-H_2)U(O)$_2$(NO_3)(CH_3OH), 4

A solution of 1,8-naphthalimide dioxime (0.0386 g, 0.170 mmol) in methanol (19 mL) was added to a solution of uranyl nitrate hexahydrate (0.0873 g, 0.173 mmol) in methanol (19 mL). The complex was formed and crystallized by slow evaporation from the methanol solution after 2 d. The remaining solution was decanted, and the red crystals were washed once with methanol before air drying (0.0453 g, 45.2% yield). ^{13}C SSNMR (Adamantane, 100.53): δ

151.92, 132.52, 127.97, 114.68. ^{13}C SSNMR (interrupted decoupling, Adamantane, 100.53): δ 151.73, 132.03, 125.32, 114.24. IR (neat): 3307, 2915, 1627, 1596, 1512, 1370, 1341, 1287, 1238, 1223, 1170, 1108, 1055, 1040, 1008, 910, 836, 808, 796, 770, 750, 705, 688 cm^{-1}. HR-ESI/MS (m/z): [M-NO_3-CH_3OH+2DMSO]$^+$ 652.1269, [M-NO_3-CH_3OH+DMSO]$^+$ 574.1144, [M-NO_3-CH_3OH]$^+$ 496.1042 (found); [M-NO_3-CH_3OH+2DMSO]$^+$ 652.1301, [M-NO_3-CH3OH+DMSO]+ 574.1162, [M-NO_3-CH_3OH]$^+$ 496.1023 (calcd). Anal. Calc. for $C_{13}H_{12}N_4O_8U$: C, 26.45; H, 2.05; N, 9.49. Found: C, 25.32; H, 1.71; N, 9.62%.

Results and discussion

Synthesis of ligand and uranyl complex

We exploited a three-step strategy to prepare the conjugated cyclic imide dioxime ligand. We synthesized acenaphtho[1,2-c][1,2,5]thiadiazole 8,8-dioxide, **1**, via an acid-catalyzed condensation reaction with sulfamide in refluxing ethanol that was modified from Qian (Scheme 2.1).[19] Following a modification of Ege's synthesis[21], compound **1** was subjected to pyrolysis under dynamic vacuum (150 mTorr) at 180 °C which caused the loss of sulfur dioxide and formation of 1,8-dicyanonaphthalene, **2**. The loss of sulfur dioxide to form aromatic dinitriles has previously been reported by Ege and Hay.[21,36] Following the method of Forrester, 1,8-dicyanonaphthalene reacted with hydroxylamine in a refluxing ethanol and water mixture to form 1,8-naphthalimide dioxime, **3**, (Np-CAO-H_3).[22] The ligand (**3**) can be purified by crystallization from absolute ethanol and must be stored under nitrogen to prevent slow decomposition. Compounds **1**–**3** were characterized by ^{1}H and ^{13}C NMR as well as HR-DART/MS and IR. The uranyl complex, (Np-CAO-H_2)$U(O)_2(NO_3)(CH_3OH)$, **4**, was prepared by mixing **3** and uranyl nitrate hexahydrate in methanol (Scheme 2.1). Red crystals of **4** that were

suitable for single crystal diffraction were formed in 45% yield after 2 days. Single crystal diffraction demonstrated that the uranyl center is coordinated to a single cyclic dioxime ligand, a bidentate nitrate group, and a methanol in the equatorial plane. This result is in contrast to the unconjugated cyclic imide dioxime ligand prepared by Rao wherein two equivalents bind to the metal center. Even addition of excess **3** still yielded **4** and not the bis tridentate amidoxime uranyl product $(Np\text{-}CAO\text{-}H_2)_2U(O)_2$. X-ray diffraction shows that the geometry about the uranium atom can best be described as hexagonal bipyramidal (Figure 2.1).[37–39] Each atom that is ligated to the uranium has a respectively ligated atom that is nearly *trans* to it. The two oxo ligands are bound in the axial positions and show only a mild distortion of the $O_1\text{-}U\text{-}O_2$ bond angle of 177.1°. The U-O bond distances are asymmetric ($U\text{-}O_1$, 1.781(6); $U\text{-}O_2$, 1.767(6)) and are well within the range of similar uranyl complexes.[40–42] Like Rao's glutarimidedioxime uranyl complex, central nitrogen (N_4) is deprotonated and a proton shift occurs on the oxime groups creating an extended aromatic structure.[15] The $U\text{-}N_4$ bond distance for **4** is 2.514(1) Å, which is slightly shorter than the UAN bond distance (2.563(3) Å) found in Rao's glutarimidedioxime uranyl complex.[15] This chelating imide dioxime is a rare example of tridentate binding to uranyl with this class of ligands[15], and contrasts to the binding motif of amidoximates to uranyl.[33]

Spectroscopic characterization of uranyl complex

Although a few similar uranyl imide dioxime complexes have been prepared previously by Rao and others, almost no detailed spectroscopic work has been undertaken outside of UV–Vis measurements.[15–17] Detailed NMR spectroscopy has not been collected for uranyl imide dioxime complexes and provides an effective method for determination of uranyl complexation. One area that would also be of potential importance for nuclear forensics is a detailed

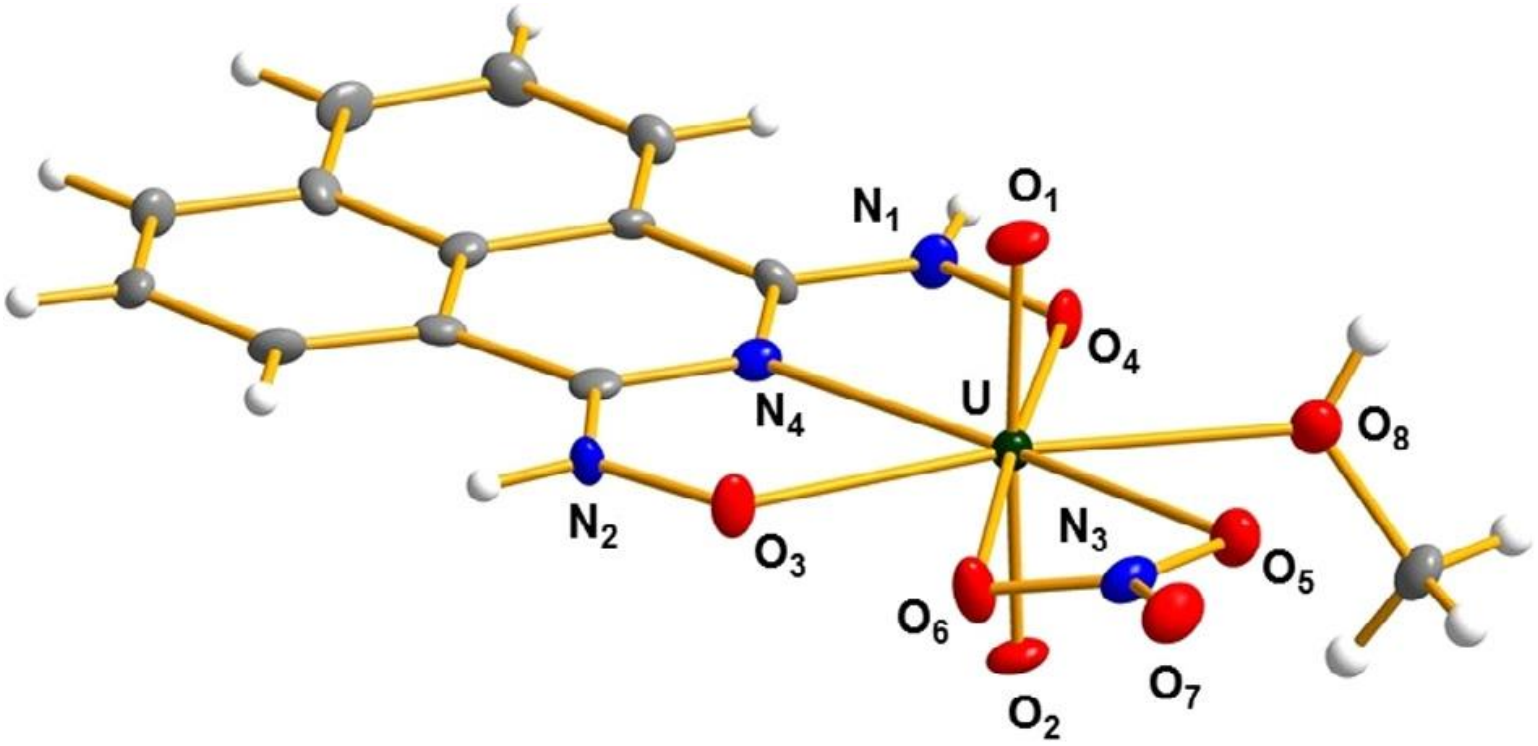

Figure 2.1. Crystal structure of (Np-CAO-H_2)U$(O)_2(NO_3)(CH_3OH)$ (4) that shows tridentate binding of cyclic amidoxime ligand. Green, blue, red, and gray ellipsoids (50% probability) represent U, N, O, and C, respectively. White spheres represent H. Selected bond distances (Å) and angles (°) are as follows: U-O_1, 1.781(6); U-O_2, 1.767(6); U-O_3, 2.398(6); U-O_4, 2.420(6); U-O_5, 2.589(6); U-O_6, 2.572(6); U-O_8, 2.462(7); U-N_4, 2.514(7); O_1-U-O_2, 177.1(3); O_3-U-O_8, 170.1(2); O_4-U-O_6, 176.8(2); O_5-U-N_4, 169.0(2).

understanding of the vibrational spectroscopy associated with binding ligands such as imide dioximes and the specific actinides targeted.

Since uranyl complex **4** has very low solubility in common organic solvents, we employed solid state ^{13}C CP MAS NMR. To unambiguously determine the peak positions for each carbon, solution state ^{1}H and ^{13}C NMR, along with HSQC and HMBC spectra, were collected for ligand **3** in DMSO-d_6 (Figures 2.5 and 2.6). These solution spectra were compared to a ^{13}C CP MAS NMR spectrum of **3** (Figure 2.7), but the width of the peaks in the ^{13}C CP MAS NMR spectrum made assignment of each individual carbon signal problematic.
To simplify the assignment of the peak positions, in particular the imine carbon as it is the closest in proximity to the bound uranyl in **4**, we turned to interrupted decoupling NMR. Interrupted decoupling serves to suppress protonated carbons, therefore removing a majority of the aromatic carbons and allowing for assignment of the individual carbon atoms of interest.[43,44] When the protonated carbons were suppressed, four clearly resolved resonances at 121.0, 125.3, 131.2, and 144.8 ppm were observed (Figure 2.2A). An interrupted decoupling NMR was then collected for complex **4** as standard ^{13}C CP MAS NMR again led to broad, unassignable peaks (Figure 2.7B) and showed four resonances at 114.7, 128.0, 132.5, and 151.9 ppm. The imine carbon (denoted ‘‘a’’ in Figure 2.2) resonance shifts significantly downfield by 7.1 ppm as the carbons are deshielded compared to the free ligand, providing evidence that the ligand is now bound.[38] Solid state ^{13}C CP MAS NMR has rarely been employed on uranyl complexes and, to our knowledge, interrupted decoupling ^{13}C CP MAS NMR has never been performed.[42] This solid state spectroscopic method is an effective technique that demonstrates that the ligand is bound to the uranyl in the bulk material.

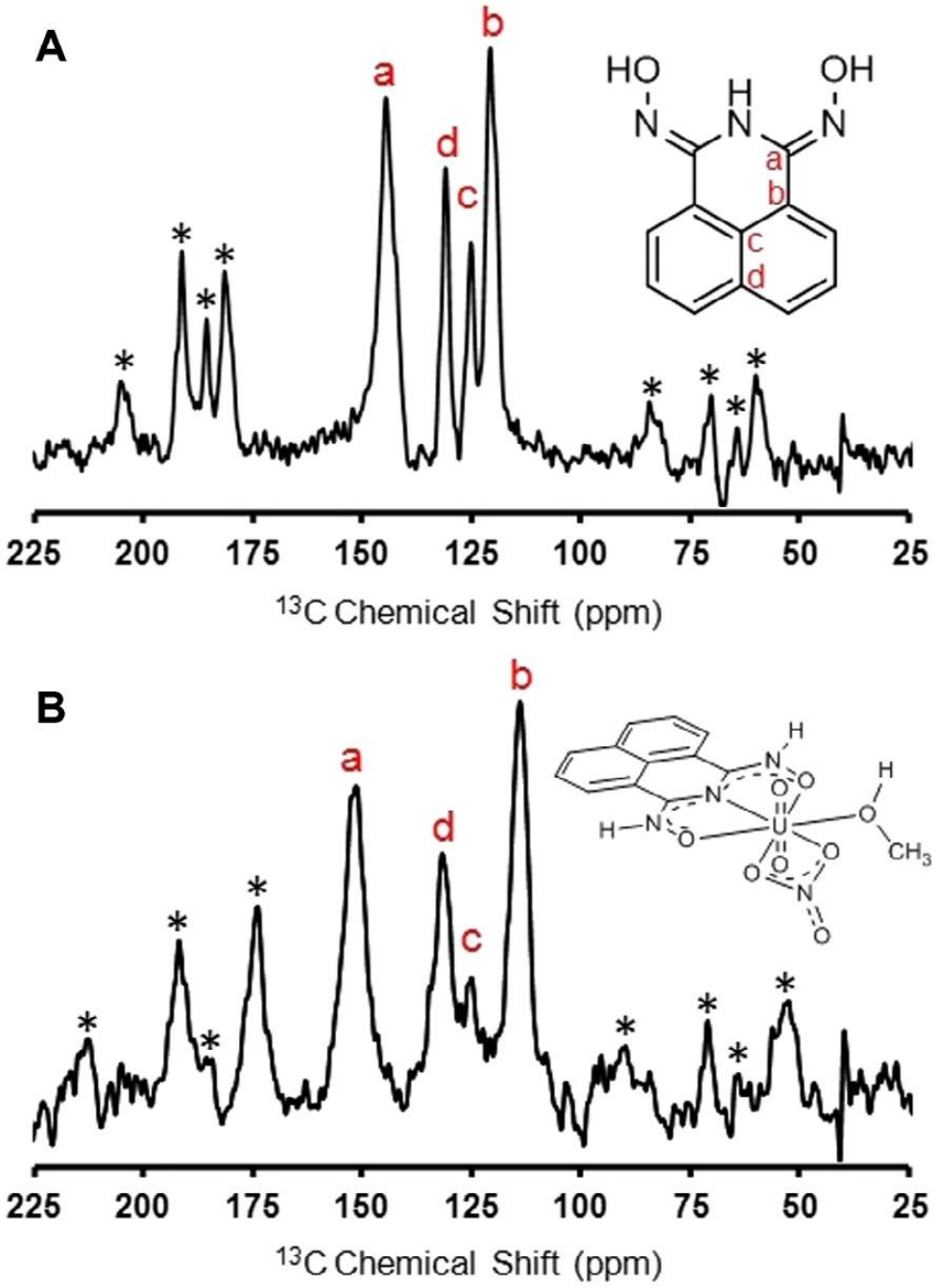

Figure 2.2. (A) The ^{13}C CP MAS NMR of 3 with interrupted decoupling exhibiting the resonances of the four quaternary carbons. (B) The ^{13}C CP MAS NMR of 4 with interrupted decoupling revealing the shifted resonances of the four quaternary carbons in the ligand. *Denote spinning sidebands.

While NMR may not be effective for nuclear forensics due to lack of portability, vibrational spectroscopy of uranyl complexes may be more insightful for field-based tests. The vibrational spectroscopy of uranyl species, $UO_2(NO_3)_2 \cdot 6H_2O$ in particular, have been previously characterized,[45–48,9] and our results are in agreement with these previous studies. The IR spectrum of the uranyl nitrate hexahydrate is dominated by the intense and broad asymmetric uranyl ($\nu_{U=O,as}$) stretch at 935 cm^{-1}, while a weak symmetric uranyl ($\nu_{U=O,s}$) stretch is visible at 867 cm^{-1}. The ligand **3** exhibits characteristic imide and oxime vibrations with the ν_{O-H} stretch at 3407 cm^{-1}, ν_{N-H} stretch at 3384 cm^{-1}, $\nu_{N=C}$ stretch at 1642 cm^{-1}, and ν_{N-O} stretch at 957 cm^{-1}. Upon mixing the ligand–UO_2 complex **4**, it exhibits a combination of stretches from the ligand, UO_2, and NO_3, moieties. Of special note is the shifting of peaks in the uranyl region (~1000–800 cm^{-1}) as shown in Figure 2.3. All of the characteristic vibrations from the UO_2 and ligand **3** in this region have shifted from their original positions.

The Raman spectrum of the uranyl salt is dominated by the $\nu_{U=O,s}$ stretch at 867 cm^{-1} while the $\nu_{U=O,as}$ stretch is virtually indistinguishable from noise. The Raman spectrum of the ligand **3** exhibits a small fluorescence background even after purification by recrystallization, although this is not unexpected from a conjugated system. The Raman spectrum is characterized by an intense mode at 1380 cm^{-1} and a weaker feature at 511 cm^{-1}. Upon binding, the large polarizability of the UO_2 group results in the spectra of the complex **4** being dominated by the $\nu_{U=O,s}$ stretch. However, as mentioned previously,[46,48,49] the $\nu_{U=O,as}$ stretch at 918 cm^{-1} is forbidden in the Raman spectrum and is practically unnoticeable. In the Raman spectrum the $\nu_{U=O,s}$ stretch is free of competing ligand vibrations, has a very strong intensity and is distinct. Thus the frequency of the stretch can serve as a clear indicator for the complexation of uranyl.

Figure 2.3. The uranyl region ($U(O)_2$) of the vibrational spectra, both IR (top) and Raman (bottom). The spectra of ligand 3, complex 4, and uranyl nitrate hexahydrate are shown from top to bottom. The positions, left to right, of the antisymmetric (ν_{as}) and symmetric (ν_s) U=O stretches are labeled for uranyl and the complex while competing vibrations are labeled for the ligand.

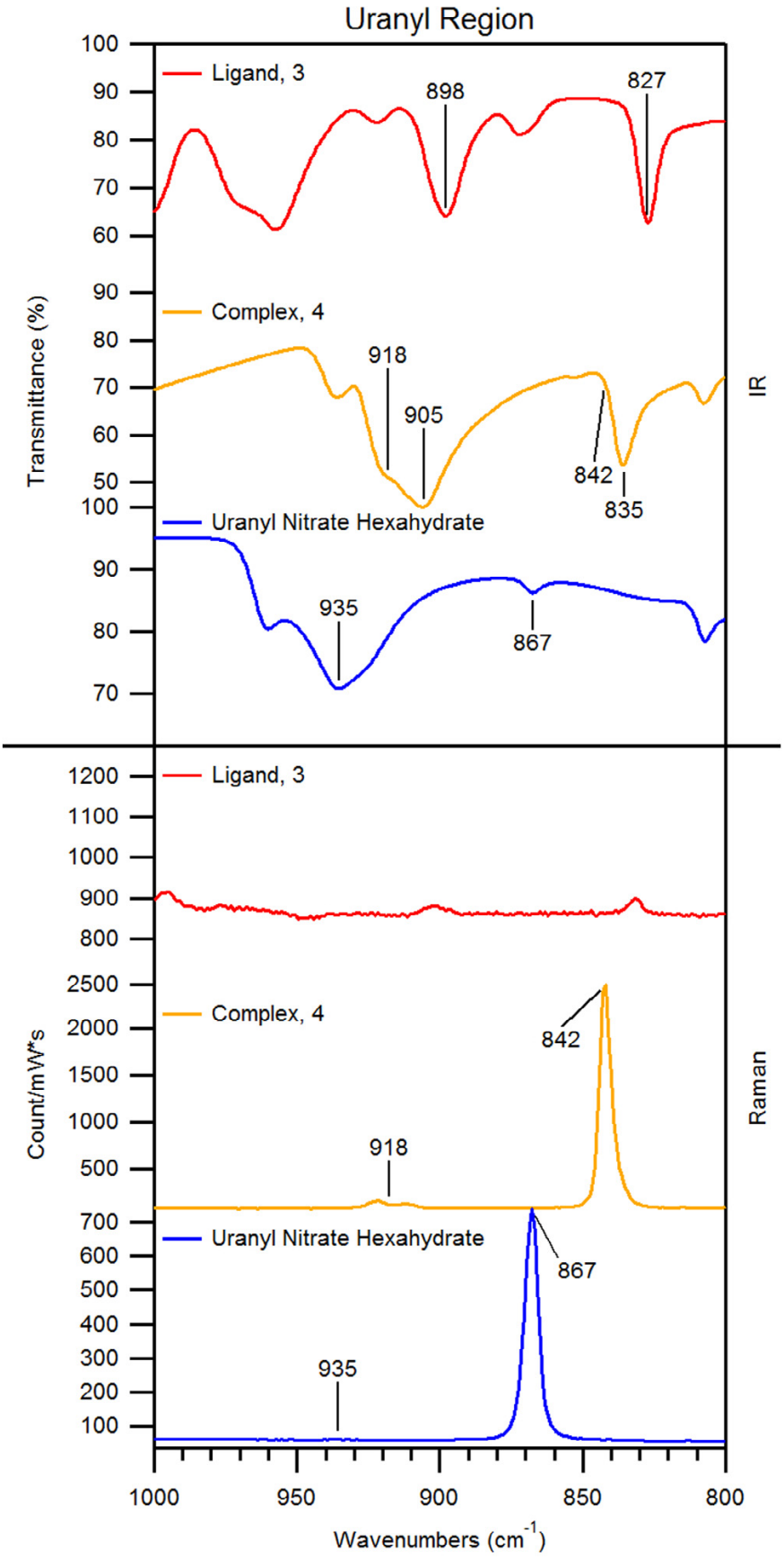
Uranyl Region
Ligand, 3
898
827
Complex, 4
918
905
842
835
Uranyl Nitrate Hexahydrate
935
867
Transmittance (%)
IR
Ligand, 3
Complex, 4
842
918
Uranyl Nitrate Hexahydrate
867
935
Count/mW*s
Raman
Wavenumbers (cm-1)

Due to the expansive, vibration free region around the $\nu_{U=O,s}$ stretch it is likely that the symmetric stretch from other actinides would also be clearly visible with this ligand system. Many theoretical and experimental studies have demonstrated the sequential trend of the $\nu_{An=O,s}$ and $\nu_{An=O,as}$ stretching frequencies of uranium, neptunium, and plutonium oxycation moieties.[50–53] We believe the sparseness of the uranyl region in the Raman spectra coupled with the sequential nature of the actinide oxycations vibrational modes presents an excellent opportunity to use ligand **3** as a detection sensor for the associated hexavalent actinide cations.

Density functional theory (DFT) calculations of vibrational modes aided in the understanding of changes between the individual molecular systems and the combined complex **4**. In particular it was noted that the $\nu_{U=O,s}$ stretch at 867 cm^{-1} is barely discernible in the IR of the uranyl complex. Once bound, the $\nu_{U=O,s}$ band is blue-shifted to 842 cm^{-1} and overwhelmed by an intense ligand **3** vibration at 835 cm^{-1}. The $\nu_{U=O,as}$ stretch at 935 cm^{-1} is clearly visible in the uranyl complex, though upon binding the uranyl mode is again blue-shifted and a competing vibration from the ligand **3** at 905 cm^{-1} again overwhelms and merges with the uranyl vibration. In both cases the U=O stretch in the IR spectrum is obscured either partially or completely by modes in the ligand **3**. The Raman spectrum of the uranyl salt lacks the $\nu_{U=O,as}$ stretch but clearly shows the $\nu_{U=O,s}$ stretch at 867 cm^{-1} that is shifted to 842 cm^{-1} in the complex. This stretch in the complex **4** is free from significant competing vibrations down to 800 cm^{-1} and up to 910 cm^{-1} which allows for it to be quickly and easily identified unlike either of the uranyl modes in the IR. Overall, the shifting of the frequencies in the uranyl region can be explained by the expansion of the conjugated system in the ligand to include the uranyl moiety. Further experimental evidence is presented in the bond lengths between uranium and the oxo ligands. The uranyl group in the uranyl nitrate has bond lengths of 1.770 and 1.749 Å while the group in the complex (**4**) has

bond lengths of 1.781 and 1.767 Å, respectively.[54] The inclusion of the uranyl moiety in the conjugated system leads to loss of electron density between the uranium and oxo ligands. This weakens the bonds, leading to elongated bond lengths.

DFT studies of uranyl complex

DFT calculations of the uranyl complex were performed to gain a greater understanding of the electronic structure of the system. Electronic orbital modeling of uranyl systems has been discussed previously.[55–63] The geometry-optimized structure was compared with the crystal structure and generally found to be in good agreement given the comparison of gas and crystal phase results (e.g., all U-O distances agreed within 0.08 Å except to the methanol oxygen which was 0.13 Å shorter in the computation). Upon binding, one significant change in the ligand geometry was a shortening by approximately ~0.09 Å of the O3-N2 and N1-O4 distances in the optimized structure of **4** compared to the experimentally determined structure. This bond shortening suggests delocalized electron density on the O-N-C-N-C-N-O ligand backbone, which could substantiate the notion of a highly conjugated system. These results were consistent with Rao's finding for a uranyl complexed to glutarimidedioxime.[15] In addition, the ligand–U bond lengths were all within 0.10 Å of the experimentally determined structures except for the bound methanol (O8), which was 0.13 Å further from uranium in the calculated structure. Overall, the accurate reproduction of the experimental complex gives us confidence that our electronic structure methods are valid.

The molecular orbitals around the HOMO and LUMO are, naturally, of special interest. When examining the highest occupied molecular orbital (HOMO) (Figure 2.4b) and adjacent lower orbitals, the majority of contributions come from ligand-based p-orbitals (Figure 2.9). In the case of the lowest unoccupied molecular orbital (LUMO) (Figure 2.4a), most of the electron

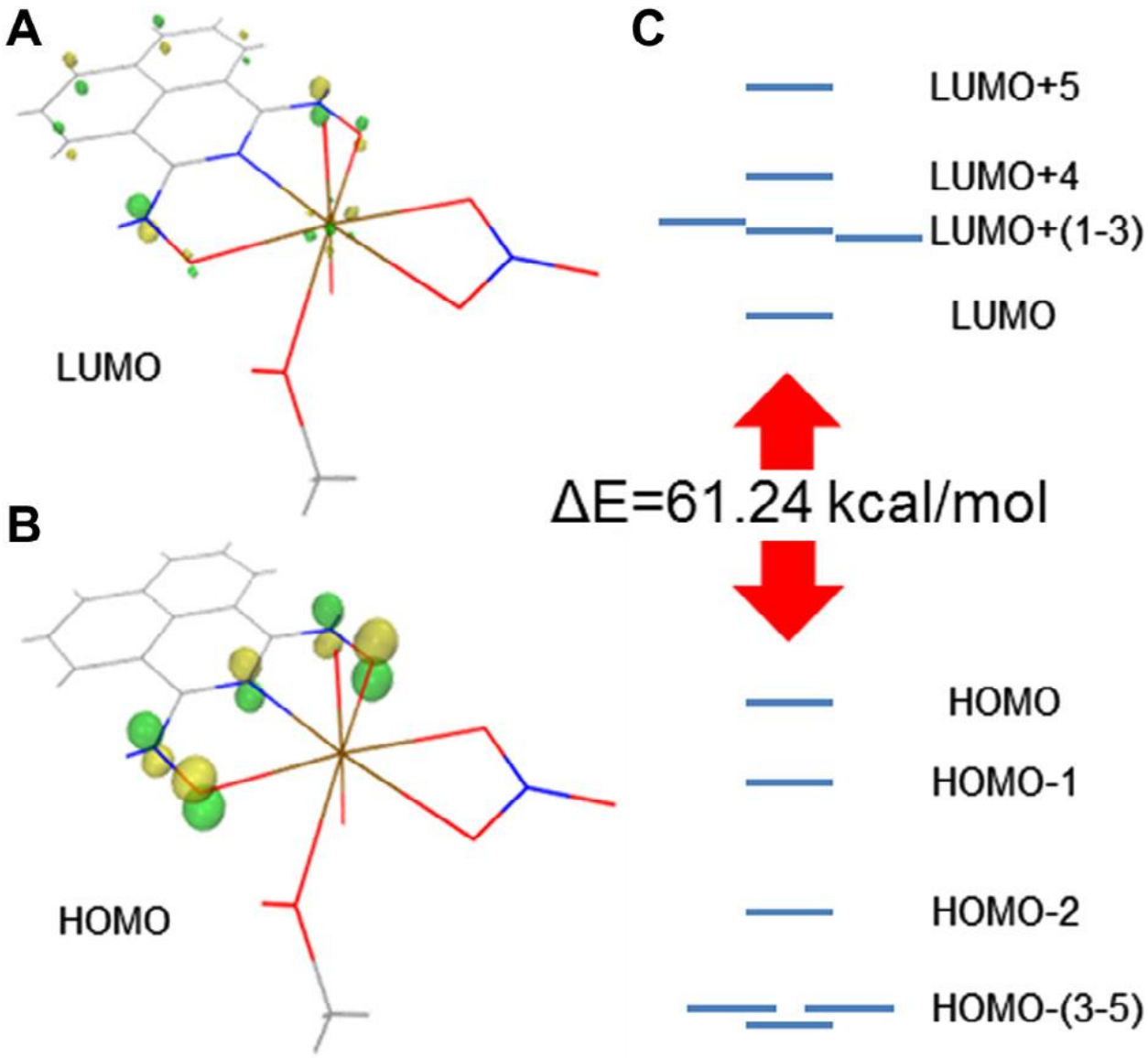

Figure 2.4. (A) LUMO of (Np-CAO-H_2)U$(O)_2(NO_3)(CH_3OH)$ (4). (B) HOMO of complex 4. (C) Orbital splitting diagram of complex 4 obtained from DFT calculations. All calculations used NWChem/B3LYP/6-311++g**

density is also ligand based, with a small contribution (10%) from an f-orbital. This result is in contrast with the LUMO+1 to LUMO+4 orbitals that show exclusively f-orbital character (Figure 2.10). Finally, we note that the complex 4 has a reasonably large HOMO–LUMO gap of approximately 61.24 kcal/mol.

Conclusion

In summary, we present a comprehensive synthetic, spectroscopic, and theoretical characterization of an aromatic tridentate amidoxime uranyl complex. The X-ray structure of the complex demonstrates that unlike Rao's tridentate amidoxime complex, only one equivalent of this aromatic ligand binds to the uranyl ion. The solid state NMR spectrum of the complex is, to our knowledge, the first NMR taken of a combined amidoxime-uranium complex and demonstrates complexation of the bulk material. DFT afforded insight into the electronic structure of this uranyl complex as well as assisted in assigning the vibrational modes. While the U=O vibrations were obscured in the IR spectrum by nearby vibrations, they were easily observed in the Raman spectrum and these signals in the Raman spectra could potentially serve as a spectroscopic marker for uranium detection. The thorough evaluation of this complex's vibrational spectra is a critical first step in the development of cyclic polydentate amidoximes for nuclear forensics and may also aid in situ investigations of extraction of uranyl from seawater.

References for Chapter 2

[1] K. Mayer, M. Wallenius, Z. Varga, Chem. Rev. 113 (2012) 884.

[2] M.J. Kristo, S.J. Tumey, Nucl. Instrum. Methods Phys. Res., Sect. B 294 (2013) 656.

[3] H. Sodaye, S. Nisan, C. Poletiko, S. Prabhakar, P.K. Tewari, Desalination 235 (2009) 9.

[4] P.S. Barber, S.P. Kelley, C.S. Griggs, S. Wallace, R.D. Rogers, Green Chem. 2014 (1828) 16.

[5] H.J. Schenk, L. Astheimer, E.G. Witte, K. Schwochau, Sep. Sci. Technol. 17 (1982) 1293.

[6] J. Kim, C. Tsouris, R.T. Mayes, Y. Oyola, T. Saito, C.J. Janke, S. Dai, E. Schneider, D. Sachde, Sep. Sci. Technol. 48 (2013) 367.

[7] R.V. Davies, J. Kennedy, K.M. Hill, R.W. McIlroy, R. Spence, Nature 203 (1964) 1110.

[8] M.J. Tamada, Jpn. Inst. Energy 88 (2009) 249.

[9] D. Bhandari, S.M. Wells, S.T. Retterer, M. Sepaniak, J. Anal. Chem. 81 (2009) 8061.

[10] L. Astheimer, H.J. Schenk, E.G. Witte, K. Schwochau, Sep. Sci. Technol. 18 (1983) 307.

[11] A. Zhang, G. Uchiyama, T. Asakura, Adsorp. Sci. Technol. 21 (2003) 761.

[12] A. Zhang, T. Asakura, G. Uchiyama, React. Funct. Polym. 57 (2003) 67.

[13] A. Zhang, G. Uchiyama, T. Asakura, Sep. Sci. Technol. 2003 (1829) 38.

[14] B.P. Hay, O. Clement, G. Sandrone, D.A. Dixon, Inorg. Chem. 37 (1998) 5887.

[15] G.X. Tian, S.J. Teat, Z.Y. Zhang, L.F. Rao, Dalton Trans. 41 (2012) 11579.

[16] X. Sun, G. Tian, C. Xu, L. Rao, S. Vukovic, S.O. Kang, B.P. Hay, Dalton Trans. 43 (2014) 551.

[17] G.X. Tian, S.J. Teat, L.F. Rao, Dalton Trans. 42 (2013) 5690.

[18] C.L. Bell, C.N.V. Nambury, L. Bauer, J. Org. Chem. 29 (1964) 2873.

[19] X.H. Qian, Y. Xiao, Tetrahedron Lett. 43 (2002) 2991.

[20] J.B. Wright, J. Org. Chem. 1964 (1905) 29.

[21] G. Ege, E. Beisiege, Synthesis (1974) 22.

[22] A.R. Forrester, H. Irikawa, R.H. Thomson, S.O. Woo, T.J. King, J. Chem. Soc., Perkin Trans. 1 (1981) 1712.

[23] Bruker, SAINT-PLUS, Bruker AXS Inc., M., Wisconsin, USA, 2007.

[24] A.L. Spek, PLATON, A Multipurpose Crystallographic Tool, Utrecht University, Utrecht, The Netherlands, 2005.

[25] M. Valiev, E.J. Bylaska, N. Govind, K. Kowalski, T.P. Straatsma, H.J.J. Van Dam, D. Wang, J. Nieplocha, E. Apra, T.L. Windus, W. de Jong, Comput. Phys. Commun. 181 (2010) 1477.

[26] A.D. Becke, J. Chem. Phys. 98 (1993) 5648.

[27] A.D. Becke, Phys. Rev. A 38 (1988) 3098.

[28] C.T. Lee, W.T. Yang, R.G. Parr, Phys. Rev. B 37 (1988) 785.

[29] M. Dolg, H. Stoll, H. Preuss, R.M. Pitzer, J. Phys. Chem. 97 (1993) 5852.

[30] R. Krishnan, J.S. Binkley, R. Seeger, J.A. Pople, J. Chem. Phys. 72 (1980) 650.

[31] D. Feller, J. Comput. Chem. 17 (1996) 1571.

[32] K.L. Schuchardt, B.T. Didier, T. Elsethagen, L.S. Sun, V. Gurumoorthi, J. Chase, J.

Li, T.L. Windus, J. Chem. Inf. Model. 47 (2007) 1045.

[33] S. Vukovic, L.A. Watson, S.O. Kang, R. Custelcean, B.P. Hay, Inorg. Chem. 51 (2012) 3855.

[34] W. Humphrey, A. Dalke, K. Schulten, J. Mol. Graph. 14 (1996) 33.

[35] Persistence of Vision (TM) Raytracer, version 3.7.0, Persistence of Vision Pty. Ltd., Williamstown, Victoria, Australia, 2004.

[36] C.D. Grant, S.O. Kang, B.P. Hay, J. Org. Chem. 78 (2013) 7735.

[37] L.L. Liang, Y.G. Cai, N.S. Weng, R.L. Zhang, J.S. Zhao, J.F. Wang, H.L. Wu, Inorg. Chem. Commun. 12 (2009) 86.

[38] S.B. Deb, S. Kannan, M.G.B. Drew, J. Coord. Chem. 63 (2010) 3620.

[39] P.S. Barber, S.P. Kelley, R.D. Rogers, RSC Adv. 2 (2012) 8526.

[40] G.X. Tian, L.F. Rao, S.J. Teat, G.K. Liu, Chem. Eur. J. 15 (2009) 4172.

[41] S. Kannan, M.A. Moody, C.L. Barnes, P.B. Duval, Inorg. Chem. 47 (2008) 4691.

[42] J. Jiang, M.J. Sarsfield, J.C. Renshaw, F.R. Livens, D. Collison, J.M. Charnock, M. Helliwell, H. Eccles, Inorg. Chem. 41 (2002) 2799.

[43] D.W. Duff, G.E. Maciel, Macromolecules 23 (1990) 4367.

[44] M.V. Luzgin, A.V. Toktarev, V.N. Parmon, A.G. Stepanov, J. Phys. Chem. C 117 (2013) 22867.

[45] C. Nguyen Trung, G.M. Begun, D.A. Palmer, Inorg. Chem. 31 (1992) 5280.

[46] K. Ohwada, Spectrochim. Acta, Part A 35 (1979) 1283.

[47] S.P. Pasilis, A. Blumenfeld, Inorg. Chem. 50 (2011) 8302.

[48] J.I. Bullock, J. Chem. Soc. A (1969) 781.

[49] A.A. Zazhogin, H.D. Lutz, A.I. Komyak, J. Mol. Struct. 482–483 (1999) 189.

[50] C. Madic, G.M. Begun, D.E. Hobart, R.L. Hahn, Inorg. Chem. 1984 (1914) 23.

[51] C. Madic, D.E. Hobart, G.M. Begun, Inorg. Chem. 22 (1983) 1494.

[52] P.J. Hay, R.L. Martin, G. Schreckenbach, J. Phys. Chem. A 104 (2000) 6259.

[53] The Chemistry of the Actinide and Transactinide Elements, 4th ed., 2011.

[54] J.C. Taylor, M.H. Mueller, Acta Crystallogr. 19 (1965) 536.

[55] J. Su, P.D. Dau, Y.H. Qiu, H.T. Liu, C.F. Xu, D.L. Huang, L.S. Wang, J. Li, Inorg. Chem. 52 (2013) 6617.

[56] J.C. Berthet, P. Thuery, J.P. Dognon, D. Guillaneux, M. Ephritikhine, Inorg. Chem. 47 (2008) 6850.

[57] P.D. Dau, J. Su, H.T. Liu, J.B. Liu, D.L. Huang, J. Li, L.S. Wang, Chem. Sci. 3 (2012) 1137.

[58] J. Su, K. Zhang, W.H.E. Schwarz, J. Li, Inorg. Chem. 50 (2011) 2082.

[59] M. Straka, P. Hrobarik, M. Kaupp, J. Am. Chem. Soc. 127 (2005) 2591.

[60] G. Nocton, P. Horeglad, V. Vetere, J. Pecaut, L. Dubois, P. Maldivi, N.M. Edelstein, M. Mazzanti, J. Am. Chem. Soc. 132 (2010) 495.

[61] C.W. Abney, S.B. Liu, W.B. Lin, J. Phys. Chem. A 117 (2013) 11558.

[62] G.M. Lombardo, A.L. Thompson, F.P. Ballistreri, A. Pappalardo, G.T. Sfrazzetto, G.A. Tomaselli, R.M. Toscano, F. Punzo, Dalton Trans. 2012 (1951) 41.

[63] P.F. Weck, E. Kim, B. Masci, P. Thuery, K.R. Czerwinski, Inorg. Chem. 49 (2010) 1465.

Appendix For Chapter 2

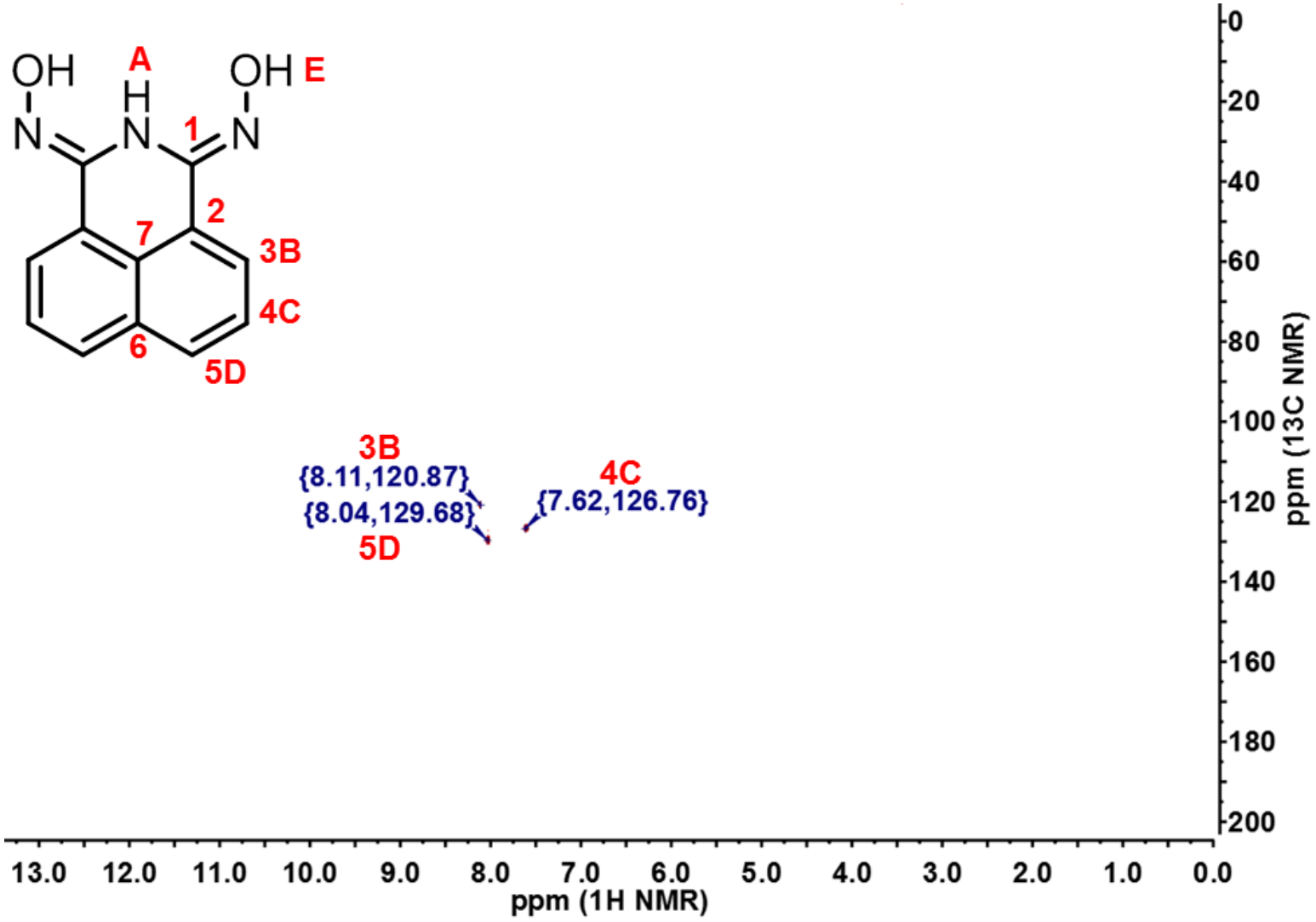

Figure 2.5. The HSQC NMR spectrum of 3 in DMSO-d_6.

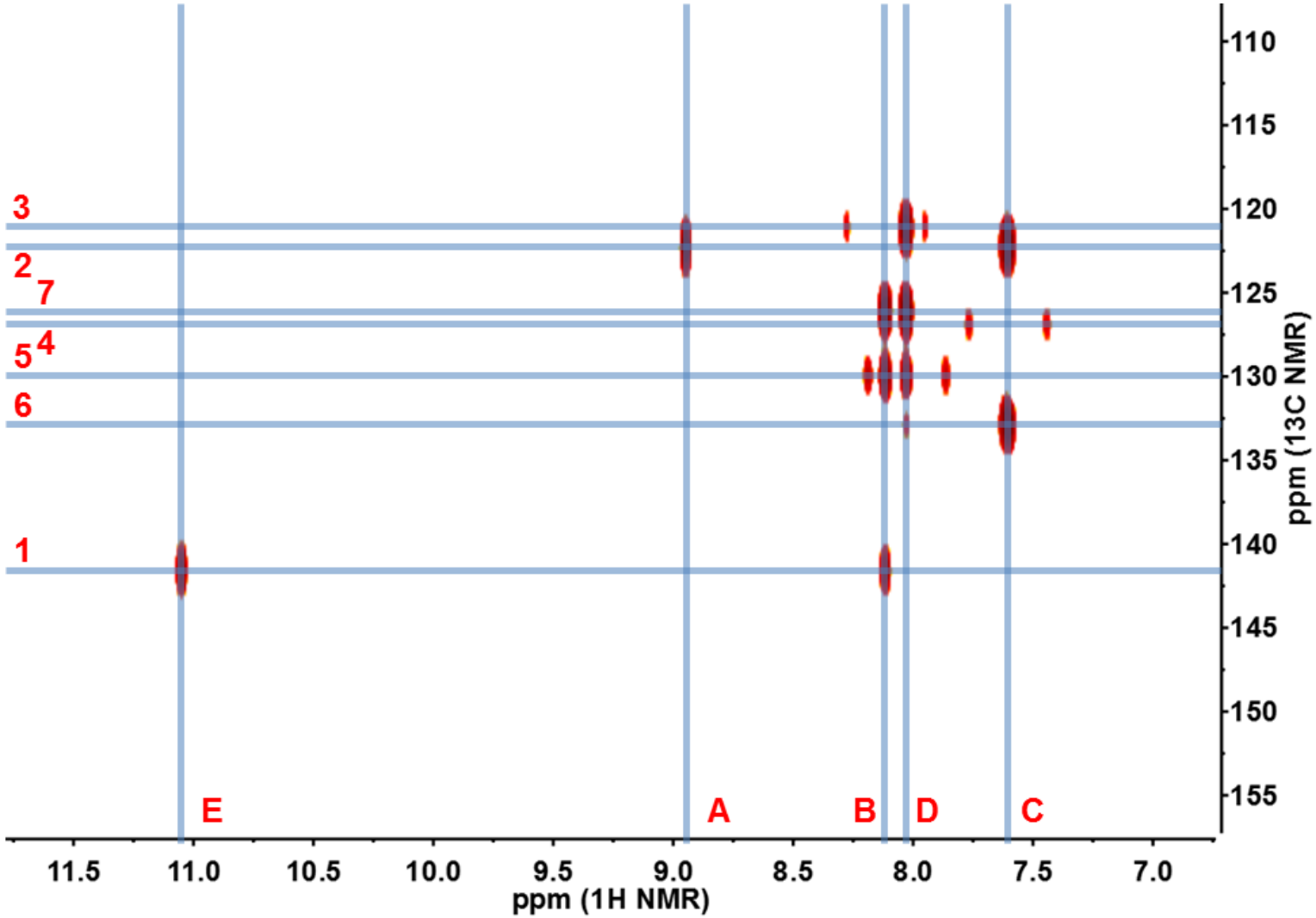

Figure 2.6. The HMBC NMR spectrum of 3 in DMSO-d_6.

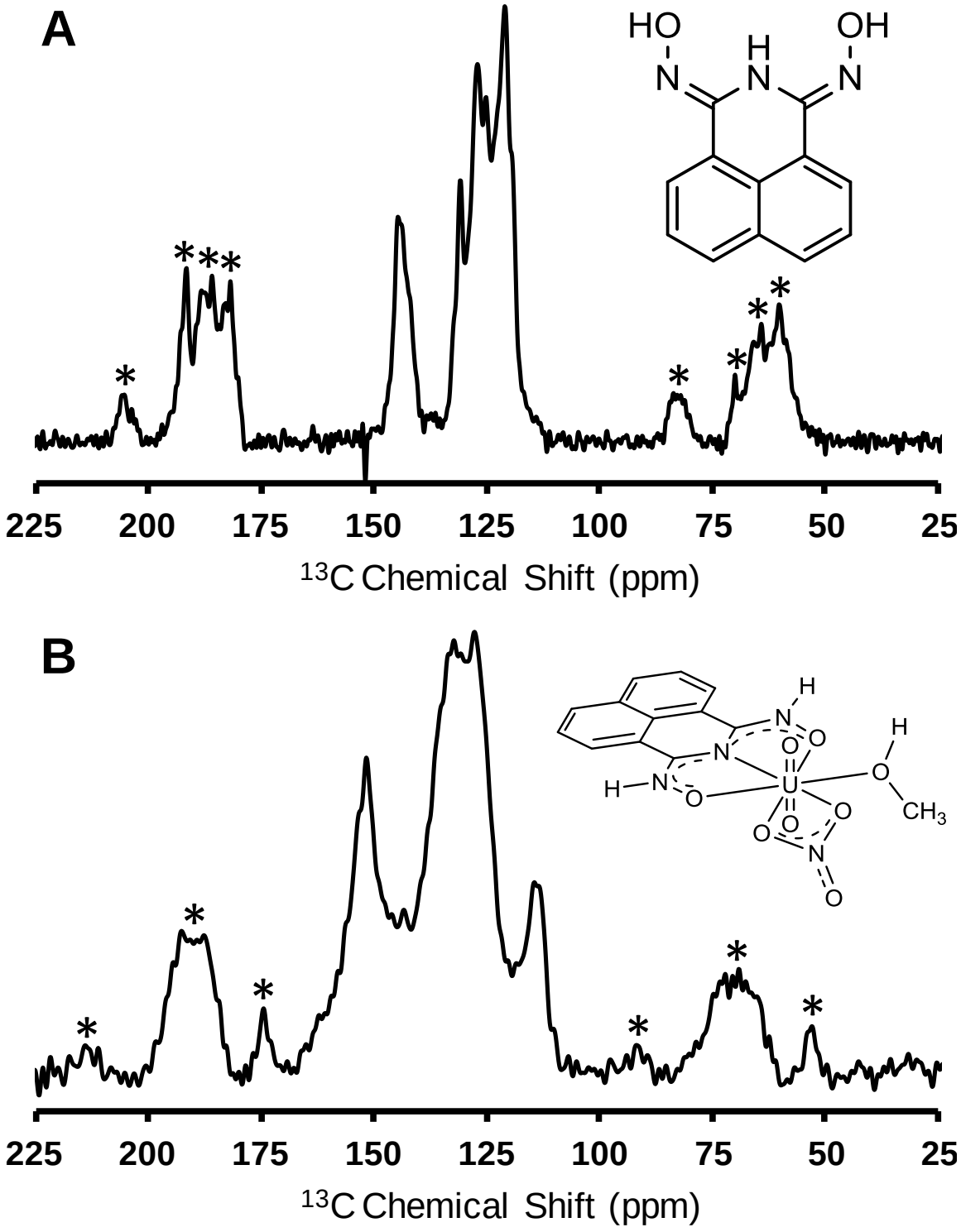

Figure 2.7. The unsuppressed solid state ^{13}C CP MAS NMR of (A) 3 and (B) 4. * denote spinning sidebands.

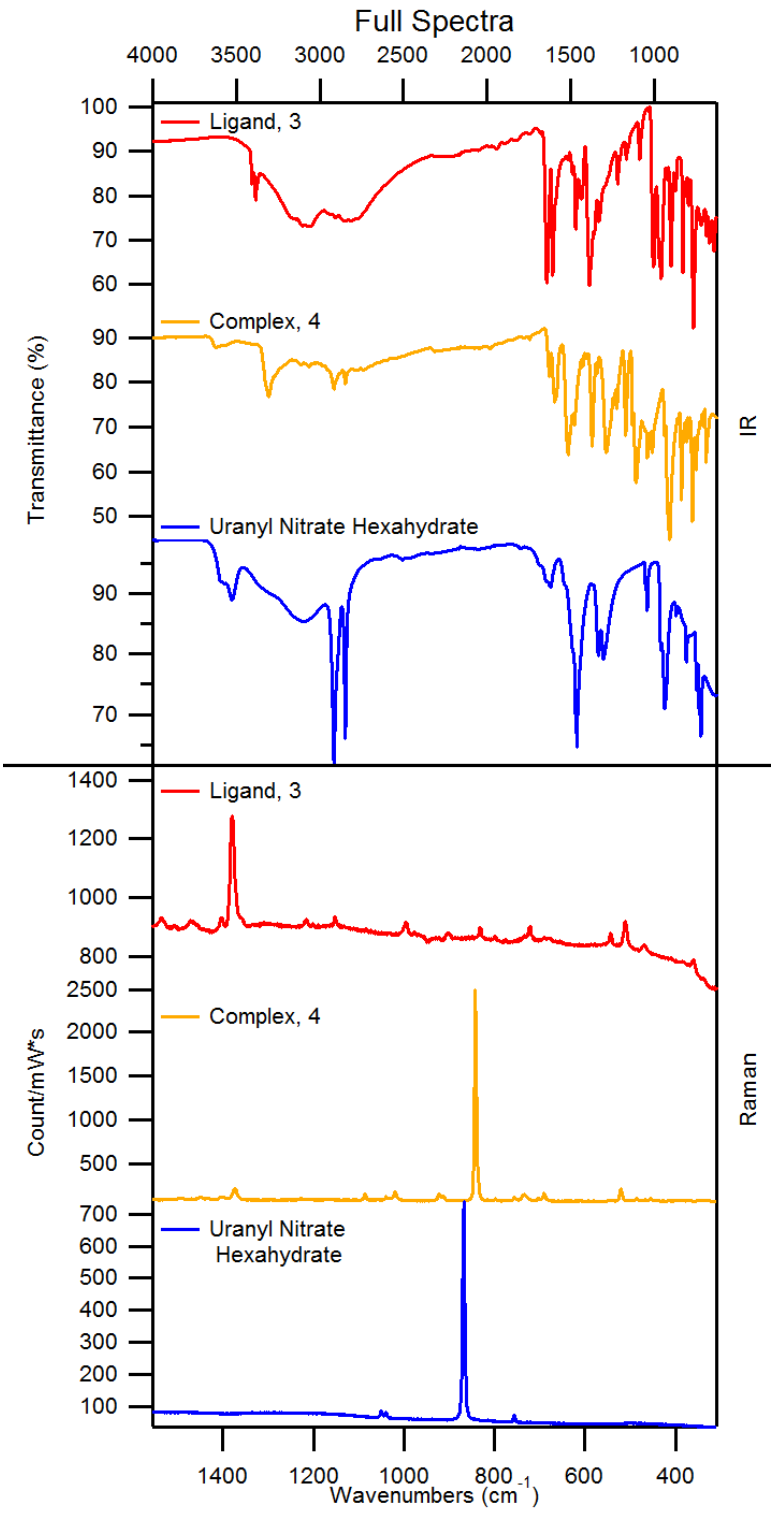

Figure 2.8. The full Raman and IR spectra of the samples collected.

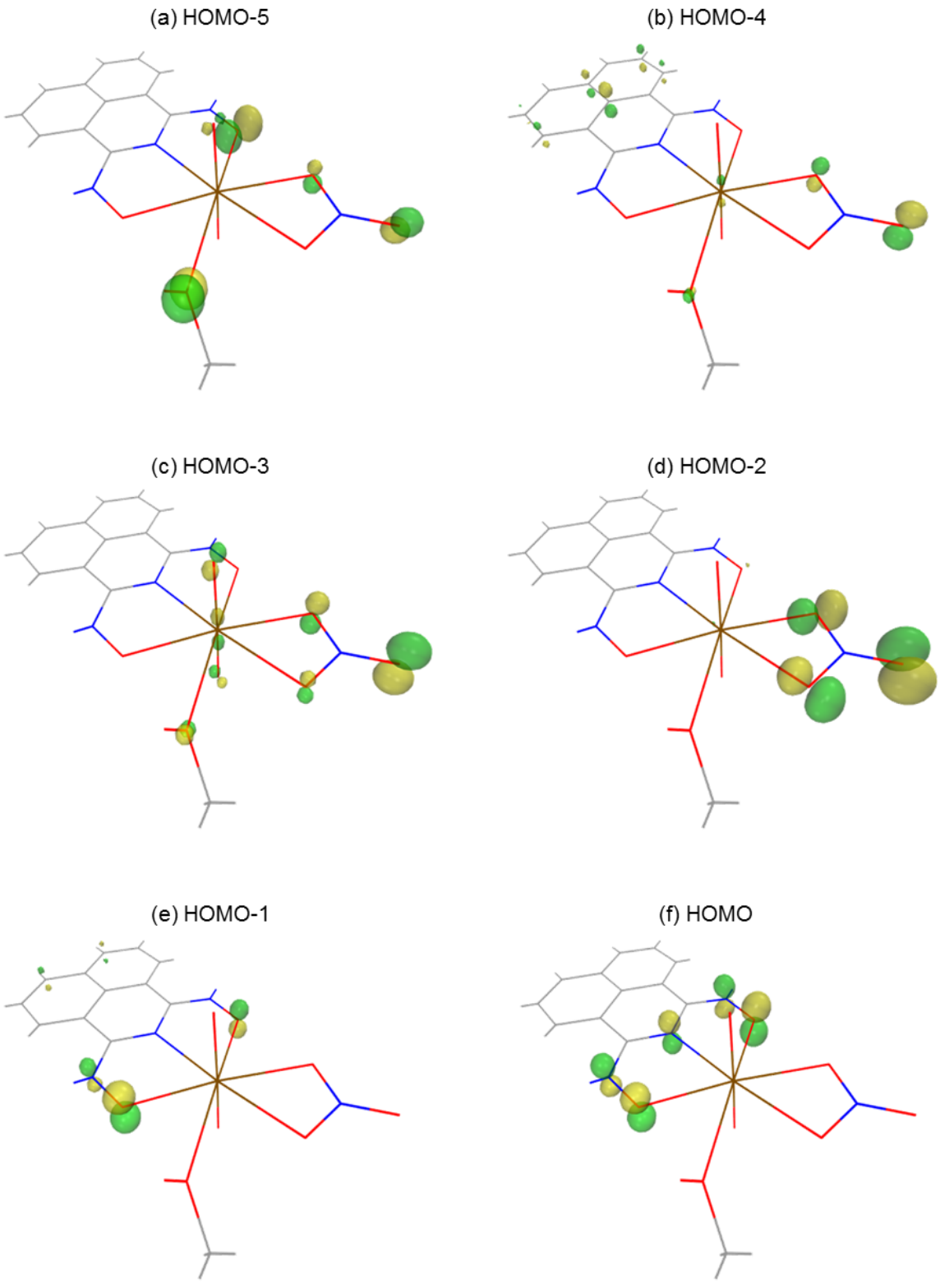

Figure 2.9. Selected molecular orbital plots from HOMO-5 (a) to HOMO (f).

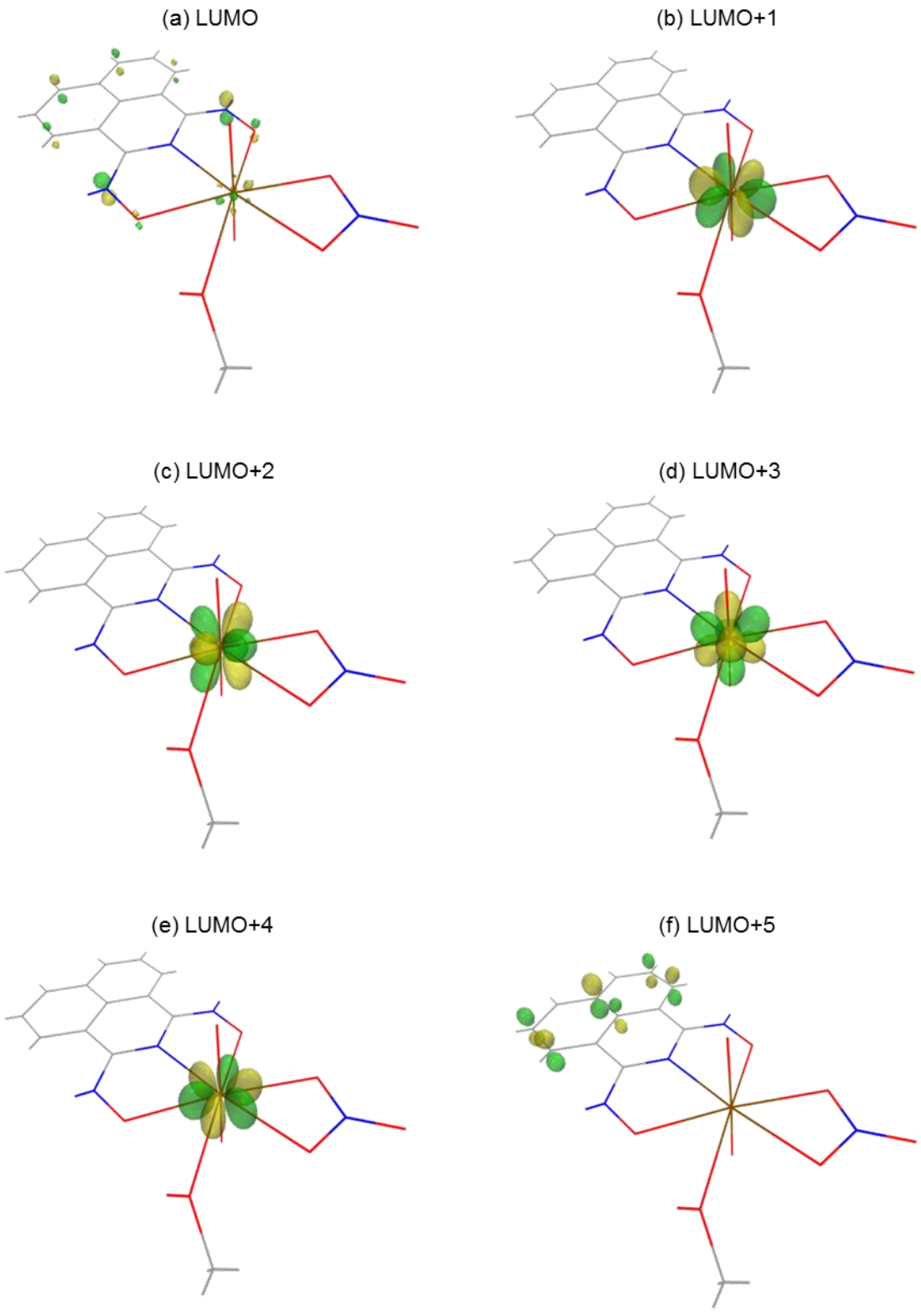

Figure 2.10. Selected molecular orbital plots from LUMO (a) to LUMO+5 (f).

Table 2.1. Selected molecular orbital data from HOMO-5 to LUMO+5.

Vector	Occupancy	E (kcal/mol)	Orbital
113	0	-41.77785877	LUMO+5
112	0	-56.05737593	LUMO+4
111	0	-62.86012399	LUMO+3
110	0	-64.62625088	LUMO+2
109	0	-65.68347973	LUMO+1
108	0	-77.99359441	LUMO
107	2	-139.2314168	HOMO
106	2	-151.9577588	HOMO-1
105	2	-172.4153379	HOMO-2
104	2	-187.5987581	HOMO-3
103	2	-187.7764689	HOMO-4
102	2	-190.3751761	HOMO-5

checkCIF/PLATON report

You have not supplied any structure factors. As a result the full set of tests cannot be run.

THIS REPORT IS FOR GUIDANCE ONLY. IF USED AS PART OF A REVIEW PROCEDURE FOR PUBLICATION, IT SHOULD NOT REPLACE THE EXPERTISE OF AN EXPERIENCED CRYSTALLOGRAPHIC REFEREE.

No syntax errors found. CIF dictionary Interpreting this report

Datablock: U

```
Bond precision:  C-C = 0.0127 A          Wavelength=0.71073

Cell:          a=7.1221(15)       b=10.601(2)      c=13.683(3)
               alpha=102.880(2)   beta=99.789(2)   gamma=98.454(2)
Temperature:   100 K

                Calculated                Reported
Volume          973.9(3)                  973.9(4)
Space group     P -1                      P -1
Hall group      -P 1                      ?
Moiety formula  C13 H12 N4 O8 U, 2(C H4 O) ?
Sum formula     C15 H20 N4 O10 U          C15 H20 N4 O10 U
Mr              654.38                    654.38
Dx,g cm-3       2.231                     2.232
Z               2                         2
Mu (mm-1)       8.397                     8.397
F000            620.0                     620.0
F000'           601.18
h,k,lmax        9,14,18                   9,14,18
Nref            5034                      4526
Tmin,Tmax       0.664,0.777               0.679,0.787
Tmin'           0.651

Correction method= MULTI-SCAN

Data completeness= 0.899          Theta(max)= 28.680

R(reflections)= 0.0465( 4098)     wR2(reflections)= 0.1325( 4526)

S = 1.073                 Npar= 289
```

```
The following ALERTS were generated. Each ALERT has the format
      test-name_ALERT_alert-type_alert-level.
Click on the hyperlinks for more details of the test.
```

Figure 2.11. Page 1 of 4 cif file.

```
Alert level B
PLAT417_ALERT_2_B Short Inter D-H..H-D       H2N    ..  H9O    ..       1.83 Ang.

Alert level C
PLAT342_ALERT_3_C Low Bond Precision on  C-C Bonds ..............     0.0127 Ang.
PLAT417_ALERT_2_C Short Inter D-H..H-D       H8O    ..  H8O    ..       2.12 Ang.

Alert level G
PLAT002_ALERT_2_G Number of Distance or Angle Restraints on AtSite         10
PLAT005_ALERT_5_G No _iucr_refine_instructions_details  in the CIF          ? Do !
PLAT083_ALERT_2_G SHELXL Second Parameter in WGHT Unusually Large.      12.48
PLAT154_ALERT_1_G The su's on the Cell Angles are Equal ..........    0.00200 Deg.
PLAT710_ALERT_4_G Delete 1-2-3 or 2-3-4 Linear Torsion Angle ... #         54
            N2  -O3  -U1  -O8   -166.40  1.10   1.555   1.555   1.555   1.555
PLAT710_ALERT_4_G Delete 1-2-3 or 2-3-4 Linear Torsion Angle ... #         63
            N1  -O4  -U1  -O6   -175.00  4.00   1.555   1.555   1.555   1.555
PLAT710_ALERT_4_G Delete 1-2-3 or 2-3-4 Linear Torsion Angle ... #         67
            C13 -O8  -U1  -O3     57.10  1.50   1.555   1.555   1.555   1.555
PLAT710_ALERT_4_G Delete 1-2-3 or 2-3-4 Linear Torsion Angle ... #         89
            N3  -O6  -U1  -O4      9.00  4.00   1.555   1.555   1.555   1.555
PLAT860_ALERT_3_G Note: Number of Least-Squares Restraints .......          6

   0 ALERT level A = Most likely a serious problem - resolve or explain
   1 ALERT level B = A potentially serious problem, consider carefully
   2 ALERT level C = Check. Ensure it is not caused by an omission or oversight
   9 ALERT level G = General information/check it is not something unexpected

   1 ALERT type 1 CIF construction/syntax error, inconsistent or missing data
   4 ALERT type 2 Indicator that the structure model may be wrong or deficient
   2 ALERT type 3 Indicator that the structure quality may be low
   4 ALERT type 4 Improvement, methodology, query or suggestion
   1 ALERT type 5 Informative message, check
```

Figure 2.12. Page 2 of 4 cif file.

It is advisable to attempt to resolve as many as possible of the alerts in all categories. Often the minor alerts point to easily fixed oversights, errors and omissions in your CIF or refinement strategy, so attention to these fine details can be worthwhile. In order to resolve some of the more serious problems it may be necessary to carry out additional measurements or structure refinements. However, the purpose of your study may justify the reported deviations and the more serious of these should normally be commented upon in the discussion or experimental section of a paper or in the "special_details" fields of the CIF. checkCIF was carefully designed to identify outliers and unusual parameters, but every test has its limitations and alerts that are not important in a particular case may appear. Conversely, the absence of alerts does not guarantee there are no aspects of the results needing attention. It is up to the individual to critically assess their own results and, if necessary, seek expert advice.

Publication of your CIF in IUCr journals

A basic structural check has been run on your CIF. These basic checks will be run on all CIFs submitted for publication in IUCr journals (*Acta Crystallographica*, *Journal of Applied Crystallography*, *Journal of Synchrotron Radiation*); however, if you intend to submit to *Acta Crystallographica Section C* or *E*, you should make sure that full publication checks are run on the final version of your CIF prior to submission.

Publication of your CIF in other journals

Please refer to the *Notes for Authors* of the relevant journal for any special instructions relating to CIF submission.

PLATON version of 01/06/2013; check.def file version of 24/05/2013

Figure 2.13. Page 3 of 4 cif file.

CHAPTER 3.

HYPER-RAMAN SCATTERING OF URANYL NITRATE HEXAHYDRATE

Abstract

A hyper-Raman (HR) based study of uranium compounds has been completed. Many issues such as low melting and boiling points, fluorescent impurities, substance based hazards and limited time were present. Initial success was found from HR spectra of uranium nitrate hexahydrate (UNH) crystals, however fluorescence hampered reproducibility. Colloidal surface-enhanced hyper-Raman spectroscopy (SEHRS) studies of UNH on silver colloids proved unsuccessful, as did HR studies of an aromatic uranium complex. Ultimately, experimental time elapsed before the fortuitous completion of this research venture.

Rational for Hyper-Raman Study of Uranyl Nitrate Hexahydrate

The use of uranium for energy and weapons has prompted an enormous amount of research into the associated chemistry.[1-3] The spectroscopy of uranium and uranium containing complexes is no exception, with entire tomes dedicated to the field.[4-6] Given the prevalence of material and the fast paced trade of today there is a greater need than ever for rapid, unambiguous identification of radiological samples.[7] While many traditional, linear, spectroscopy methods have been studied in detail, little work has been performed using non-linear methods such as hyper-Raman (HR) spectroscopy. Nonlinear spectroscopies offer the ability to observe one-photon forbidden modes and provide promising new methods for detection. Given the fast pace of technology there now exist several examples in the hands of public servants which could be utilized for HR with little to no modification. Thus with this in mind, and in light of increasing fundamental understanding of uranium and uranium complexes, this study attempted to obtain hyper-Raman spectra of a uranium compound.

Experimental Challenges

Experimentation was started with crystalline uranyl nitrate hexahydrate (UNH). Early on it was obvious that the high powers utilized for HR spectroscopy were going to be a challenge due to modest melting and boiling points of 60.2 °C and 118 °C respectively.[8] This rapidly limited experimentation to lower power levels in order to prevent vaporizing the samples. The added precaution of sealing samples in containers to contain any gaseous UNH produced from escaping was also taken.

Further complicating the experimental endeavor was the lack of aromaticity in the UNH compound. Molecules with extensive aromaticity typically have very large HR cross-sections. Well known examples include frequently used targets such as rhodamine 6G (R6G) and crystal violet (CV). Recent publication used R6G with two-photon SERS, surface-enhanced hyper-Raman spectroscopy (SEHRS), to achieve single molecule sensitivity.[9] However, without aromaticity UNH was likely to have a rather small HR cross-section. This means that higher power would be required to attain sufficient signal. Given that power was limited by the low melting and boiling point of the analyte, UNH would be challenging to study using HR spectroscopy.

Another benefit of R6G and CV were strong, visible absorptions. Choosing an incident radiation that coincided with these absorptions will lead to the virtual state being very close in energy to an electronic transition of the molecule and greatly enhances the intensity of the Raman scattering. This method is called Resonance Raman spectroscopy and is often used in conjunction with SERS and SEHRS experiments to obtain single molecule sensitivity.[9-11] Unfortunately, UNH absorptions are deep in the ultraviolet region with only very weak

absorptions in the visible region. This means that resonance enhancements for UNH are to be weak at best.

A frequent issue in Raman spectroscopy is fluorescence; which was a constant issue in the process of this work. The crystalline starting material was found to be heterogeneous in purity with some crystals providing only modest fluorescence (Figure 3.1) and others to extensively fluorescence. Previously, with the work on phosphines, this issue was combatted by additional purification, typically through sublimation. The difference in results from the additional purification was stark as illustrated in Figure 3.2. Additional purification was not possible with UNH for a number of reasons. Instead the issue was combatted by visual examination of individual crystals under the microscope, panning from crystal to crystal until a low enough glow was achieved that a spectrum was attempted. Initial results proved promising as seen in Figure 3.3 with a peak in the uranium symmetric ($\nu_{U=O,s}$, 867 cm^{-1}) and anti-symmetric ($\nu_{U=O,as}$, 935 cm^{-1}) range of 800-950 rel cm^{-1} and a peak at roughly 1700 rel cm^{-1}. However, a quick background acquisition also showed the same peak at 1700 rel cm^{-1} as seen in Figure 3.4. Subsequent repeated scans of UNH failed to reproduce the peak observed in the 800-950 rel cm^{-1} range (Figure 3.5). After efforts to reduce stray light and other interferences a promising spectrum was captured (Figure 3.6). Regrettably, this result could not be reliably reproduced.

Attempted Remedies

In an attempt to utilize higher power, UNH was dissolved in water. It was hoped that by taking advantage of the high water solubility (122 g in 100 g) of UNH and the high heat capacity of water, higher laser powers could be used to achieve greater signal.[12] However, all that resulted was incredibly homogeneous, spectacularly intense fluorescence as seen in Figure 3.7.

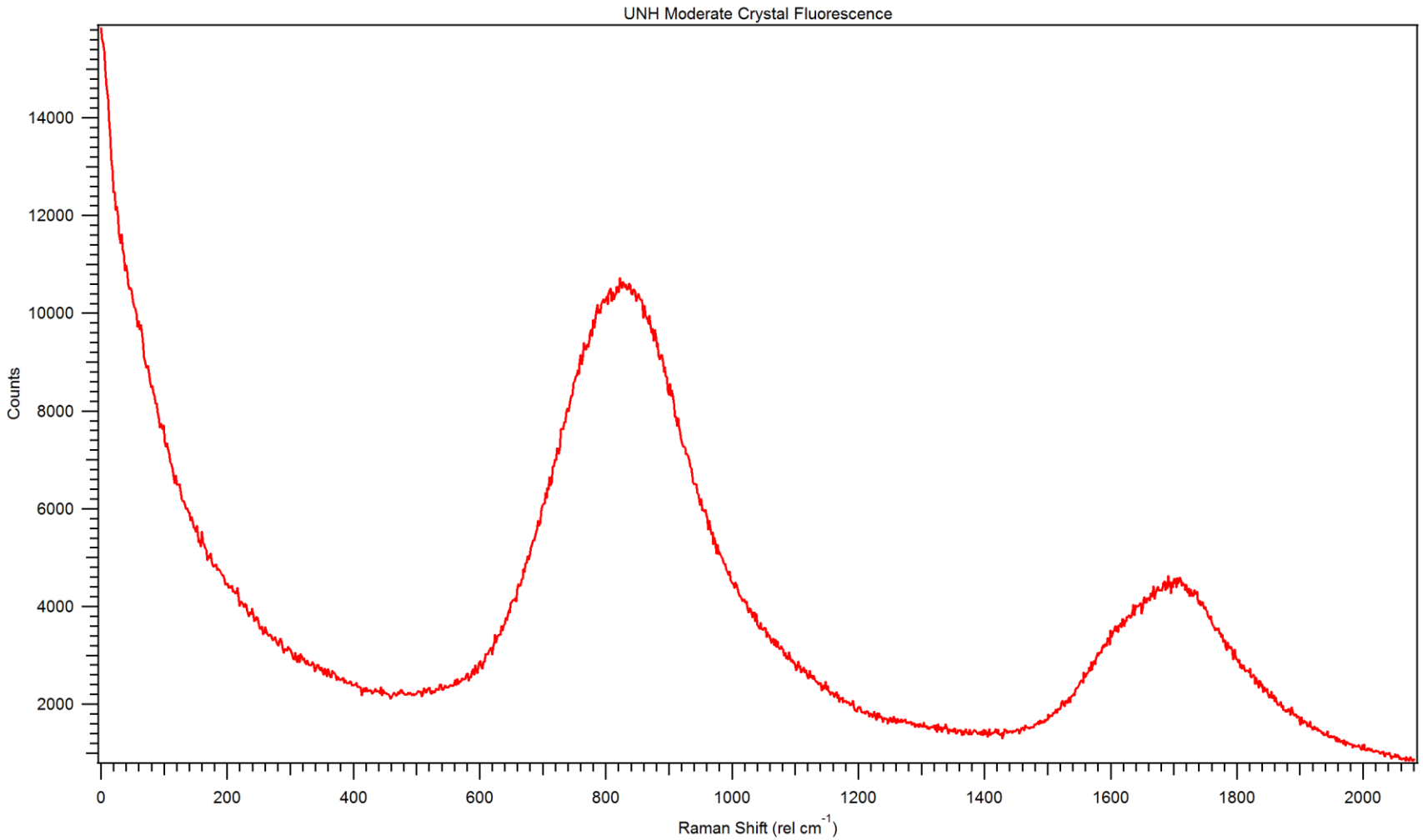

Figure 3.1. An example of an UNH crystal with moderate fluorescence. The majority were far more fluorescent. Laser frequency of 1018 nm, Rayleigh line at 509 nm, 60s scan, 1200 grove grating.

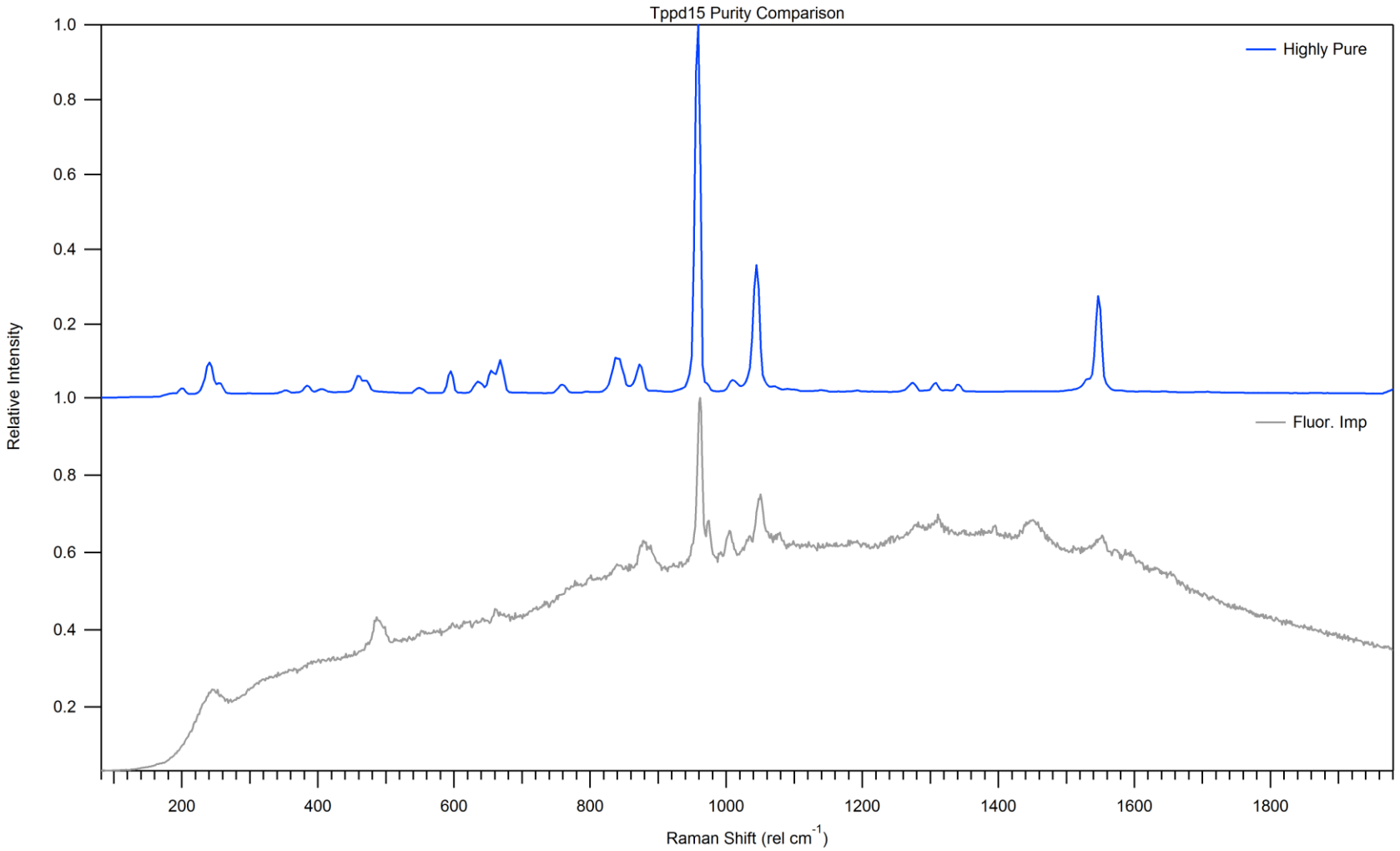

Figure 3.2. A comparison of Tppd15 with fluorescent impurities on the bottom and the highly purified compound on the top.

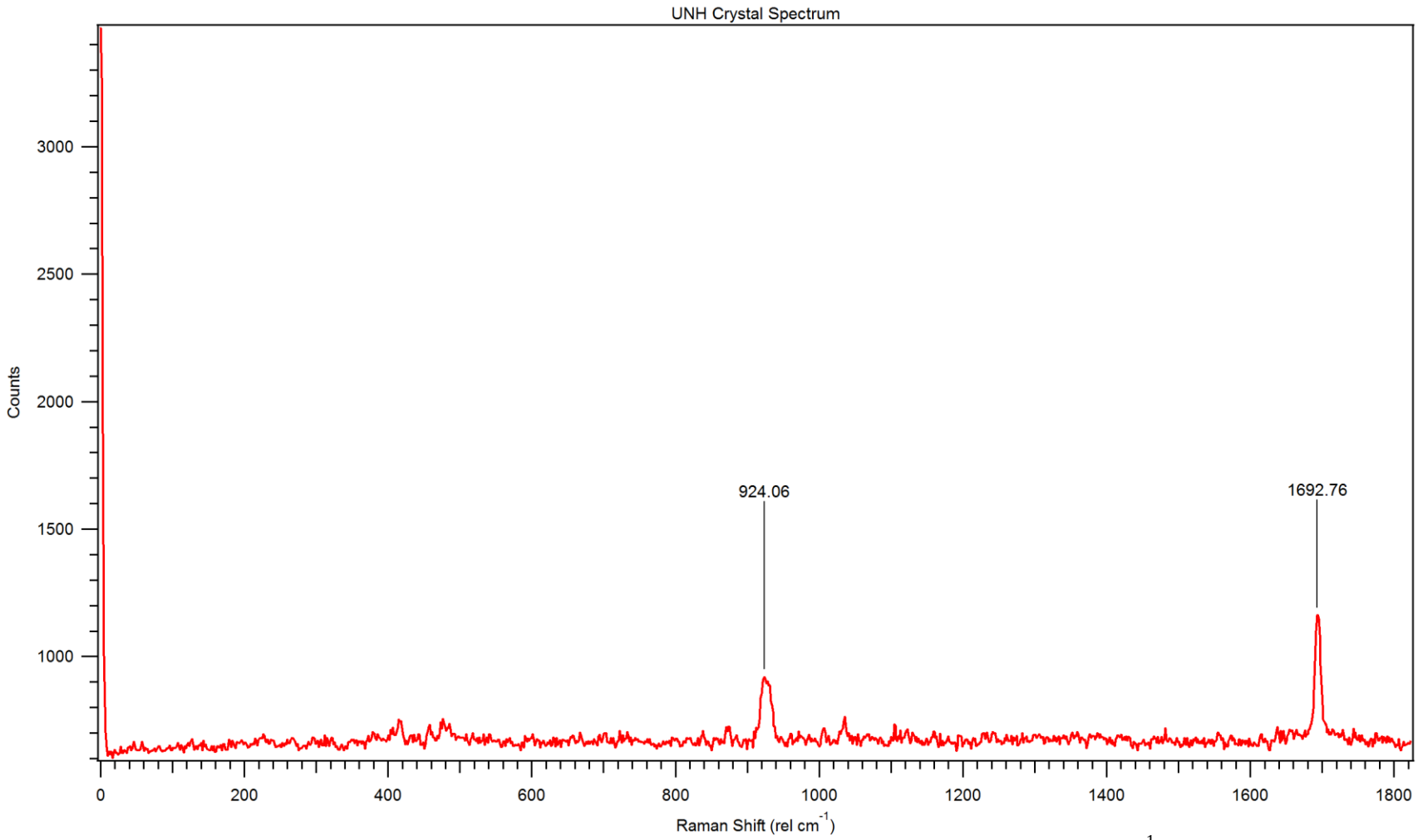

Figure 3.3. Two peaks of interest were seen in this UNH crystal spectrum. The peak in the 800-950 rel cm^{-1} uranyl region at 924 rel cm^{-1} is within experimental error of the $\nu_{U=O,as}$ stretch at 935 cm^{-1}. Laser frequency of 1064 nm, Rayleigh line at 532 nm, 300s scan, 1200 grove grating.

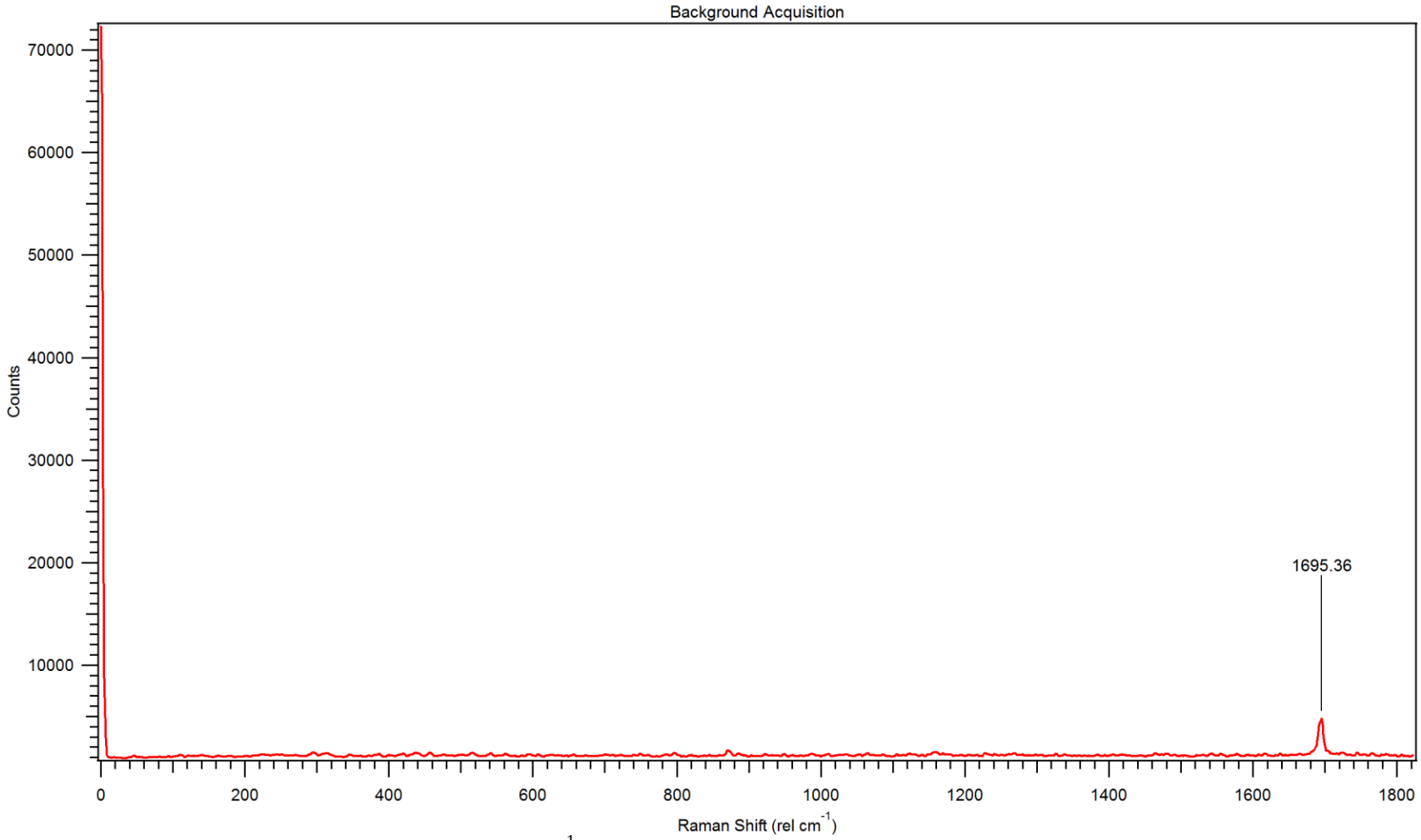

Figure 3.4. The peak of interest around 1700 rel cm^{-1} shows up again in the background scan, demonstrating that it is not from the sample. Laser frequency of 1064 nm, Rayleigh line at 532 nm, 300s scan, 1200 grove grating.

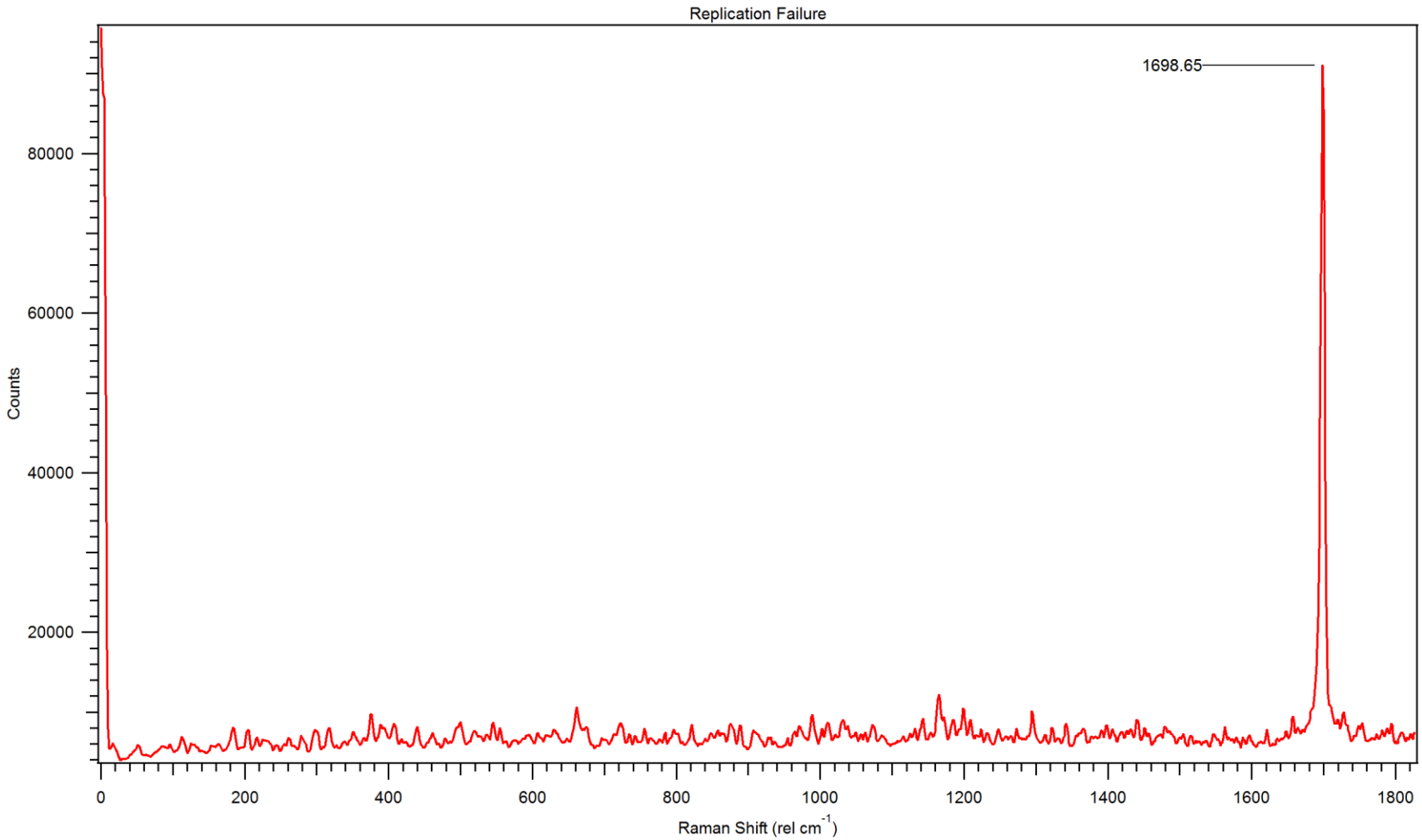

Figure 3.5. The background peak of around 1700 rel cm^{-1} is again present; however the peak from the uranyl region is missing from this replication attempt. Laser frequency of 1064 nm, Rayleigh line at 532 nm, 300s scan, 1200 grove grating.

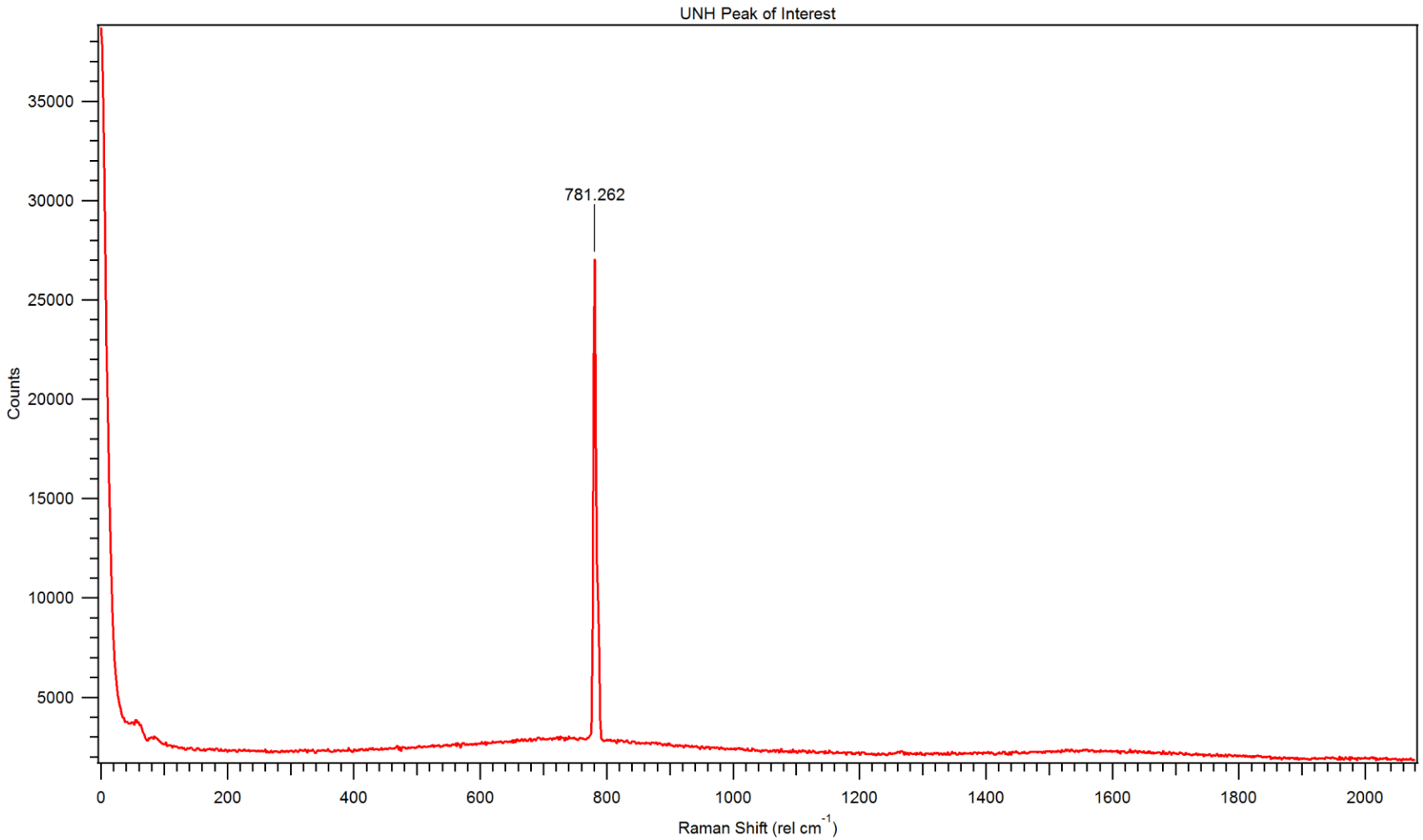

Figure 3.6. The intense peak of around 800 rel cm^{-1} is close to the region of the urayl stretches, but the peak could not be reliably reproduced. Laser frequency of 1018 nm, Rayleigh line at 509 nm, 600s scan, 1200 grove grating.

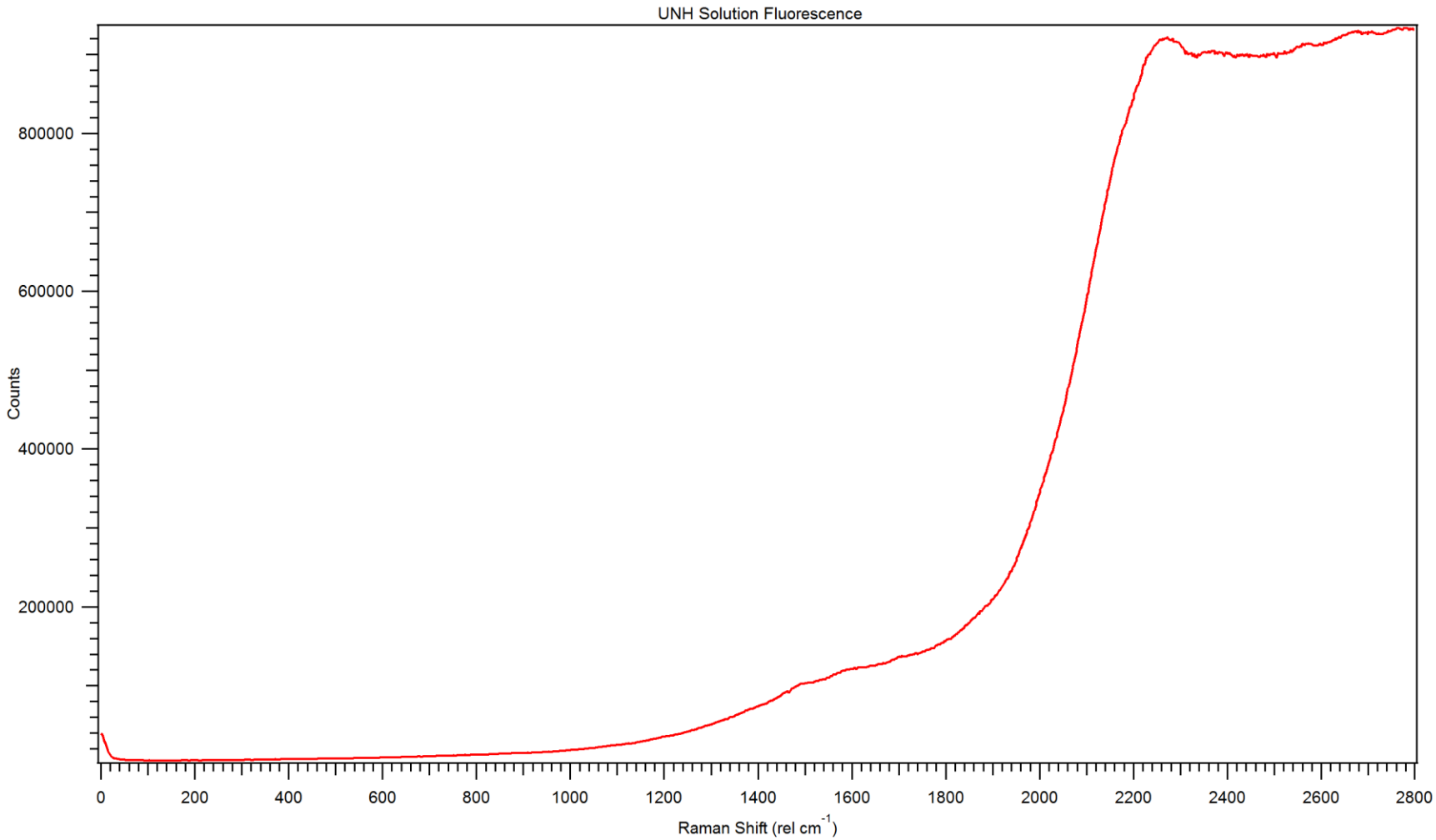

Figure 3.7. A UNH solution scan, the luminous fluorescence overshadowing the Rayleigh peak illustrates the excessive intensity of the competing fluorescence encountered in solution samples. Laser frequency of 1018 nm, Rayleigh line at 509 nm, 600s scan, 1200 grove grating.

It became obvious that in order to obtain a satisfactory HR scan of UNH other methods would have to be utilized. The first thought was to use an incident radiation further in the red. Initial work had been performed in the 800-1100 nm range in the hope of achieving some resonance enhancement. Given this failure, higher wavelengths were utilized. Unfortunately, little headway was made in this area of work. Another method of negating the impact of fluorescence is through the use of SERS. It was believed that the utilization of SERS would sufficiently quench the fluorescence and allows for legible spectra. In order to test this, several different concentrations of UNH were combined with silver colloids. These samples were crashed and then investigated. Initial results were promising with a broad peak at a little past 800 rel cm^{-1}, close to the $\nu_{U=O,s}$ stretch (Figure 3.8). Further investigation proved this peak to be incredibly broad (>100 rel cm^{-1}) and to actually be lower than 800 rel cm^{-1} and thus not a uranium stretch (Figure 3.9). No other noticeable activity was observed with SEHRS.

In a final effort to obtain a HR scan of uranium compound, crystals of an unnamed uranium complex, *(Np-CAO-H2)U(O)2(NO3)(CH3OH)* Figure 3.10, from a previous publication was used. A large advantage of this complex was the high level of aromaticity. It was hoped that this aromaticity would result in a larger HR cross-section. A larger cross-section would allow for lower power usage to obtain a spectrum, reducing interference from fluorescence. Unfortunately, after many recorded spectra this did not prove to be the case as seen in Figure 3.11.

Further Work

The prevalent issue of fluorescence greatly impeded progress in obtaining a well resolved hyper-Raman spectrum of a uranium compound. The issue of fluorescence was present in previous works when attempting to obtain normal Raman spectra of uranyl nitrate hexahydrate and it is likely that the uranium compounds themselves are fluorescing and not just impurities.

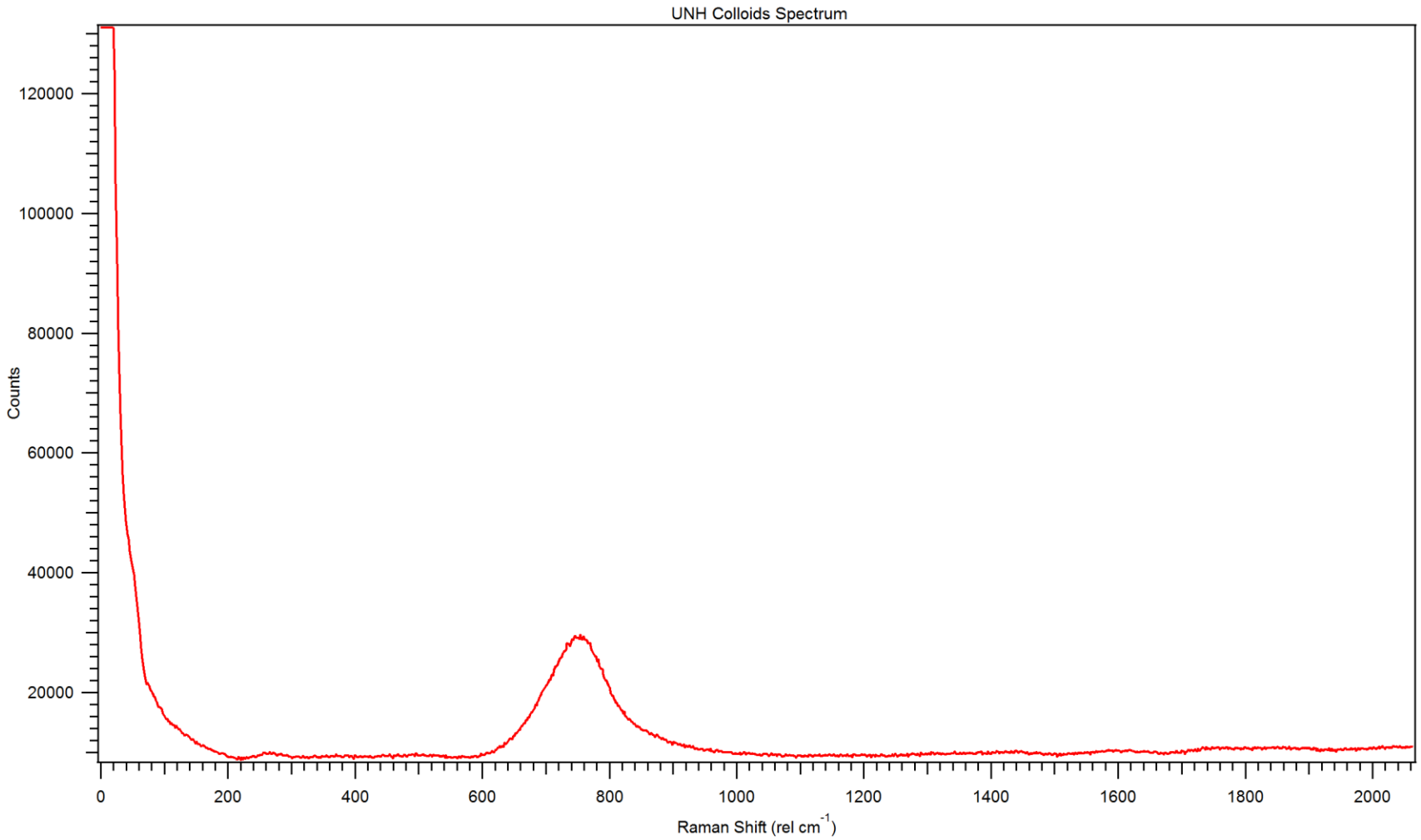

Figure 3.8. The intense peak of around 800 rel cm^{-1} is in the region of the urayl stretches, but the peak is much broader than would be expected. Laser frequency of 1018 nm, Rayleigh line at 509 nm, 120s scan, 1200 grove grating.

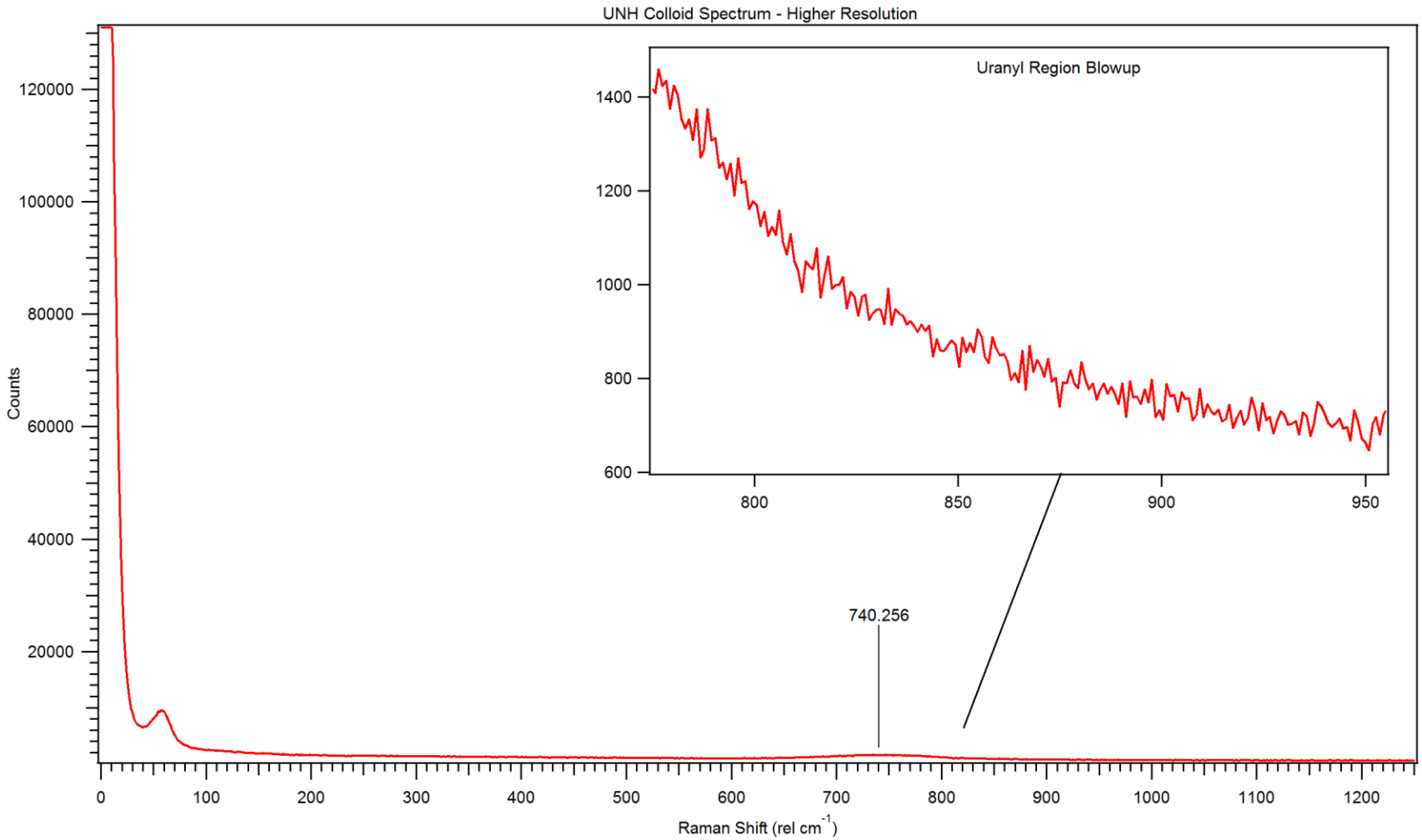

Figure 3.9. The higher resolution demonstrates the previously seen intense peak of around 800 rel cm^{-1} has shifted to the mid 750 rel cm^{-1} and is far too broad to be a uranyl stretch. Laser frequency of 1018 nm, Rayleigh line at 509 nm, 120s scan, 1800 grove grating.

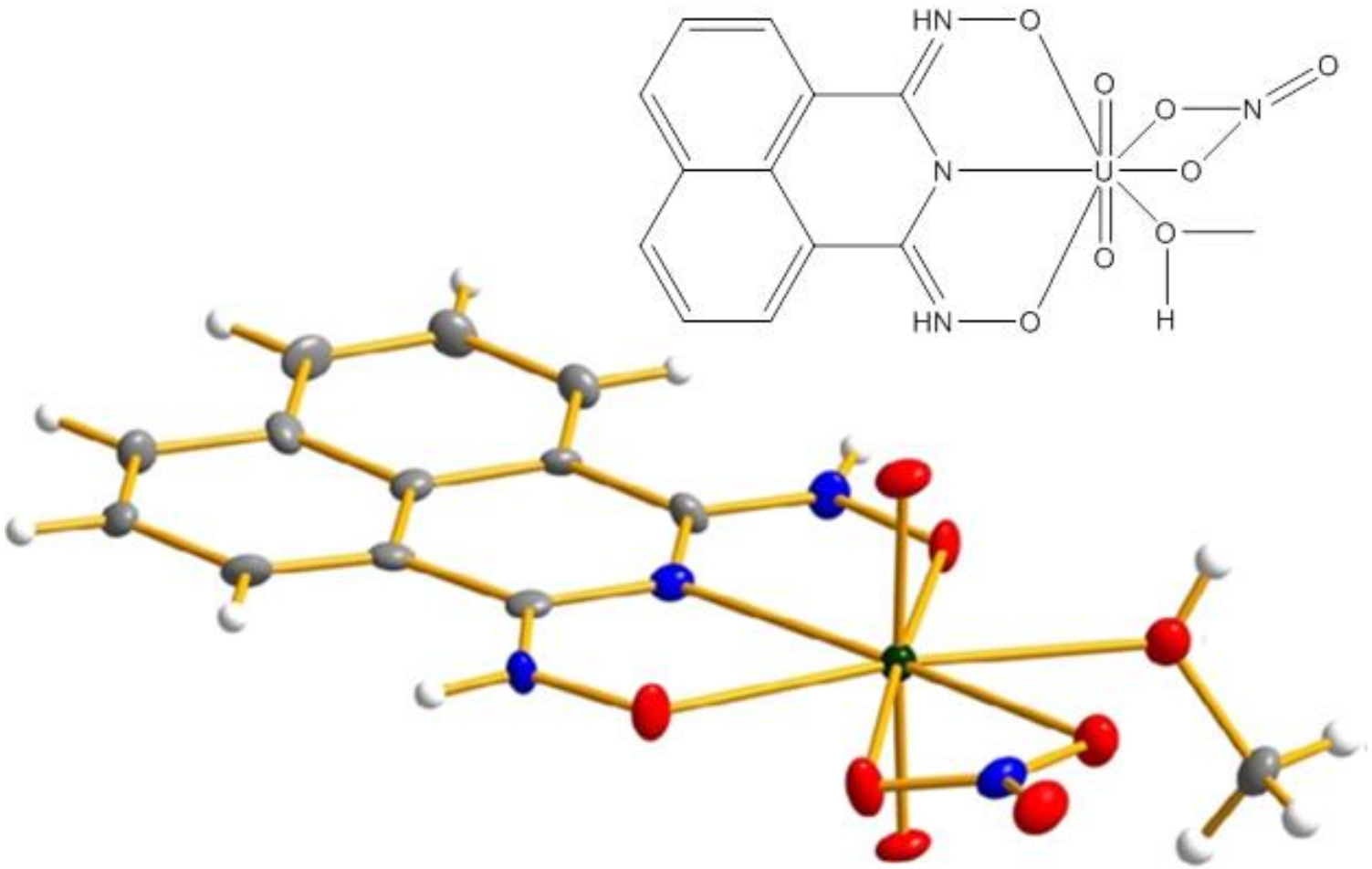

Figure 3.10. The unnamed uranium complex, *(Np-CAO-H2)U(O)2(NO3)(CH3OH)*.

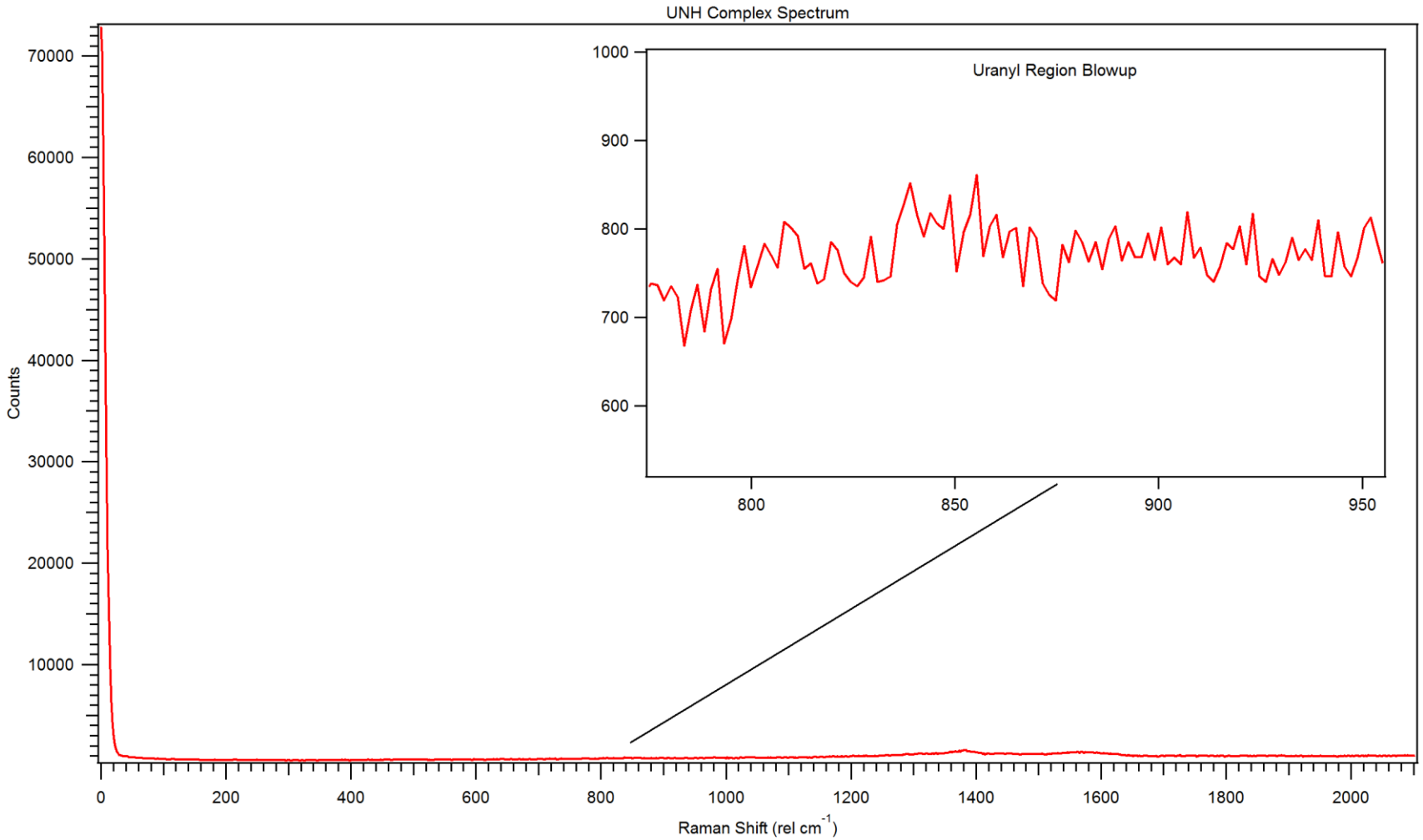

Figure 3.11. No peaks of interest are noted over the minor fluorescence observed. Laser frequency of 1018 nm, Rayleigh line at 509 nm, 300s scan, 1200 grove grating.

Thus while purification of the uranium compounds is likely to be of some help, not all of the fluorescence will be overcome by this method.

Ultimately, issues with fluorescence would be solved by using an excitation source deeper in the IR. Progress would likely be made on hyper-Raman spectra if the excitation source used was in the 1266 nm to 1570 nm region, which would give a hyper-Rayleigh line between 633 nm or 785 nm. This would entail the use of a different laser, as the excitation source, than the mode-locked Ti:sapphire laser used for the 700-1040 nm excitation. A significant benefit to and reason much of the current work used the Ti:sapphire laser was power output, with average power of three watts obtainable. The picoEmerald OPO would be the laser used for 1064-1570 nm excitation and has an average power of roughly 500 mW, a significant disadvantage for hyper-Raman, which has a squared dependence on power. However, the much higher wavelength excitation should prevent the inherent fluorescence and allow for well resolved hyper-Raman spectra of a uranium containing compound.

Switching to excitation sources deeper in the IR is likely to be the most successful method at combatting fluorescence as a sensing method for routine field analysis as well, when the practicality will not allow for purification of the material. Thus, the innate fluorescence of the uranium compounds would be negated and the fluorescence from various matrix elements should be nullified in the switch.

Conclusion

In conclusion, this work illustrates many of the challenges associated with recording hyper-Raman spectra. However, the asymmetric uranyl stretches was observed, though was challenging to reproduce. Additional work, as described, is required before total fruition of this project is realized.

Experimental

Excitation was provided by a frequency doubled ND:YAG laser (Millennia Pro, Princeston Instruments) with a laser line of 532 nm, a mode-locked Ti:sapphire laser (Tsunami, Spectra-Physics) and a OPO (picoEmerald, APE). Incident radiation between 700 and 1600 nm were used with power at the objective between 0.01 mW and 1.5 W. An inverted microscope (Ti-U, Nikon Eclipse) with a 10x, 0.30 NA dry objective (Nikon) in the 180° configuration was used in conjunction with Rayleigh filter and dichroic (Semrock) to collect the Raman scattering. Spectra were recorded with a 300 cm focal length spectrometer (Acton, Princeton Instruments) containing a 600, 1200, 1800 groove mm^{-1} holographic grating, and a 10 μm slit with an attached liquid-nitrogen-cooled deep-depletion charge-coupled device (CCD, Spec10, Princeton Instruments).

Uranyl nitrate hexahydrate was purchased from Fisher Scientific and used as is. The uranium compound *(Np-CAO-H2)U(O)2(NO3)(CH3OH)* was synthesized according to the literature.

References for Chapter 3

[1] Burns, P. C.; Ewing, R. C.; Hawthorne, F. C. *Canadian Mineralogist* **1997**, *35*, 1551.

[2] Ephritikhine, M. *Dalton Transactions* **2006**, 2501.

[3] Selbin, J.; Ortego, J. D. *Chemical Reviews* **1969**, *69*, 657.

[4] Groenewold, G. S.; Gianotto, A. K.; Cossel, K. C.; Van Stipdonk, M. J.; Moore, D. T.; Polfer, N.; Oomens, J.; de Jong, W. A.; Visscher, L. *Journal of the American Chemical Society* **2006**, *128*, 4802.

[5] Baird, C. P.; Kemp, T. J. *Progress in Reaction Kinetics* **1997**, *22*, 87.

[6] Geipel, G. *Coordination Chemistry Reviews* **2006**, *250*, 844.

[7] Science, J. W. G. o. t. A. P. S. a. t. A. A. f. t. A. o. *Nuclear Forensics: Role, State of the Art, and Program Needs*, 2008.

[8] Pohanish, R. P. *Sittig's Handbook of Toxic and Hazardous Chemicals and Carcinogens*; Elsevier Science, 2008.

[9] Milojevich, C. B.; Mandrell, B. K.; Turley, H. K.; Iberi, V.; Best, M. D.; Camden, J. P. *Journal of Physical Chemistry Letters* **2013**, *4*, 3420.

[10] Kneipp, K.; Wang, Y.; Kneipp, H.; Perelman, L. T.; Itzkan, I.; Dasari, R.; Feld, M. S. *Physical Review Letters* **1997**, *78*, 1667.

[11] Nie, S. M.; Emery, S. R. *Science* **1997**, *275*, 1102.

[12] Speight, J. *Lange's Handbook of Chemistry, 70th Anniversary Edition*; McGraw-Hill Companies,Incorporated, 2004.

CHAPTER 4.

DENSITY FUNCTIONAL THEORY FOR NICKEL COMPLEXES

A version of this chapter was originally published as a part of a publication by Heather M. Bass, S. Alan Cramer, A. Scott McCullough, Karl J. Bernstein, Chris R. Murdock, and David M. Jenkins:

Bass, H. M.; Cramer, S. A.; McCullough, A. S.; Bernstein, K. J.; Murdock, C. R.; Jenkins, D. M., "Employing Dianionic Macrocyclic Tetracarbenes To Synthesize Neutral Divalent Metal Complexes." *Organometallics* **2013**, *32*, 2160-2167.

The article is represented as part of the published form from Organometallics, including the sections titled Abstract, Introduction and DFT Calculations for Nickel Complexes. The Supporting Information section of the manuscript has been added in part as an appendix. The dissertation author was primarily responsible for the execution of the DFT calculations and was aided by S. A. Cramer in the interpretation and discussion. All authors participated in the discussion of results and approved the final manuscript.

Abstract

Macrocyclic tetraimidazolium diborate ligand precursors with two different ring sizes have been synthesized by ring-forming reactions between diimidazoles and haloboranes. Deprotonation of the macrocyclic tetraimidazoliums with n-butyllithium followed by the addition of divalent metal salts of palladium or nickel leads to macrocyclic tetracarbene complexes with an 18-atom macrocycle, but not the 16-atom variant. These neutral palladium and nickel complexes are the first examples of macrocyclic tetracarbene diborate complexes, and unlike their cationic counterparts, they are highly soluble in nonpolar solvents. All macrocyclic tetraimidazoliums and their corresponding metal complexes were characterized by single-crystal X-ray diffraction and spectroscopic techniques.

Introduction

In myriad instances, the addition of a borate moiety to the backbone of tridentate ligands has led to fascinating reactivity that is distinct from that exhibited by complexes with isostructural ligands featuring carbon in the same position.[1] Addition of a borate decreases the overall charge of a metal complex, often allowing for increased solubility in nonpolar solvents. In addition to increasing solubility, a borate positioned near the metal center can subtly change the electronic structure of the complex.[2] This seemingly small tweak in electron donation properties of the ligand can induce novel oxidation states and spin states at the metal center, which leads to innovative reactivity.[3]

These phenomena have been documented extensively for tripodal ligands for both triphosphines and tricarbenes in comparison of the neutral versus anionic versions.[4] In the case of the triphosphine ligands, the Peters group has shown that the tris(phosphino)borate ligand can support complexes which stabilize novel iron−nitrogen bonds that can then be functionalized.[5] For the tricarbenes, both the neutral and anionic versions have been found to support metal−ligand multiple bonds;[6] however, the anionic version has stabilized unprecedented oxidation states for iron nitrides that exhibited reactivity in instances where complexes with the neutral version of the tricarbene ligand did not.[7] Despite the importance of these tripodal ligands with a borate in the backbone, to date, there are no known tetracarbenes with borates in the macrocyclic ring.

Macrocyclic tetracarbene ligands are a class of strong σ-donor ligands that were first reported by Hahn via a templating synthesis on platinum in 2005.[8] Since his publication, macrocyclic tetraimidazoliums have now been employed to prepare a wide variety of transition-metal tetracarbene complexes.[9] Many of these complexes have demonstrated important

properties such as electron transfer reagents,[10,11] aziridination catalysis,[12,13] and stabilization of non-heme iron oxos.[14] Despite the growing importance of this class of macrocyclic N-heterocyclic carbene (NHC) ligands, no examples with borates in the macrocycle have been prepared. Nevertheless, previous syntheses suggest that it would be possible to prepare a macrocyclic tetraimidazolium with borates in the backbone that could be ligated to form tetracarbenes. Siebert and co-workers synthesized imidazolium borate macrocycles that contained either four or five imidazoliums per ring with an equal number of borates.[15] While they noted that they were unable to form carbenes with these complexes, perhaps because the borates decrease the acidity of the C2 proton, they demonstrated that this type of cyclic structure is possible.[15] In contrast, Fehlhammer[16] and Smith[17] independently prepared bis-dicarbene borate complexes on group 10 metals. Their complexes only had one borate moiety per two carbenes. We intend to meld these concepts to synthesize macrocyclic tetracarbene complexes with two borate moieties per macrocycle.

The expansion of the family of macrocyclic tetracarbenes to include examples with borates in the macrocycle would be advantageous for two reasons. First, metal complexes would have a reduced charge that would increase their solubility in nonpolar solvents. Improved solubility in noncoordinating solvents such as toluene is particularly beneficial for catalytic reactions, such as the aforementioned aziridination.[12] Second, the addition of borates should improve the electron-donating ability of the carbenes to the metal, if the imidazolium can be successfully deprotonated. This electron donation comparison can be investigated through spectroscopic methods[18] as well as TD-DFT calculations.[19] The combined properties of increased electron donation and reduced charge on the complex may assist in stabilizing metal ions in high-valent oxidation states in the same manner that Smith and Peters demonstrated with tripodal

borate ligands.[20-26] In this paper, we describe the first synthesis of borate-containing macrocyclic tetracarbene ligand precursors and provide two examples of complexation on palladium and nickel with the larger ring precursor. Unlike Siebert's macrocyclic rings, we were able to synthesize exclusively the tetraimidazolium as the sole product.[15] The ligand precursors and metal complexes were characterized by single-crystal X-ray crystallography and spectroscopic techniques. Finally, DFT and TD-DFT calculations were performed on structurally similar neutral and cationic metal complexes to assist in comparing the electron donor strength of these novel tetracarbene ligands.

Computational Methods

Density functional theory (DFT) and time-dependent density functional theory (TD-DFT) calculations are relatively new techniques to chemistry but have already found wide acceptance and use.[27,28] DFT is a quantum mechanical modeling approach used to examine the electronic structure of many-body systems. The technique is centered on the use of functionals to describe spatially dependent electron density. The use of the approach was greatly accelerated in the 1990s with the advancement of the correlation and exchange interaction approximations. TD-DFT varies from DFT in that the computation must take into account time-dependent potentials, such as magnetic or electric fields. As computational methods, DFT and TD-DFT are a step removed from the laboratory, yet serve as methods to aid in the understanding of typical bench experiments and to make predications in advance of experimentation. Both aspects of the methods were utilized in this work, as our investigation into ($^{B(Me)_2,Et}TC^{H}$)Ni and [($^{Me,Et}TC^{Ph}$)Ni]$^{2+}$ served to deepen our understanding of the work performed in the lab and the work with the hypothetical complex [($^{Me,Et}TC^{H}$)Ni]$^{2+}$ allowed us to draw conclusions not yet tested.

DFT Calculations for Nickel Complexes

In order to gain a better understanding of the effects of installing two borate moieties in the macrocycle, we performed DFT calculations on our nickel complexes and evaluated the corresponding d-orbital splitting. We chose the nickel complexes specifically to compare them to the already published DFT results of the structurally similar compounds ($^{Pr,Pr}TC^{H}$)Ni and [($^{Pr,Pr}TC^{H}$)Ni]$^{2+}$ (**15**), prepared by Murphy.[11] The former compound facilitates fascinating reduction reactions due to its unusual ligand-based radical.[11] Our DFT calculations were performed with NWChem using the functional B3LYP and the basis set 6-31g**. Single-point electronic structure calculations were performed on ($^{B(Me)_2,Et}TC^{H}$)Ni and [($^{Me,Et}TC^{Ph}$)Ni]$^{2+}$ using the experimentally determined X-ray coordinates and a singlet ground state. Each structure was allowed to relax to a global minimum without the use of geometric constraints. Time-dependent DFT (TD-DFT) energy calculations were performed on the optimized ground state DFT geometries also using functional B3LYP and basis set 6-31g**.

An energy minimization for ($^{B(Me)_2,Et}TC^{H}$)Ni (**11**) shows no appreciable change in the Ni−C bond distances versus the experimental structure and only a small change in the C−Ni−C bond angles (Table 4.1). The calculated orbital splitting diagram for **11** shows that the LUMO is centered primarily on the p_z orbitals of the carbene carbons and their adjacent nitrogens (Figure 4.1A). The LUMO p_z orbital of **11** is consistent with the calculated LUMO for [($^{Pr,Pr}TC^{H}$)Ni]$^{2+}$ (**15**).[11] However, the HOMO orbital for **11** is a d_{z^2} orbital (Figure 4.1B) and not a ligand-based orbital as was observed for **15**.[11] The other orbitals with energies that are near the HOMO and LUMO orbitals are consistent with typical square-planar d^8 complexes.

To help determine if the change in the HOMO orbital is due to the boron atoms being part of the macrocycle, we performed the same calculations on the previously described

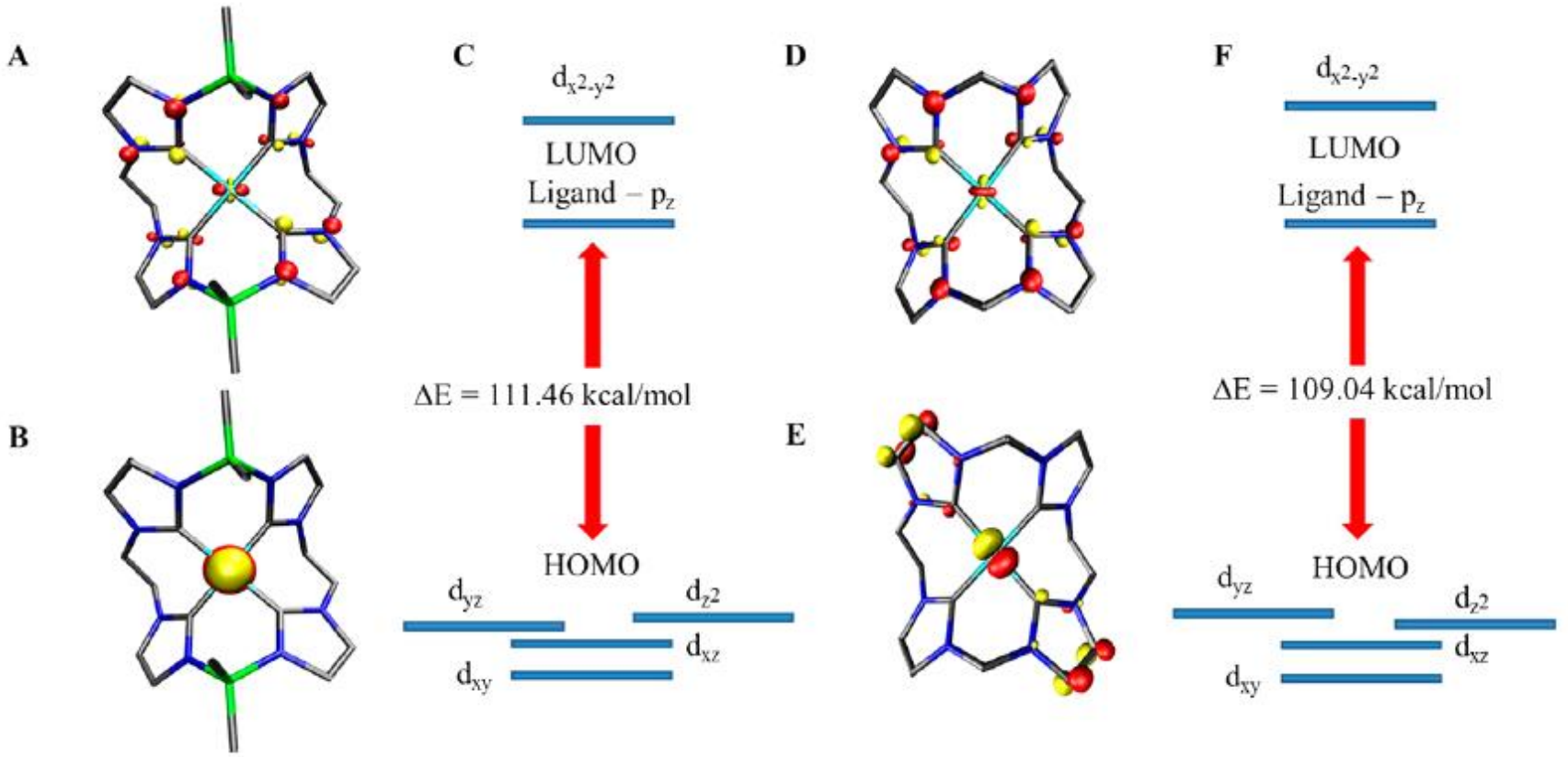

Figure 4.1. (A) LUMO of ($^{B(Me)_2,Et}TC^{H}$)Ni. (B) HOMO of ($^{B(Me)_2,Et}TC^{H}$)Ni. (C) Orbital splitting diagram of ($^{B(Me)_2,Et}TC^{H}$)Ni obtained from TDDFT calculations. (D) LUMO of [($^{Me,Et}TC^{H}$)Ni]$^{2+}$. (E) HOMO of [($^{Me,Et}TC^{H}$)Ni]$^{2+}$. (F) Orbital splitting diagram of [$^{Me,Et}TC^{H}$)Ni]$^{2+}$ obtained from TD-DFT calculations. All calculations used NWChem/B3LYP/6-31g**.

$[(^{Me,Et}TC^{Ph})Ni]^{2+}$ (**13**).[29] In a manner similar to that for **11**, there is almost no change in the metal−ligand bond lengths but a slightly more appreciable flexing which causes one of the trans C−Ni−C bond angles to contract (Table 4.1). Notably, the LUMO is the same ligand-based p_z orbital that we observed for **11** and a similar d orbital splitting pattern was found for $[(^{Me,Et}TC^{Ph})Ni]^{2+}$. However, a direct comparison was problematic, since several ligand-based orbitals were interspersed between the LUMO and the highest occupied d orbital. All of these orbitals have electron density primarily on the phenyl rings of the macrocyclic ligand. To simplify the interpretation of the DFT results, an additional calculation was performed on the hypothetical complex $[(^{Me,Et}TC^{H})Ni]^{2+}$. The phenyl rings on the 4- and 5-positions of each carbene ring for $[(^{Me,Et}TC^{Ph})Ni]^{2+}$ were removed and replaced by hydrogen atoms and then the calculation was performed as described previously. In the same manner as for **11**, the LUMO remains a p_z ligand-based orbital (Figure 4.1D), but for $[(^{Me,Et}TC^{H})Ni]^{2+}$ the HOMO is now a d_{yz} orbital (Figure 4.1E). This change in HOMO orbital is likely due to the near-degeneracy of the d_{z2}, d_{yz}, and d_{xz} orbitals. The simplified structure of $[(^{Me,Et}TC^{H})Ni]^{2+}$ allows for a closer comparison of the HOMO−LUMO gap between the cationic and neutral complexes. The HOMO−LUMO gap for $[(^{Me,Et}TC^{H})Ni]^{2+}$ is 109.04 kcal/mol (Figure 4.1F) which is slightly smaller than the calculated value of 111.46 kcal/mol for $(^{B(Me)_2,Et}TC^{H})Ni$ (Figure 4.1C).

We can draw two conclusions from the DFT calculations. First, the tetracarbene borate macrocycles appear to have σ-donor strength comparable to that of their neutral counterparts. This conjecture is supported by the ^{13}C NMR experimental evidence, which shows that the carbene resonance is only slightly shifted by the addition of borates to the macrocycle. Both the experimental and theoretical observations suggest that the borate containing macrocycles may be slightly more electron donating with regards to their nickel complexes. Second, the calculations

suggest that it is the size of the macrocyclic ring and the accompanying change in torsion angle of the NHC rings in relation to the metal−ligand plane (formed by four carbons and the nickel) that affect the energies of the ligand-based HOMO orbital and not the presence of boron atoms in the macrocyclic ring.

Conclusion

The calculations performed, along with NMR, suggest the 18-atom borate containing macrocycle is equivalent in σ-donor strength to our previously prepared isostructural ligand. This new class of tetracarbene complexes, despite structural conformity, presents two possible benefits compared to equivalent compounds synthesized from neutral macrocyclic ligands. Cardinally, the incorporation of borate in the macrocyclic ring could allow for different reactivity analogous to that of the tripodal carbenes and phosphines, principally when bound to metals which form nonsaturated complexes. Subsequently, the exceptional solubility in nonpolar solvents (e.g. toluene) should serve as auspicious for numerous catalytic reactions.

References

[1] Saouma, C. T.; Peters, J. C. *Coordination Chemistry Reviews* **2011**, *255*, 920.

[2] Smith, J. M. *Comments on Inorganic Chemistry* **2008**, *29*, 189.

[3] Scepaniak, J. J.; Harris, T. D.; Vogel, C. S.; Sutter, J.; Meyer, K.; Smith, J. M. *Journal of the American Chemical Society* **2011**, *133*, 3824.

[4] Hu, X.; Meyer, K. *Journal of Organometallic Chemistry* **2005**, *690*, 5474.

[5] Brown, S. D.; Betley, T. A.; Peters, J. C. *Journal of the American Chemical Society* **2003**, *125*, 322.

[6] Hu, X.; Meyer, K. *Journal of the American Chemical Society* **2004**, *126*, 16322.

[7] Smith, J. M.; Subedi, D. *Dalton Transactions* **2012**, *41*, 1423.

[8] Hahn, F. E.; Langenhahn, V.; Lügger, T.; Pape, T.; Le Van, D. *Angewandte Chemie International Edition* **2005**, *44*, 3759.

[9] McKie, R.; Murphy, J. A.; Park, S. R.; Spicer, M. D.; Zhou, S.-z. *Angewandte Chemie International Edition* **2007**, *46*, 6525.

[10] Park, S. R.; Findlay, N. J.; Garnier, J.; Zhou, S.; Spicer, M. D.; Murphy, J. A. *Tetrahedron* **2009**, *65*, 10756.

[11] Findlay, N. J.; Park, S. R.; Schoenebeck, F.; Cahard, E.; Zhou, S.-z.; Berlouis, L. E. A.; Spicer, M. D.; Tuttle, T.; Murphy, J. A. *Journal of the American Chemical Society* **2010**, *132*, 15462.

[12] Cramer, S. A.; Jenkins, D. M. *Journal of the American Chemical Society* **2011**, *133*, 19342.

[13] Jenkins, D. M. *Synlett* **2012**, *23*, 1267.

[14] Meyer, S.; Klawitter, I.; Demeshko, S.; Bill, E.; Meyer, F. *Angewandte Chemie International Edition* **2013**, *52*, 901.

[15] Weiss, A.; Pritzkow, H.; Siebert, W. *Angewandte Chemie International Edition* **2000**, *39*, 547.

[16] Fränkel, R.; Kniczek, J.; Ponikwar, W.; Nöth, H.; Polborn, K.; Fehlhammer, W. P. *Inorganica Chimica Acta* **2001**, *312*, 23.

[17] Nieto, I.; Bontchev, R. P.; Smith, J. M. *European Journal of Inorganic Chemistry* **2008**, *2008*, 2476.

[18] Baker, M. V.; Barnard, P. J.; Brayshaw, S. K.; Hickey, J. L.; Skelton, B. W.; White, A. H. *Dalton Transactions* **2005**, 37.

[19] Wasbotten, I. H.; Ghosh, A. *Inorganic Chemistry* **2007**, *46*, 7890.

[20] Rohde, J.-U.; Betley, T. A.; Jackson, T. A.; Saouma, C. T.; Peters, J. C.; Que, L. *Inorganic Chemistry* **2007**, *46*, 5720.

[21] Thomas, C. M.; Mankad, N. P.; Peters, J. C. *Journal of the American Chemical Society* **2006**, *128*, 4956.

[22] Hendrich, M. P.; Gunderson, W.; Behan, R. K.; Green, M. T.; Mehn, M. P.; Betley, T. A.; Lu, C. C.; Peters, J. C. *Proceedings of the National Academy of Sciences of the United States of America* **2006**, *103*, 17107.

[23] Scepaniak, J. J.; Vogel, C. S.; Khusniyarov, M. M.; Heinemann, F. W.; Meyer, K.; Smith, J. M. *Science* **2011**, *331*, 1049.

[24] Scepaniak, J. J.; Young, J. A.; Bontchev, R. P.; Smith, J. M. *Angewandte Chemie International Edition* **2009**, *48*, 3158.

[25] Scepaniak, J. J.; Fulton, M. D.; Bontchev, R. P.; Duesler, E. N.; Kirk, M. L.; Smith, J. M. *Journal of the American Chemical Society* **2008**, *130*, 10515.

[26] Betley, T. A.; Peters, J. C. *Journal of the American Chemical Society* **2004**, *126*, 6252.

[27] Ittel, S. D.; Johnson, L. K.; Brookhart, M. *Chemical Reviews* **2000**, *100*, 1169.

[28] Herebian, D.; Wieghardt, K. E.; Neese, F. *Journal of the American Chemical Society* **2003**, *125*, 10997.

[29] Lu, Z.; Cramer, S. A.; Jenkins, D. M. *Chemical Science* **2012**, *3*, 3081.

Appendix For Chapter 4

Table 4.1. Experimentally obtained data compared to DFT calculations using NWChem using functional B3LYP and basis set 6.31g**.

	Experimental		**Calculated**	**Calculated**
Complex	**($^{B(Me)_2,Et}TC^{H}$)Ni**	**Complex**	**($^{B(Me)_2,Et}TC^{H}$)Ni**	**[($^{Me,Et}TC^{H}$)Ni]$^{2+}$**
Ni-C1 (Å)	1.927(3)	Ni-C1 (Å)	1.9304	1.9296
Ni-C2 (Å)	1.891(3)	Ni-C2 (Å)	1.8926	1.8853
C1-Ni-C2 (°)	93.8(1)	Ni-C3 (Å)	1.9304	1.9298
C1-Ni-C2' (°)	86.5(1)	Ni-C4 (Å)	1.8926	1.8854
C1-Ni-C1' (°)	172.0(2)	C1-Ni-C2 (°)	93.311	87.684
C2-Ni-C2'(°)	175.8(2)	C2-Ni-C3 (°)	87.237	92.519
		C3-Ni-C4 (°)	93.311	87.677
		C1-Ni-C4 (°)	87.237	92.536
		C1-Ni-C3 (°)	167.409	168.369
		C2-Ni-C4 (°)	175.006	177.948

CONCLUSION

The field of Raman spectroscopy has been further broadened, if even slightly in these undertakings. They were permitted in part by the advent of inexpensive, monochromatic laser sources and high resolution spectrometers. Undertakings such as the investigation into the binding of aryl phosphines which was conducted utilizing tertiary phosphines illustrated a Lewis acid/base adduct or L-type binding and the secondary phosphine oxides demonstrated no bonding, suggesting that without lone pair electrons directly on the phosphorus atom binding will not ensue. While SIFs were unsuccessful for the study of secondary phosphines, it is likely that FONs are likely to rectify the issue and allow for completion of the study.

The second project presented a novel synthetic, spectroscopic, and theoretical characterization of an aromatic, tridentate amidoxime uranyl complex. The X-ray structure of the complex established a singular complexation with uranium as opposed to other known tridentate amidoxime complexes. The inaugural solid state NMR spectra in this work confirmed bulk complexation and extension of aromaticity. DFT calculations served to provide insights into the electronic and vibrational morphology. The IR spectroscopy was cluttered with numerous active modes while the Raman spectra provided clear and concise evidence of uranium binding, hinting at the potential of serving as a spectroscopic method for uranium detection.

The triennial project pursued Raman based spectroscopic detection of uranium in nonlinear spectroscopy via hyper-Raman spectroscopy. While the anti-symmetric stretch was observed, fluorescence prohibited reproducibility, which stymied progress. Further work at longer wavelengths is likely to overcome the obstruction and allow for advancement.

A slew of Raman spectroscopy techniques have been drawn on to analyze a number of different inorganic compounds. Advantages such as reduced interference, lack of sample

preparation, differing selection rules, clarity of spectra, and many other benefits have aided the included works. There are sure to be many more reasons to continue utilizing variations on Raman spectroscopy for research moving forward.

VITA

Karl J. Bernstein was born on June 1st, 1985. He graduated Andrews University in 2008 having majored in Chemistry, minored in Physics, and accomplished significant studies in engineering, computer science and mathematics. Following graduation, he worked at Physics Enterprises, a small company that manufactures Physics based devices for university level teaching and instruction. In 2010 he began his pursuit of a Doctorate of Philosophy at the University of Tennessee Knoxville. He joined the Camden group and pursued studies in Analytical Chemistry. His research focused on new techniques for spectroscopic detection of Uranium via Raman based approaches.